BIRLA CENTRAL LIBRARY

PILANI (RAJASTHAN)

Call No. 620·1123
H382I

Accession No. 51167

Blackie's "TECHNIQUE" Series

An Introduction to Photo-elastic Analysis

BLACKIE & SON LIMITED
66 Chandos Place, LONDON
17 Stanhope Street, GLASGOW

BLACKIE & SON (INDIA) LIMITED
103/5 Fort Street, BOMBAY

BLACKIE & SON (CANADA) LIMITED
TORONTO

An Introduction to
Photo-elastic Analysis

BY

ARNOLD W. HENDRY
B.Sc.(Eng.), Ph.D., A.M.Inst.C.E., A.M.I.Struct.E.
Lecturer in Engineering, University of Aberdeen

BLACKIE & SON LIMITED
LONDON AND GLASGOW

First published 1948

Printed in Great Britain by Blackie & Son, Ltd., Glasgow

PREFACE

Although it is not always realized, photo-elasticity is one of the oldest experimental methods available for determining the stress distribution in engineering constructions—it is now nearly fifty years since the late Professor Coker began his long series of investigations which firmly established the value of the method. Notwithstanding this fact, photo-elastic analysis has generally remained something of a mystery to the practising engineer, with the result that he remains unaware of its possible applications to his particular problems, and finds difficulty in assessing the results of a research in which it has been used. The lack of a book giving a practical outline of the subject within a small compass has contributed to this and tended to retard the use of photo-elasticity by those who have not the time to study highly detailed textbooks or to extract the necessary information from a rather scattered literature.

I have therefore ventured to write the present volume as a general survey of the method for the non-specialist and for the student, for whom it may serve as an introduction to the more advanced works such as Coker and Filon's *Treatise*.

The treatment is mainly descriptive, and mathematical discussions are restricted to those necessary for a satisfactory understanding of the matter under consideration.

I am indebted to the Institutions of Civil and Structural Engineers for permission to reproduce several diagrams and photographs from my papers published by them. Information quoted directly from other sources has been acknowledged in the text.

ARNOLD W. HENDRY.

ENGINEERING DEPARTMENT,
ABERDEEN UNIVERSITY.

17th February, 1948.

CONTENTS

CHAP. Page

INTRODUCTION - - - - - - - 1

I. ELASTIC THEORY - - - - - - - 3

II. ESSENTIAL OPTICS - - - - - - - 20

III. STRESSED TRANSPARENT MATERIALS IN THE POLARISCOPE - - - - - - - - 40

IV. THE REDUCTION OF DATA FROM PHOTO-ELASTIC TESTS 53

V. PHOTO-ELASTIC APPARATUS - - - - - 75

VI. COMPENSATORS AND OTHER INSTRUMENTS - - - 91

VII. PHOTO-ELASTIC MATERIALS - - - - - 106

VIII. THE PREPARATION OF MODELS AND TEST PROCEDURE - 117

IX. PRACTICAL APPLICATIONS OF PHOTO-ELASTICITY - 128

X. FROZEN STRESS PATTERNS AND THEIR PRACTICAL APPLICATIONS - - - - - - - - 138

BIBLIOGRAPHY - - - - - - - 143

INDEX - - - - - - - - - 150

LIST OF PLATES

Facing Page

Fringe Patterns for Beam and L Models - - - 46

Polariscope with Glass-plate Reflection Polarizer - 89

Polariscope with "Polaroid" Filters - - - - 90

Straining Frame for Polariscope - - - - - 92

Mica-plate Compensator: Shaping Model on Milling Machine - - - - - - - - - 102

"Talymit" Gauge - - - - - - - - 103

Fringe Patterns for Bent Notched Beam: Cam and Roller: and L Frame - - - - - - 121

Fringe Patterns for Vierendeel Girder: Eccentrically Loaded Rivet Group - - - - - - 136

Introduction

When a stress-distribution problem is encountered in engineering design it is usually dealt with by a mathematical analysis of a more or less idealized conception of the factors involved. This procedure, when supported by experience, is satisfactory in many cases, but frequently a new problem is encountered which is not at all amenable to mathematical treatment and for which an accurate solution is essential in the interests of safety, economy, and efficient design. Such a problem may become the subject of a laboratory research in which the stress distribution in the member concerned is explored by means of suitable strain gauges. The results of this investigation may then be used to develop mathematical formulæ for the solution of future problems or to check a proposed theoretical solution. The stress analysis of full-sized constructions by strain gauges is expensive, both in time and money, so that alternative methods have been developed in which a solution is obtained by tests on small-scale models. Photo-elasticity is such a method—in it, small-scale transparent models are examined in polarized light and the stress distribution deduced from the optical effects observed.

The optical phenomenon upon which the photo-elastic method is based—the quasi-crystalline behaviour of stressed transparent materials—was first observed by Brewster in 1816. Brewster was fully aware that the effect which he had discovered might be used as a method of stress measurement and suggested that the stresses in arches might be investigated by optical methods. Many nineteenth-century physicists—including Fresnel, Wertheim, Clerk Maxwell, Mach, Kerr and Pockels—investigated and contributed to the theory of artificial double refraction, but little was done towards applying it to engineering problems. This is not surprising when we consider the practical difficulties of cutting glass—then the only available photo-elastic material—to the shape of even the simplest type of model.

The introduction of celluloid for photo-elastic models opened the way for the great advances made by Coker and Filon and their co-workers; they developed the experimental technique, the design of apparatus, and investigated a large number of engineering problems. Their photo-elastic work was usually paralleled by theoretical analyses and the results of many years' work are contained in their monumental *Treatise on Photo-elasticity*.

During the 1930's further progress was due mainly to American workers who were able to make use of new transparent plastics in their investigations and extended the method to the analysis of three-dimensional stress systems.

As a result of these efforts photo-elasticity has been raised from the status of a difficult and laborious laboratory experiment, yielding mainly qualitative results, to a rapid and economical method of stress analysis giving a reliable quantitative solution of the problem under consideration. One of the chief merits of the method is its inherent attractiveness to the engineer, giving as it does an immediate and tangible picture of the stress conditions in the structure or detail being investigated.

In the succeeding chapters the aim is to give a general introduction to the theory and practice of photo-elasticity, and an indication of the types of problems in engineering where the method is likely to be of particular value.

CHAPTER I

Elastic Theory

As this book is addressed primarily to engineers it will be assumed that the reader is familar with the elementary principles of elasticity. The intention of the present chapter is therefore to summarize the stress formulæ, theorems and definitions which are of particular importance in photo-elastic analysis. The scope of this summary is restricted to two-dimensional analysis as it is in this field that the photo-elastic method is of the most immediate value. The extension of photo-elasticity to three-dimensional work will be discussed in this book only briefly, and is only likely to be attempted after some experience with two-dimensional analysis.

Stress at a Point

It is convenient to refer the stresses at a point in a body to three rectangular axes, X, Y and Z. When the stress say in the direction of the Z-axis is zero at every point in the body we have a system of *plane stress*. If the strain is everywhere zero in the direction of the Z-axis, the problem is one of *plane strain*. The photo-elastic method is usually applied to problems of plane stress or to problems which can be approximately represented by such a condition.

Suppose that ABCD in fig. 1 is an infinitely small element cut from a thin stressed plate. Then, in general, the stresses on the element can be reduced to normal stresses f_x and f_y and a shear stress s_{xy}. The stress in the direction of the Z-axis is zero, and there is no shearing stress on the surface of the plate. The stresses f_x and f_y may be tensile or compressive and the shearing stresses s_{xy} are, by a well-known theorem, of equal magnitude; s_{xy} is counted positive if the shear diagonal passes through the first quadrant formed by the X- and Y-axes, and negative if it passes through the second quadrant. The meaning of the term " shear diagonal " will be understood from fig. 1. We may now consider the state of stress across a section AE, the normal to which is inclined at angle θ to the X-axis. For equilibrium there must evidently be components normal and parallel to AE, so that, resolving in the directions of the X- and Y-axes (fig. 2), we have

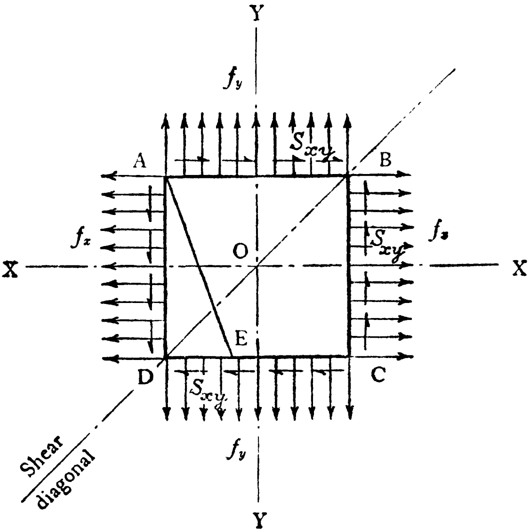

Fig. 1.—Stresses on an element cut from a thin plate

$$f_\theta \cos\theta \, \mathrm{EA} + s_\theta \sin\theta \, \mathrm{EA} = f_x \, \mathrm{AD} + s_{xy} \, \mathrm{DE},$$

i.e. $$f_\theta \cos\theta + s_\theta \sin\theta = f_x \cos\theta + s_{xy} \sin\theta.$$

$$f_\theta \sin\theta\,\mathrm{EA} - s_\theta \cos\theta\,\mathrm{EA} = f_y\,\mathrm{DE} + s_{xy}\,\mathrm{AD},$$

i.e. $$f_\theta \sin\theta - s_\theta \cos\theta = f_y \sin\theta + s_{xy} \cos\theta.$$

From which

$$s_\theta = \frac{f_x - f_y}{2} \sin 2\theta - s_{xy} \cos 2\theta, \quad . \quad . \quad (1)$$

and

$$f_\theta = f_x \cos^2\theta + f_y \sin^2\theta + s_{xy} \sin 2\theta, \quad . \quad . \quad (2)$$

$$= \frac{f_x + f_y}{2} + \frac{f_x - f_y}{2} \cos 2\theta + s_{xy} \sin 2\theta. \quad . \quad (3)$$

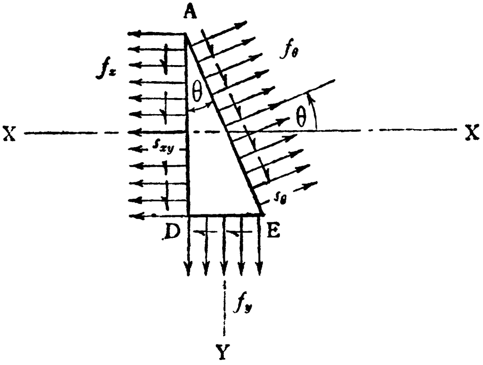

Fig. 2.—Stresses on section AE of element ABCD of fig. 1

On a section at right angles to AE (BF in fig. 3) it is easily found that

$$s_{\theta+90} = -\left(\frac{f_x - f_y}{2} \sin 2\theta - s_{xy} \cos 2\theta\right), \quad . \quad (4)$$

and $$f_{\theta+90} = \frac{f_x + f_y}{2} - \frac{f_x - f_y}{2} \cos 2\theta - s_{xy} \sin 2\theta. \quad (5)$$

That is, the tangential (shearing) stresses are equal in magnitude on planes at right angles to one another, and on an element inclined at angle θ to the X-axis the state of stress is as indicated in fig. 3.

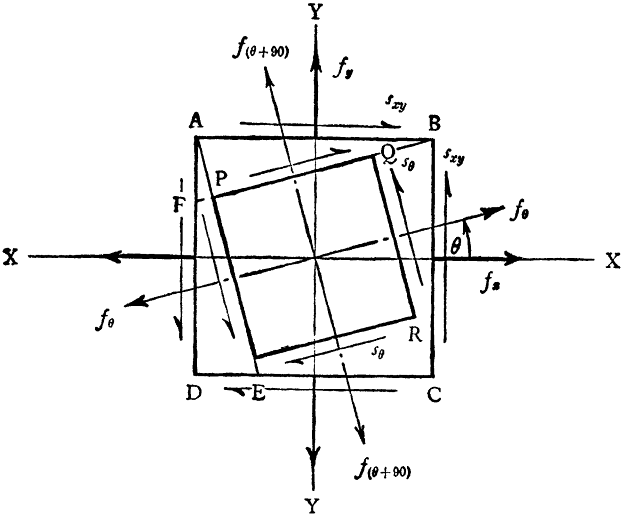

Fig. 3.—Stresses on an element PQRS inclined at angle θ to the original element ABCD

Principal Stresses

There is one particular value of θ for which the shearing stresses s_θ given by equations (1) and (4) above are equal to zero; this value is obtained by equating (1) to zero and is given by

$$2\theta = \tan^{-1}\frac{2s_{xy}}{f_x - f_y}. \quad . \quad . \quad . \quad (6)$$

The stresses on the sides of the element PQRS of fig. 3 are then purely normal, either tensile or compressive, and are known as *principal stresses*. In terms of f_x, f_y and s_{xy} the principal stresses are

$$p = \frac{f_x + f_y}{2} + \sqrt{\left(\frac{f_x - f_y}{2}\right)^2 + s_{xy}{}^2}, \quad . \quad (7)$$

$$Q = \frac{f_x + f_y}{2} - \sqrt{\left(\frac{f_x - f_y}{2}\right)^2 + s_{xy}^2}. \quad . \quad (8)$$

Counting tensile stress positive, P is the algebraically larger principal stress, i.e. P is the major and Q the minor principal stress.

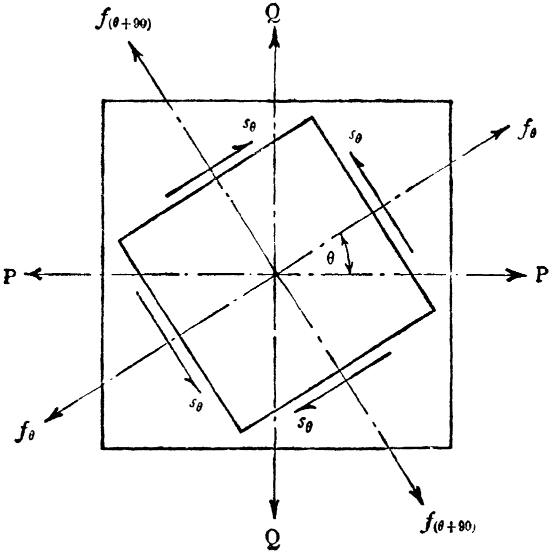

Fig. 4.—Stresses on an element inclined at angle θ to the direction of major principal stress

If at any point the principal stresses and their directions relative to a fixed reference axis are known, the normal and shearing stresses on any other element at the point can readily be calculated from the expressions

$$f_\theta = \frac{P+Q}{2} + \frac{P-Q}{2} \cos 2\theta, \quad . \quad (9)$$

$$f_{\theta+90} = \frac{P+Q}{2} - \frac{P-Q}{2} \cos 2\theta, \quad . \quad (10)$$

$$s_\theta = \frac{P-Q}{2}\sin 2\theta, \quad . \quad . \quad . \quad (11)$$

where θ has the value indicated in fig. 4. The principal stresses and their directions thus completely specify the state of stress at a point.

Maximum Shearing Stress

It is easily shown, by differentiating equation (1) with respect to θ and equating to zero, that a maximum value of s_θ occurs when

$$2\theta = \tan^{-1}\left(-\frac{f_x - f_y}{2s_{xy}}\right). \quad . \quad . \quad (12)$$

This stress is the *maximum shearing stress* at the point. It is evident that the value of 2θ given by equation (12) differs from that of equation (6) by 90°, thus the inclination of the maximum shearing stress at a point is 45° to the direction of the principal stresses. The maximum shearing stress in terms of the principal stresses is

$$s_{max} = \frac{P-Q}{2}. \quad . \quad . \quad . \quad . \quad (13)$$

As will be found later, the maximum shearing stress is of special significance in photo-elastic stress analysis.

Lines of Principal Stress

In a field of non-uniform stress, the directions of the principal stresses vary from point to point. If a curve be drawn in such a way that the direction of one of the principal stresses is tangential to it at every point along its length, then such a curve is termed a *line of principal stress* or *stress trajectory*. This is illustrated in fig. 5 from which it is apparent that there must be two orthogonal sets of curves, corresponding to the maximum and minimum principal stresses.

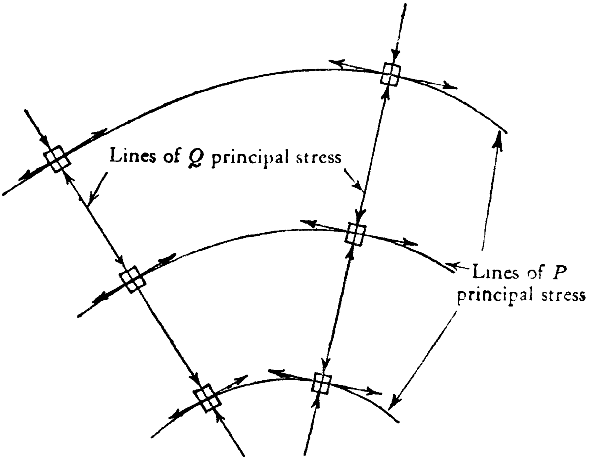

Fig. 5.—Lines of principal stress

The principal stress network for a portal frame model is shown in fig. 6. The lines of maximum principal stress are shown thin and the lines of minimum principal stress thick. An inspection of this diagram gives a valu-

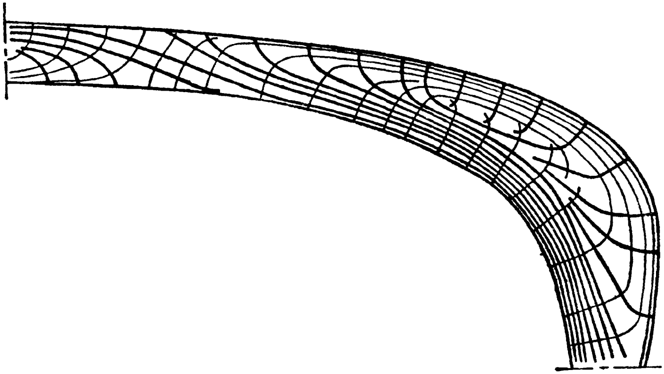

Fig. 6. Lines of principal stress in a portal frame model

able impression of the stress distribution in the model. For example, the crowding together of the lines of minimum principal stress towards the inner edge at the right of the model indicates a stress concentration there, and the cross-over of the two sets of lines in the horizontal part shows that the stress on the inner edge changes from compression to tension in this region.

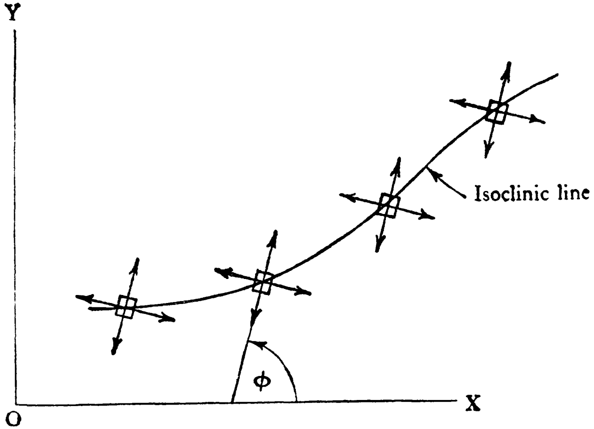

Fig. 7.—Illustrating the definition of an isoclinic line

Isoclinic Lines

The locus of points at which the principal stresses have the same inclination to an arbitrary reference axis is termed an *isoclinic line*; this is indicated in fig. 7. The angle ϕ which the direction of the principal stress makes with the reference axis is the *parameter* of the isoclinic. In a given model there will be an isoclinic line corresponding to every value of ϕ between zero and 180°. An axis of symmetry is always an isoclinic of some parameter.

The isoclinic lines for parameters 0° to 180° by 10° intervals are shown in fig. 8 for the portal frame model of fig. 6.

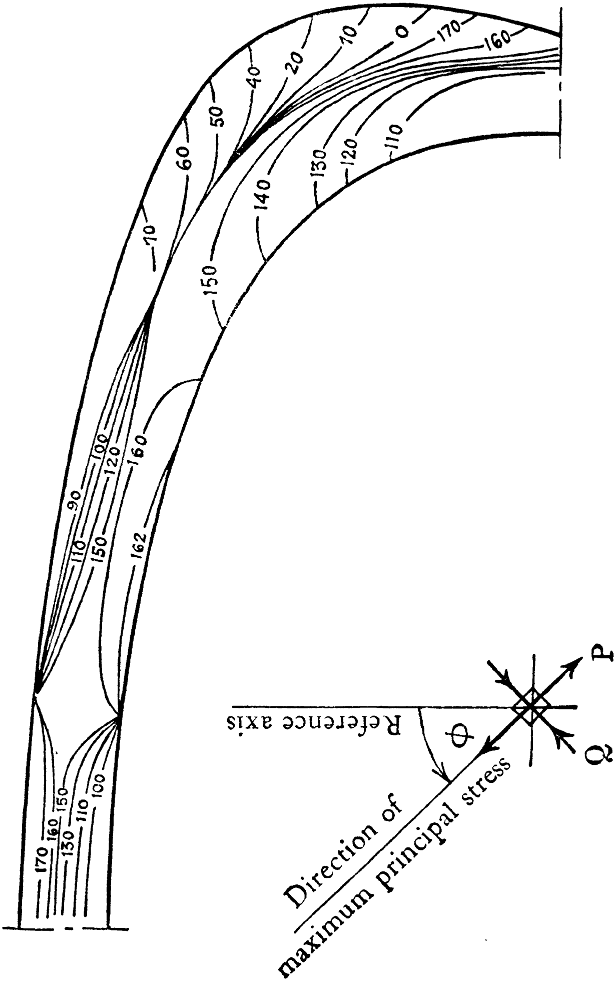

Fig. 8.—Isoclinic lines in the portal frame model of fig. 6

As will be seen later, the isoclinic lines are very readily obtained for a given model by photo-elastic experiment, and once they are known, it is an easy matter to construct the lines of principal stress. A simple construction for doing this is indicated in fig. 9, but the matter will be discussed in detail in Chapter IV.

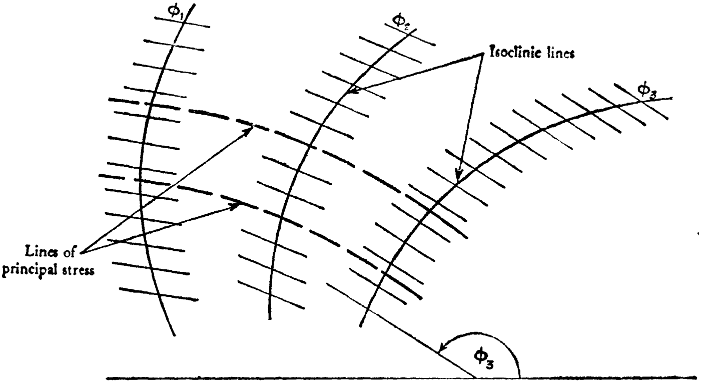

Fig. 9.—Construction of the lines of principal stress from the isoclinics

Mesnager's Theorem of the Isoclinic Lines

It can be shown that the principal stress tangent to a given line of principal stress reaches a maximum or a minimum value when that line is cut at right angles by an isoclinic. This is Mesnager's theorem, and is illustrated in fig. 10; the angle ψ between the tangents to the line of principal stress and the isoclinic is 90° at point A and respectively less and greater than this value at points B and C. The principal stress P is thus a maximum or a minimum at A which is termed a *cupic point.*

It follows from Mesnager's theorem that an isoclinic must be normal to a free boundary where the boundary stress is a maximum or minimum.

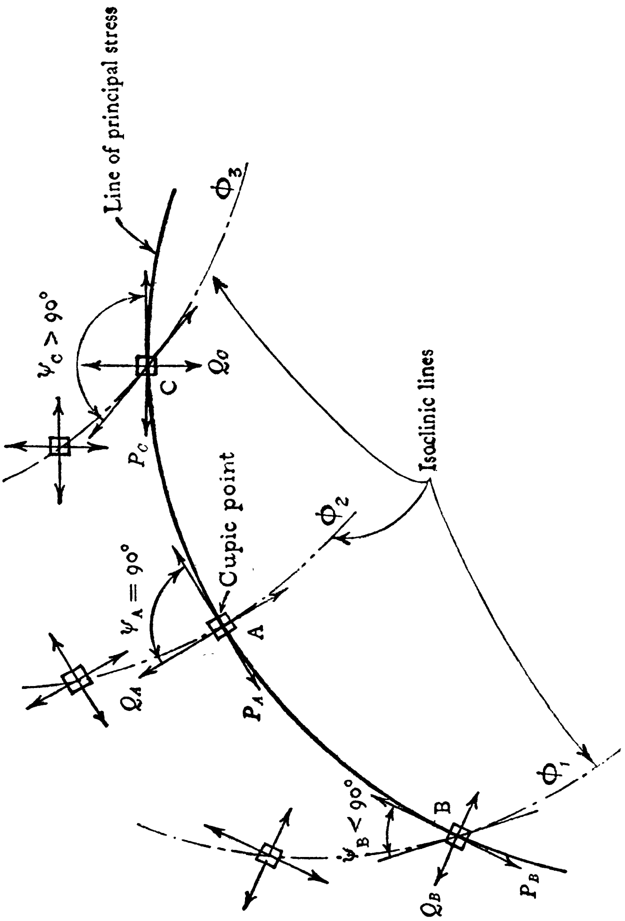

Fig. 10.—Mesnager's theorem of the isoclinic lines

Isotropic Points

A point at which the principal stresses are equal is termed an *isotropic point.* If the two principal stresses are zero, i.e. $P = Q = 0$, we have a special type of isotropic point usually referred to as a *singular point.*

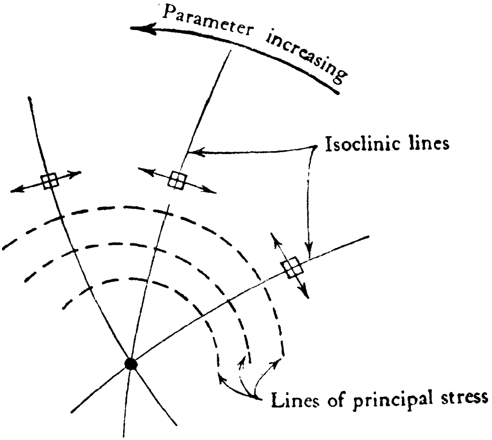

Fig. 11.—(*a*) Positive isotropic point

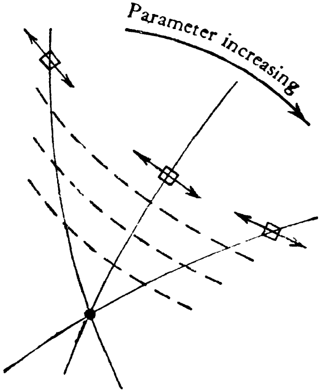

Fig. 11—(*b*) Negative isotropic point

Isoclinic lines of many parameters pass through an isotropic point, which is designated positive or negative according to the convention of fig. 11.

The formation of the lines of principal stress around isotropic points is of some interest. Figs. 12(*a*) and (*b*) are typical of the systems formed around positive and negative isotropic points. While there are many possible variations in detail from one model to another, they are all similar in type, being classified either as *interlocking* or *non-interlocking* systems.

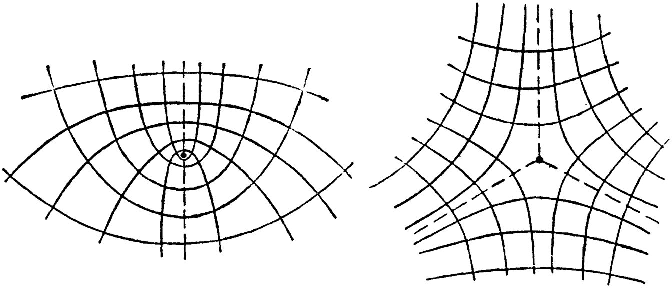

Fig. 12.—Typical arrangements of the lines of principal stress at isotropic points

(*a*) An interlocking system at a positive isotropic point

(*b*) A non-interlocking system at a negative isotropic point

The Stress Distribution in Geometrically Similar Plates

In the photo-elastic method the stresses in full-sized engineering constructions of steel or other material are determined by the optical effects observed in small-scale models made of transparent plastic. The question therefore arises as to whether the stress distribution is identical in plates of different materials subjected to the same external loads on their edges. It has been shown theoretically, and confirmed by experiment, that the stresses in elastic plates, under a system of plane stress, are independent of the ratio of the elastic constants provided that there are no holes. If there are holes in the plates this statement is only true if the forces applied to the boundary of any one hole form a system in equilibrium or reduce to a couple. If there is a resultant load on the boundary of a hole, as for example in the case of an eye-bar loaded through shackles and pins, a correction is necessary if the results are to be transferred from a plate of one material to a plate of a different material.

The theory underlying this correction is exceedingly complex and only the results of the mathematical investigation will be quoted.

Suppose that it is desired to find the stresses in the head of a steel eye-bar by a photo-elastic test on a Bakelite model which we will assume to be the same size as the steel prototype. In order to find the correction to be applied in transferring from Bakelite to steel, we must make a cut in the Bakelite model across a section AB, as shown in fig. 13, which is at right angles to the direction of the resultant load W on the boundary of the hole. The head of the bar is now strained, so that the upper surface of the cut is displaced by a distance h, relative to the lower surface, in the direction of AB. The cut section is now recemented, so as to maintain this displacement. This is known as a *dislocation*. The stresses set up by the dislocation alone are now determined by photo-elastic analysis.

Suppose that P', Q' are the principal stresses at any point C due to the external load W; P_d, Q_d are the principal stresses at C due to the dislocation, and P, Q are the principal stresses at the corresponding point in the steel bar; ϕ', ϕ_d, and ϕ are the directions of these principal stresses relative to an arbitrary axis.

Then

$$(P - Q)\cos 2\phi = (P' - Q')\cos 2\phi' + k(P_d - Q_d)\cos\phi_d,$$

$$(P - Q)\sin 2\phi = (P' - Q')\sin 2\phi + k(P_d - Q_d)\sin\phi_d,$$

$$(P + Q) = (P' + Q') + k(P_d + Q_d),$$

where $$k = \frac{W(1/m - 1/m')}{E'hd},$$

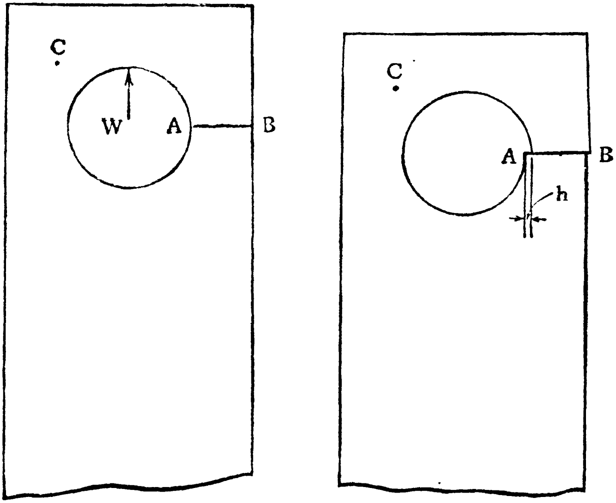

Fig. 13.—Construction of a dislocation

in which $1/m$, $1/m'$, are Poisson's ratios for steel and Bakelite respectively, E' is Young's modulus for Bakelite, and d is the thickness of the plate. $(P' - Q')$, $(P_d - Q_d)$, ϕ' and ϕ_d are known from the photo-elastic experiments, so that from the first two equations it is possible to calculate $(P - Q)$ and ϕ in the steel plate. The separate principal stresses in the steel plate are then determined by one of the methods described in Chapter IV.

If there is more than one hole in the plate it is necessary to construct dislocations for each hole in turn and add up the separate effects.

To carry out this procedure for a large number of points would be most laborious, and in practice it will usually be sufficient to find whether the correction is appreciable at a few points in the immediate vicinity of the hole. In most cases the correction will be negligible—Poisson's ratios for Bakelite and steel differ by about 0·04 and Young's modulus is of the order of 600,000 lb/in^2 for Bakelite, so that generally k will be small.

A further condition, tacitly assumed in the above discussion, is that the stresses in both model and prototype are within the elastic range of the material. If this is not the case, the stress distributions will in general be different as the plastic behaviour of the materials will be different. Highly localized plastic zones, however, as for example in the immediate vicinity of a concentrated load, will have no appreciable effect.

The model will usually be smaller than the prototype and the loads on it will be reduced by some convenient ratio. If F_d is the ratio of the linear dimensions of the model to the linear dimensions of the prototype, F_t the ratio of thickness of model to thickness of prototype and F_p the ratio of the loads on model and full-size, then the stresses at corresponding points in the model and prototype are in the ratio

$$\frac{f}{f_m} = \frac{F_d \times F_t}{F_p}.$$

Models of Framed Structures

In dealing with pin-jointed structures, the applied loads must be in a constant ratio F_p and the linear dimensions in the ratio F_d, as above. Then if the frame is statically determinate the *total loads* in the members will also be in the ratio F_p.

If the structure is redundant the product of the quantities E and A (E being Young's modulus and A the cross-sectional area of the member) in model and full size must bear a constant ratio F_m in order that the loads in the members shall be proportional. Redundant frameworks are sometimes fitted with members which are made deliberately too long or too short and to reproduce the effects of such members in the model it will generally be necessary to exaggerate the proportional amount of the misfit in the following manner: let dl be the length by which the member would have to be lengthened or shortened to fit into a just-stiff framework and let dl' be the corresponding quantity in the model, then

$$dl' = \frac{F_d \, . \, F_p}{\mathrm{F}_m} \, . \, dl,$$

where F_d, F_p and F_m are the dimensional, load, and modular scales as defined above.

A structure which has rigid connexions, so that the members are under bending in the plane of the frame, is rather more difficult to represent accurately by a model cut from a sheet of material. In addition to the above conditions the stiffness EI (where I is the relevant moment of inertia) must be proportional in corresponding members. The members being of rectangular section in the model and of constant thickness, can only be adjusted by varying the depth, so that it is rather difficult to get the ratios of EA and EI correct at the same time. However, it has been found that the bending moment distribution is usually satisfactorily reproduced if the depths of the model members are made proportional to the cube root of the inertias of the corresponding full-size members. In certain cases it is possible to construct flanged models so that the members may then be correctly represented.

CHAPTER II

Essential Optics

This chapter is to be devoted to a description of those optical phenomena which are of fundamental importance in photo-elasticity, but which are not as a rule familiar to engineers. We may first of all consider the nature of light, as it is very necessary to have some appreciation of this in order to understand the phenomena of polarization and double refraction which we will have to study in some detail.

The Nature of Light

The first systematic theory of light was elaborated by Newton and others and was based on the assumption that a light source emits minute material particles in all directions. This was termed the corpuscular theory of light and, while it satisfactorily explained a number of observed phenomena, there were effects which were quite inconsistent with the theory and led to its being abandoned in favour of the *ether-wave theory*. In this, a light wave is assumed to be a *transverse* vibration in the ether, that is, the particles of the *ether*, which is the medium through which the wave is transmitted, vibrate at right angles to the direction of propagation. To clarify this statement, we may consider the waves which spread across the surface of still water when a disturbance is originated at a point, say by dropping a stone into the water; the particles on the surface move up and down, but not at all in the direction in which the waves are travelling. Energy is thus transmitted along the surface of the water although the water particles do not move in the direction of propagation. Light is assumed to be transmitted in a similar fashion through a hypothetical medium called the ether.

We may represent such a wave by a sinusoidal wave train (fig. 14), as the motion of any particular ether particle is periodic. Harmonic vibrations of this type are so familiar to engineers that it is hardly necessary to define the elements of the curve. In the case of visible light the wavelength (λ) varies between 3900×10^{-8} cm and 7700×10^{-8} cm. The shorter wavelength corresponds to violet light and the longer to deep red light; between these limits we have the wavelengths corresponding to the various colours of the spectrum. It is customary to express wavelengths of visible light in *Angström units*, equal to 10^{-8} cm, so that the wavelengths are all four-figure numbers.

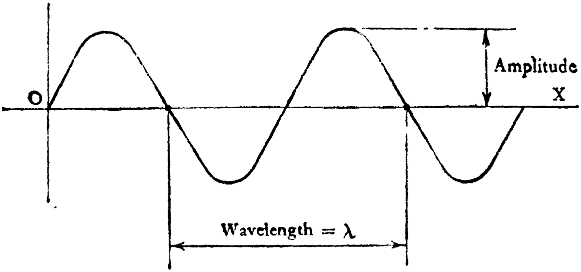

Fig. 14.—Sinusoidal wave train

As is well known, white light consists of a mixture of lights of different wavelengths. Light which contains waves of only one wavelength is *monochromatic*, a self-explanatory term. Strictly monochromatic light is unobtainable, as all known light-sources emit waves of more than one wavelength, but approximately monochromatic light may be obtained, for example, from a sodium-vapour lamp.

The velocity of light is 3×10^{10} cm/sec and the periodic time—the time for one complete vibration of an ether particle — is $\tau = \lambda/v$ seconds, where v is the velocity. $1/\tau$ is the *frequency* of the vibration, i.e. the number of vibrations per second.

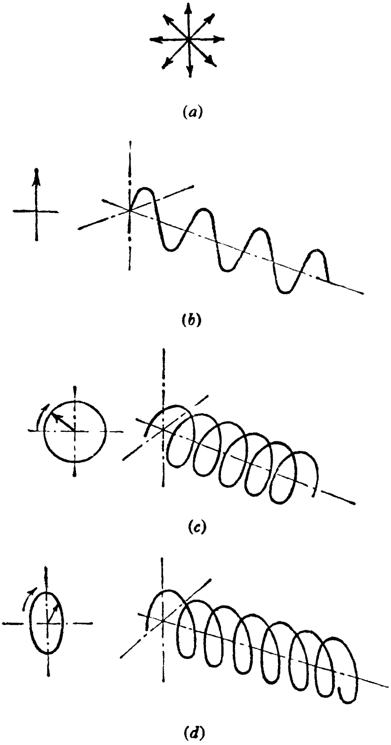

Fig. 15.—Polarized light waves and their conventional representation

(a) unpolarized wave, (b) plane polarized wave, (c) right-hand circularly polarized wave, (d) right-hand elliptically polarized wave.

The magnitude and direction of the displacement of an ether particle from its original position can be represented at any instant by a vector, called the *light vector*. If the plane containing the light vector and the direction of propagation remains fixed from instant to instant, the light is said to be *plane polarized*. The inclination of the plane of polarization relative to an arbitrary reference plane is termed the *azimuth of polarization*. Ordinary light, say from an electric lamp, is not polarized but may be regarded as consisting of polarized lights of all possible azimuths.

If the light vector at any point remains of constant amplitude while continually altering its azimuth in such a way that its extremity traces out a circular path, the light wave is said to be *circularly polarized.* The light wave travels forward in a circular helical path, which is either right- or left-handed, according to the direction of propagation and direction of rotation of the light vector. If the extremity of the light vector traces out an elliptical path the light is *elliptically polarized.*

The various types of polarized waves and their symbolic representations are shown in fig. 15.

All the optical phenomena encountered in photo-elasticity may be satisfactorily explained in terms of the above conception of light and the theory is sufficiently accurate for present purposes. It has been found, however, that light is electromagnetic in nature and a more accurate theory has been built up by Maxwell and others, explaining the various phenomena in terms of rapidly rising and falling electric and magnetic fields along the line of propagation of the light wave. This theory does not require the existence of the ether and has considerable experimental support. In addition, all kinds of radiation from the extremely short wavelength γ-rays to the long wavelength radio waves appear to be of the same fundamental nature as light, the essential difference being the wavelength of the radiation. Even this theory is not final and still newer theories concerning the nature of light are formulated in the quantum mechanics.

The Propagation of Light through Isotropic Media

Optically isotropic substances are those which have the property of transmitting light waves with equal velocity in all directions. Examples include air, water, strain-free glass, and certain plastics. If a light source is surrounded by any of these media, light waves will be transmitted in such a way that after a given time-interval the locus of the farthest points reached by the waves will be a sphere. Such a sphere is termed a *wave surface*, and a tangent plane to the wave surface at a point is the *wavefront* at that point. Any limited portion of the spherical wave surface, provided it is at a considerable distance from the light source, is sensibly plane and we thus have a *plane wave*.

A line along which light energy flows from the source to some point on the wavefront is a *ray*. Light being propagated in straight lines, the rays are straight and, in the case under discussion, are radii of the spherical wave surface. The ray thus coincides with the normal to the wavefront (the *wave normal*) at any point on the wave surface.

We may now consider the phenomena of reflection and refraction at the interface between two isotropic media in terms of the wave theory. Part of the incident light will be reflected and part refracted through the second medium.

In fig. 16 let OB represent the trace of the interface of the two media on the plane of the paper; OA represents the trace of the incident plane wavefront and N_i is its wave normal (assumed to lie in the plane of the paper). After a certain time interval, t, point A on the wavefront has reached B, i.e. the wave travels distance AB in time t, in the first medium. Thus, after time t, the reflected wavefront will be in position BC, where OC is perpendicular to BC and equal to AB. N_R is the normal to the reflected wavefront, and it is clear that the angle of incidence, i, is equal to angle of reflection, R. If light is transmitted through the second medium at a lower velocity than through the first, the refracted wavefront BD will have travelled a shorter distance in time t than the reflected wave; thus OD is less than OC. It is easily seen that the ratio

$$\frac{\sin i}{\sin r} = \frac{\text{Velocity of light in first medium}}{\text{Velocity of light in second medium}} = \mu,$$

where μ is the *refractive index* for the two media. It will be noted that in passing from one medium to another in which the velocity of light is less than in the first, the wave normal is deflected towards the normal to the interface. It should also be noted that the value of μ depends on the wavelength of the light transmitted; this, of course, gives rise to the well-known phenomenon of the dispersion of white light by a prism.

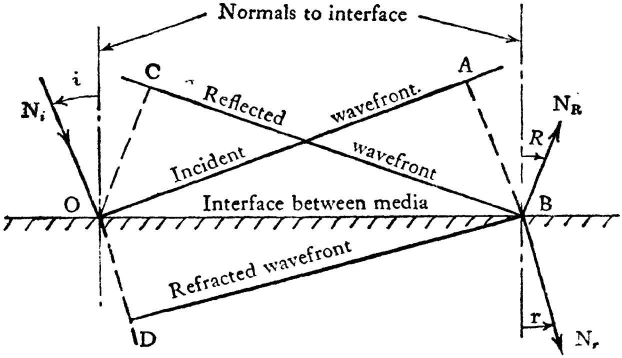

Fig. 16.—Reflection and refraction at the interface between two media

The Propagation of Light in Anisotropic Media: Double Refraction

Anisotropic substances are those which have the property of transmitting light with a velocity which depends on the direction of propagation. All crystals and also strained glass and plastics have this property. If a light source were placed at the centre of a crystal block it would be found that two distinct sets of waves would be radiating outwards from it. The wave surface relative to these two sets of waves may be of a rather complicated two-sheeted form, but the case of particular importance in photo-elastic theory is that in which the wave surface consists of a sphere and an ellipsoid.

The sphere may lie outside or inside the ellipsoid as indicated in fig. 17, which shows typical sections through the wave surfaces; in the first case the crystal is said to be *positive*, and in the second *negative*. The common axis of the sphere and ellipse is termed the *optic axis* of the crystal, which in this case is *uniaxial*, having but one optic axis.

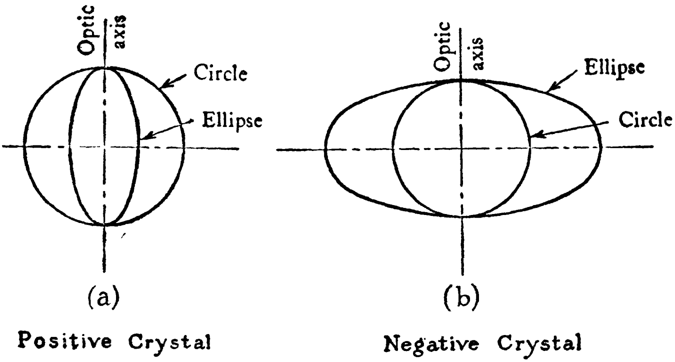

Fig. 17.—Wave surface on a uniaxial crystal

We may now consider the propagation of light through a block of calcite, which is a typical negative uniaxial crystal. We shall assume that the optic axis of the crystal lies in the plane of the paper and at an angle ϕ to the normal to the crystal face, as in fig. 18. The incident wave normal makes an angle θ with this direction. As explained above, any light disturbance originating at point O will be transmitted through the crystal as a two-sheeted wave surface, the trace of which on the plane of the paper is a circle and an ellipse. The refracted wave normal is deflected towards the normal to the interface and corresponding to it are two wavefronts. The traces of these at a particular instant are shown in the figure, being tangents to the circle and ellipse. The former wavefront corresponds to the case of an isotropic medium in that the wave surface is a sphere and is thus called the *ordinary wavefront*; the ray relative to this wavefront coincides with the wave normal. The other wavefront is called the *extraordinary wavefront*, and in this case the ray does not coincide with the wave normal. Thus, corresponding to a single incident ray there are two emergent rays; corresponding to a single incident wavefront there are two

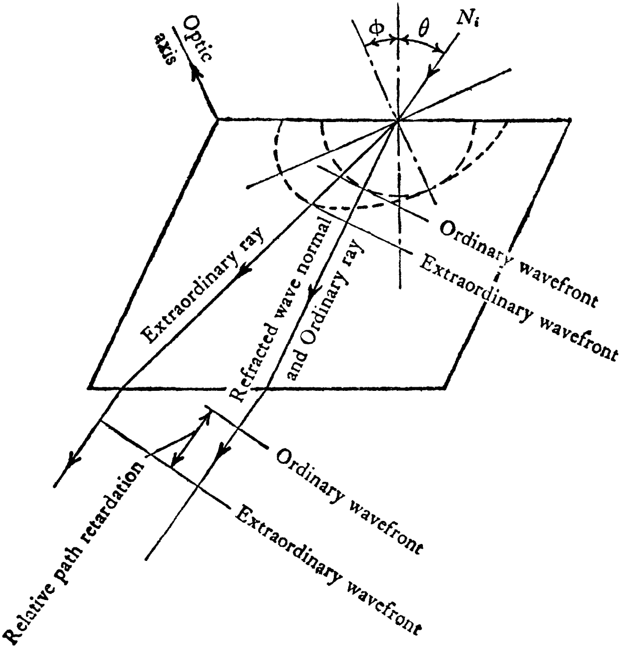

Fig. 18.—Double refraction in a negative uniaxial crystal

emergent wavefronts, one of which has travelled through the crystal faster than the other. This gives rise to the peculiar effect, known as *double refraction*, whereby two images of the same object are observed on looking through a piece of calcite. If, however, the refracted wave normal should coincide with the optic axis OX of the crystal, only one image would be observed, as the ordinary and extraordinary rays and wavefronts coincide. If the refracted wave normal lies along OY, again only one image will be observed as the two rays coincide, but in this case there are two wavefronts.

After the two wavefronts emerge from the plate they will travel (through air) with equal velocities so that the distance between them (which is termed the *relative path retardation* or simply the *relative retardation*) will remain constant after the wavefronts leave the plate. The relative retardation will evidently depend on the thickness of the crystal plate and on the relative velocities of light corresponding to the two wavefronts, or, in other words, on the difference between the relevant refractive indices. Thus,

$$\text{Relative retardation} = R = (\mu_0 - \mu_e)d,$$

where μ_0 = refractive index for ordinary wave in crystal (passing from air to calcite),

μ_e = refractive index for extraordinary wave in crystal.

We may notice one further important phenomenon in connexion with the transmission of light through the calcite plate, namely, that the ordinary and extraordinary waves are plane polarized in directions at right angles to one another.

In the above discussion, calcite has been quoted merely as a typical example of a uniaxial crystal—there are of course many others. Bi-axial crystals, as the name implies, have two optic axes and a more complicated wave surface; they behave in a somewhat similar manner to the uniaxial crystals. Mica is a biaxial crystal and, as will be seen later, is used for certain purposes in photo-elastic apparatus.

Interference

The elementary principles of optical interference may be understood by considering a simplified account of the optical system shown in fig. 19. This consists of four parallel mirrors set at the corners of a rectangle and inclined at 45° to the sides of the rectangle. Light waves from the source L (which we will assume to be monochromatic) strikes the half-silvered glass mirror M_1; the light will be partly reflected and partly refracted through the plate. The reflected beam is again reflected from the full silvered mirror M_3 and transmitted through the half-silvered plate M_4. Here it is reunited with the part of the beam which was transmitted through M_1 and reflected at M_2 and M_4. The reunited beam finally falls on the screen S as a bright spot of light.

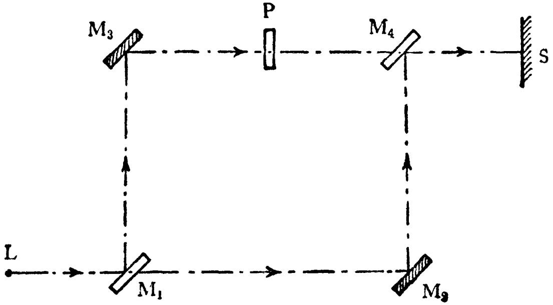

Fig. 19.—Optical interference

We have assumed that the mirrors are so adjusted that the two components of the light beam travel precisely equal distances between the point at which the original beam was split up, and the point at which the two components are reunited. This being the case, there will obviously be no difference in path length between the reuniting components, the light waves in which will therefore be exactly in step or *in phase*, and will combine to form a beam, the intensity of which is reduced relative to that of the original beam only by losses due to reflection and refraction at the mirrors.

If now we place a plate, P, in the path of one of the component beams, the effective path length of that component will be increased due to the lower velocity of light through the plate, and there will be some difference in path length between the light waves at the point where the two components reunite. This is indicated in fig. 20, where the wave which has passed through P is shown to be retarded by an amount R relative to the other wave.

The light wave which results from the combination of the two components, which are now out of phase, is shown in fig. 20 and is obviously of smaller amplitude than the wave which would result from the combination of the two components when in phase. There is therefore a reduction of intensity due to *interference* of the two waves and, if the relative retardation is exactly half a wavelength, the two components will exactly oppose each other. The troughs of one wave will coincide with the crests of the other; they will thus cancel each other out, and no light will reach the screen.

If we arrange the apparatus so that the retardation due to P can be varied at will, we shall find that the light beam thrown on the screen will be extinguished at regular intervals, whenever the waves cancel each other out.

The apparatus shown in fig. 19 is not really practicable but it serves to explain the nature of interference. Interference can only be observed between two light beams which have been produced by splitting a single beam from a source, and which have been reunited after traversing paths of slightly different lengths. Interference effects between light waves from two different light sources—or even from two parts of the same source—are never observed, as in this case the relative phases of the uniting waves would be entirely random and only a mean effect would be observed. If two light sources could be found to emit continuously, absolutely homogeneous monochromatic light, then of course these waves could be made to interfere. But such conditions are never found—indeed, each point of a flame or incandescent body behaves as an independent light source, and the frequency of the waves emitted from it varies continually.

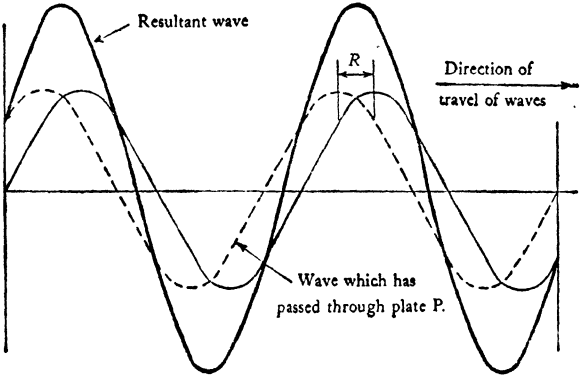
Resultant wave
R
Direction of travel of waves
Wave which has passed through plate P.

Fig. 20.—The addition of two periodic waves

Beams of polarized light can only be made to interfere when their azimuths of polarization are coincident. Thus, although light emerging from a crystal plate consists generally of two plane-polarized components having a certain relative path retardation, interference phenomena will not be observed as the two components are polarized in planes at right angles to one another; but if components of the emergent plane-polarized waves are brought to a common plane by suitable means, interference effects are now observed.

The Plane Polariscope

As already stated, ordinary light may be regarded as a mixture of polarized lights of every possible azimuth. It is possible to isolate plane-polarized light of any desired azimuth by passing ordinary light through a suitable filter. The various types of polarizing filters will be described in Chapter V and in the meantime their existence may be taken for granted.

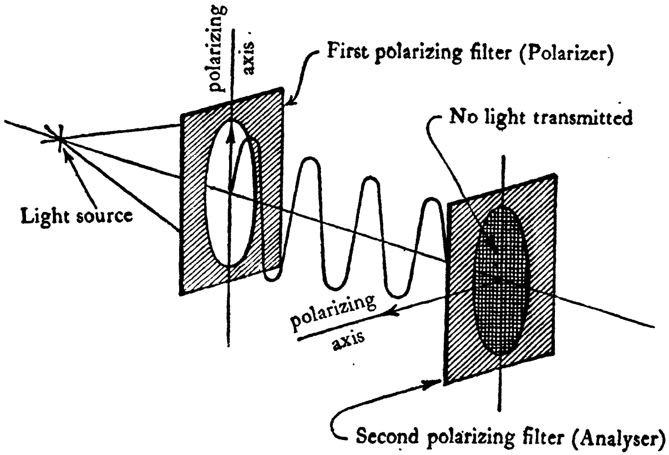
polarizing axis
First polarizing filter (Polarizer)
No light transmitted
Light source
polarizing axis
Second polarizing filter (Analyser)

Fig. 21.—The plane polariscope

A *plane polariscope* is a device which consists essentially of two polarizing filters set as shown in fig. 21. Light from the source is polarized in, say, the vertical plane by the first filter, which is termed the *polarizer*. The second filter, *the analyser*, is generally set with its polarizing axis at right angles to that of the polarizer, so that none of the light polarized in the vertical plane by the first filter will pass through the second and on looking through the analyser in the direction of the light source no light beam will be seen. Two filters set thus are said to be "crossed"; this is the usual setting of the polarizing filters for photo-elastic observations, but occasionally the axes of the polarizer and analyser are set parallel, and in this case, all the light from the polarizer is transmitted and the field appears light.

Uniform Crystal Plate in the Plane Polariscope

We may now discuss the phenomena which are observed when a crystal plate of uniform thickness is placed between the polarizer and analyser of the simple polariscope of fig. 21. We shall assume first that the light source is monochromatic and that the action of the crystal is as discussed in a previous section (see p. 25), that is, the incident plane-polarized wave is broken up into two components and there emerge from the crystal two waves polarized in directions at right angles to one another, one lagging slightly behind the other as indicated in fig. 22. In general, the directions of polarization of the emergent waves from the crystal do not coincide with the polarizing axis of the analyser and the components of these waves parallel to this direction are transmitted. Thus, beyond the analyser we have two waves polarized in the same plane and with a certain relative retardation between them. We have here the necessary conditions for interference, and we may determine the conditions for extinction of the transmitted beam in the following manner: let the light wave entering the crystal plate be represented by

$$y = a \sin \phi.$$

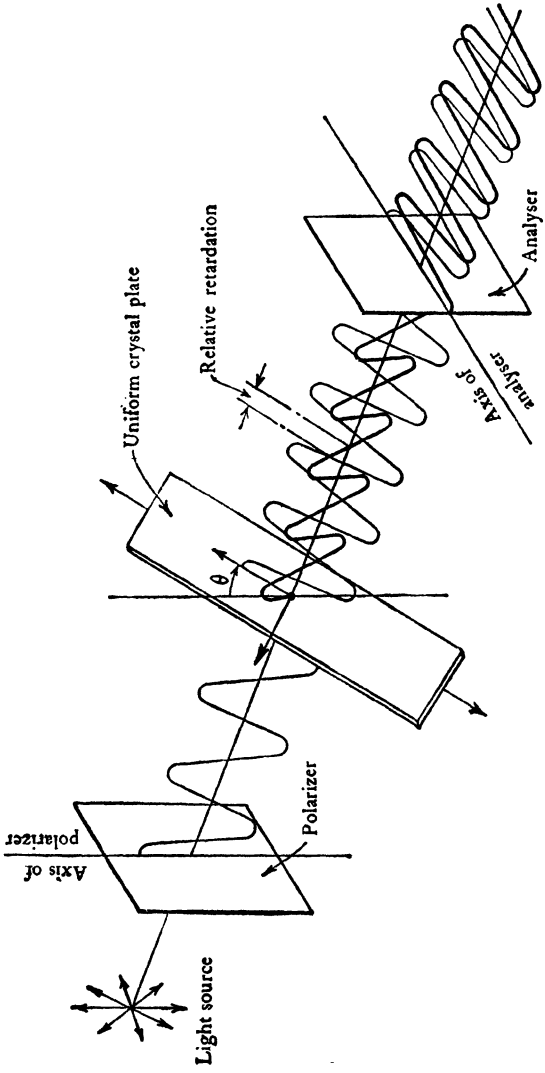

Fig. 22.—Uniform crystal plate in the plane polariscope

If the direction of polarization of one of the emergent waves is inclined at angle θ to the direction of polarization of the incident wave, as indicated in fig. 22, then the latter is broken up into two components on entering the plate, viz.

$$u = a \sin\phi \cos\theta,$$
$$v = a \sin\phi \sin\theta.$$

After transmission through the crystal these waves will be of the form

$$u = ka \sin(\phi' + \epsilon) \cos\theta,$$
$$v = ka \sin\phi' \sin\theta,$$

where k is a factor covering reduction of amplitude due to absorption in the crystal and

$$\epsilon = \frac{2\pi d}{\lambda} (\mu_1 - \mu_2)$$

is the relative phase retardation corresponding to a relative path retardation of $(\mu_1 - \mu_2)d$; μ_1 and μ_2 are the refractive indices of the ordinary and extraordinary waves in the crystal for light of wavelength λ, and d is the thickness of the crystal plate.

The analyser transmits components of u and v parallel to its polarizing axis; these are $u \sin\theta$ and $v \cos\theta$. These transmitted components then combine to give the observed wave, which will be of the form

$$\begin{aligned} v\cos\theta - u\sin\theta &= k'a \sin\phi' \sin\theta \cos\theta \\ &\qquad - k'a \sin(\phi + \epsilon) \cos\theta \sin\theta', \\ &= \tfrac{1}{2} k'a \sin 2\theta \{\sin\phi' - \sin(\phi' + \epsilon)\}, \\ &= k'a \sin 2\theta \cos(\phi' + \epsilon/2) \sin\epsilon/2. \end{aligned}$$

Examination of this last equation shows that the amplitude of the resultant vibration is zero whenever one of the following conditions is satisfied:

(*a*) When θ is equal to 0 or $\pi/2$, in other words, *when the direction of polarization of the incident beam coincides with the polarizing axes in the crystal.*

(*b*) When ϵ is equal to an even multiple of π, as will be the case *when the path retardation is an integral number of wavelengths.*

The resultant is at its maximum when θ is 45° and when the relative path retardation is an odd number of half wavelengths (or, otherwise stated, when ϵ is an odd multiple of π).

From the foregoing it will be clear that if we place a crystal plate between the crossed polarizer and analyser of a polariscope, and rotate the polarizer and analyser together, we will find two positions at which the light will be extinguished. As the filters are rotated from these positions in either direction the intensity of the transmitted light will gradually increase to a maximum at 45°, then decrease again to zero as the angle of rotation reaches 90° from the original setting.

If we examine in the polariscope a wedge of crystal plate, which in effect is a plate whose thickness varies from zero upwards, we will find that it is crossed by a series of alternate light and dark bands as indicated in fig. 23. Equally spaced dark bands will be seen along the wedge where the thickness is such that the retardation is an integral number of wavelengths of the light transmitted. We are assuming, of course, that the optic axis in the plate is suitably oriented and that neither of the polarizing axes coincides with the direction of polarization of the light from the polarizer.

If monochromatic light is replaced by white light, then any light wave whose wavelength happens to be equal to (or a submultiple of) the relative retardation will be extinguished by interference; light waves whose wavelengths approach this critical value will be partially extinguished. Thus the balance of the colour making up the white light will be upset, and the light transmitted by the analyser will be the complementary colour of the light extinguished. For example, if the retardation is such that wavelengths corresponding to red light are extinguished, then the light transmitted will be blue.

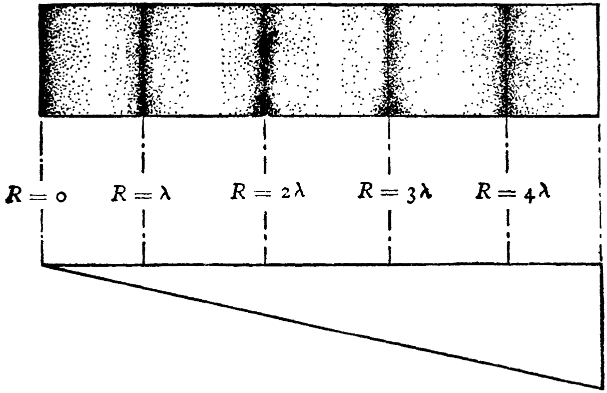

Fig. 23.—Appearance of a crystal wedge in the polariscope in monochromatic light

It is obvious that if the relative retardation is increased progressively from zero all the colours of the spectrum will be extinguished in turn, beginning with the shorter wavelengths at the violet end of the spectrum. Thus, on examining the crystal wedge of fig. 23 in the polariscope in white light, we would find that, instead of simply being crossed by a number of dark bands, it would be crossed by coloured bands, the colours varying along the length of the wedge according to a definite sequence. We shall consider this sequence in detail in the next chapter.

The Circular Polariscope

As we have seen, a plane-polarized wave on passing through a crystal plate is split into two components, plane-polarized in directions at right angles to one another. In general, these two components combine to give an elliptically polarized wave, but if they have a relative phase retardation of $\pi/2$, corresponding to a relative path retardation of quarter of a wavelength, they combine to give a circularly polarized wave. A crystal plate which converts an incident plane-polarized wave into a circularly polarized wave is therefore referred to as a *quarter-wave plate.*

A polariscope which has two quarter-wave plates placed between the polarizer and analyser in the manner indicated in fig. 24 is termed a *circular polariscope*, the light entering the specimen under examination being circularly polarized by the first quarter-wave plate. The second quarter-wave plate is set with its polarizing axes at right angles to those of the first, that is the " fast " axis of the first plate lines up with the " slow " axis of the second. The second plate therefore exactly undoes the effect of the first, and if there is no specimen in the polariscope, the light emerging from the second plate is plane-polarized in the same direction as the light from the polarizer.

If the circularly polarized light from the first quarter-wave plate passes through a crystal specimen, the emergent light may once again be resolved into two components plane-polarized at right angles to one another in directions parallel to the polarizing axes of the specimen. The relative retardation between these two components will be the retardation due to the crystal specimen plus quarter of a wavelength, due to the first quarter-wave plate, so that, in general, the emergent light is elliptically polarized.

After passing through the second quarter-wave plate,

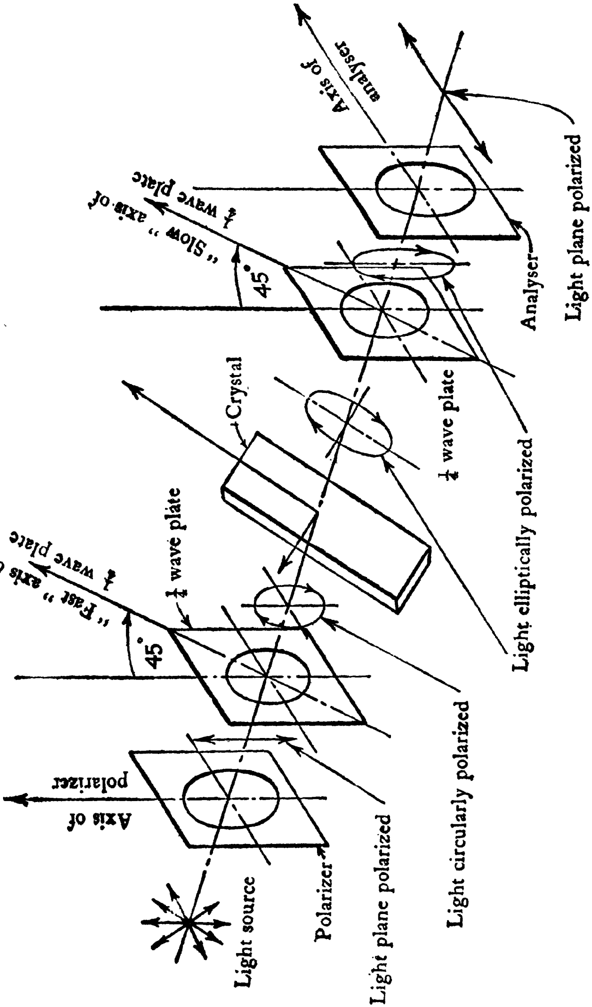

Fig. 24.—Crossed circular polariscope

the light is still elliptically polarized, but the relative retardation between the two rectangular components is quarter of a wavelength less than before. This wave, which may of course be regarded as two waves plane-polarized in directions at right angles to one another with a certain relative retardation, is analysed in exactly the same way as in the plane polariscope and the appearance of the specimen is also the same *except that its orientation does not affect the intensity of the light transmitted.* As will be seen in the next chapter this is of great practical importance in photo-elastic work.

CHAPTER III

Stressed Transparent Materials in the Polariscope

Certain transparent materials such as glass, celluloid, Bakelite, and other plastics are optically isotropic when unstrained, but when subjected to stress, they become anisotropic and exhibit in the polariscope certain features characteristic of natural crystals. On this phenomenon is based the whole science of photo-elasticity.

The Photo-elastic Effect

If a plate of one of the above-mentioned materials is subjected to stress, it is found to behave in the polariscope like a uniaxial crystal, the optic axis of which is parallel to the surface of the plate. In general, a plane-polarized wave entering the plate is split into two components plane-polarized in the directions of the principal stresses at the point of entry. As in the case of a natural crystal, these components are not transmitted with the same velocities, so that when they emerge from the plate they have a certain relative path retardation, the magnitude of which, at any point in a given plate, *is directly proportional to the difference of the principal stresses.* Also, the retardation is proportional to the *thickness* of the plate, so that we can write:

$$\text{Relative retardation} = R = C(P - Q)d,$$

where P and Q are the principal stresses, d the thickness of the plate, and C a constant known as the *stress-optical coefficient.* Examination of the equation shows that C must have the dimensions of the reciprocal of stress. The unit adopted for C is the *Brewster*, which is equal to 10^{-13} sq. cm/dyne. This apparently unwieldy unit is chosen since it gives the retardation in Ångström units when $(P - Q)$ is in bars (approximately, kilogrammes/sq. cm) and d is in millimetres. It is very easy to convert the formula for use with inch-pound units; thus

$$R = 1{\cdot}752C(P - Q)d,$$

where R is in Ångström units, C in Brewsters, $(P - Q)$ in lb/sq. in, d in inches.

If the retardation is equal to one wavelength or multiple of a wavelength of the light used, the components transmitted by the analyser cancel each other out and the transmitted light is extinguished.

Suppose now that we place a strip of Bakelite between the polarizer and analyser, and subject it to a gradually increasing tensile stress. We will assume first that the light source of the polariscope is monochromatic. When the specimen is unstressed the material is isotropic and the field of the polariscope remains dark. If the stress is now gradually increased, the specimen appears bright, the brightness reaching a maximum when the retardation is

TABLE I

Colour Sequence

Colour sequence shown by a Bakelite tensile specimen 0·26 in. thick, in crossed polariscope. If viewed in a parallel polariscope the colours observed and extinguished are reversed.

	Stress (lb/in²)	Approximate Relative Retardation A.U.	Colour Observed	Colours Extinguished	Remarks
First Order Colours	22	500	Grey		Retardation is less than wavelength of visible light.
	88	2,000	White		
	176	4,000	Lemon-yellow	Violet	Violet is extinguished first as it has the shortest wavelength.
	198	4,500	Orange	Blue	
	220	5,000	Deep red	Green	Retardation is equal to wavelength of spectrum colours in turn.
	260	5,900	Purple	Yellow	The colour between red and blue is termed the " tint of passage ".
	286	6,500	Deep blue	Orange	
	308	7,000	Green	Red	
Second Order	352	8,000	Pale yellow	Deep red (1st), Deep violet (2nd)	The second extinction of violet (4000 A.U.) almost coincides with the first extinction of extreme red (7700 A.U.), so that the orange and red tints are paler than those of the 1st order.
	396	9,000	Orange	Glue	
	440	10,000	Red	Green	
	520	11,800	Purple	Yellow (2nd), Violet (3rd)	Paler than tint of passage of 1st order.
	573	13,000	Emerald green	Orange-red (2nd), Indigo blue (3rd)	

Third Order	616	14,000	Pale yellow	Red (2nd), Blue (3rd)	As the retardation is increased the overlapping of the extinguished colours becomes more and more pronounced; the colour sequence above the third order becomes a repetition of white, pink and green, getting paler each time until about the 7th order when the transmitted light is practically white.
	682	15,500	Pink	Deep red (2nd), Green (3rd), Deep violet (4th)	
	748	17,000	Pale green	Yellow (3rd), Indigo (4th)	
	836	19,000	White	Orange (3rd), Blue (4th)	
Fourth Order	925	21,000	Pale pink	Red (3rd), Green (4th), Violet (5th)	
	1056	24,000	Pale green	Deep red (3rd), Yellow (4th), Blue (5th), Violet (6th)	
	1100	25,000	White	Orange (4th), Green (5th), Indigo (6th)	

half a wavelength. Thereafter the intensity of the transmitted light is once more diminished. As the stress is still further increased this cycle of events is repeated—the field appearing alternately light and dark as the transmitted beam is extinguished, whenever the retardation is an integral number of wavelengths.

If white light is used in the experiment just described, the specimen appears coloured, the colours going through the sequence indicated in Table I. When a small stress is applied to the specimen the retardation is less than the wavelength of the shortest visible light waves and all the colours of the spectrum are transmitted through the analyser. The specimen then appears white, but as the retardation is increased, it becomes equal to the wavelength of violet light which is therefore extinguished, and the transmitted light is of a pale lemon-yellow colour. As the stress, and thus the retardation, is further increased, each spectrum colour is extinguished in turn in the order indigo, blue, green, yellow, orange, red. The model thus shows the colour sequence, yellow, orange, red, indigo, blue, green, i.e. the complementary colour of that extinguished by interference.

As the retardation is still further increased, it becomes equal to twice the wavelength of each spectrum colour in turn; these are extinguished a second time, and the colour sequence is repeated. The colours, however, are not quite the same as those of the first sequence (or *order*) since, for example, the first extinction of deep red of wavelength 7600 A.U. takes place at the same time as the second extinction of violet of wavelength 3800 A.U. This overlapping of the colours extinguished makes the colours of the second and subsequent orders appreciably paler than those of the first. When the colours are extinguished for the fourth, fifth and sixth times the colour sequence has degenerated into an alternation between rose-pink and pale green tints. When the retardation is greater than about six wavelengths of the spectrum colours, the overlapping is so great that all the colours are transmitted and the field appears white.

Monochromatic Fringe Patterns

In a field of non-uniform stress $(P - Q)$, and thus the relative path retardation, varies from point to point. Wherever $(P - Q)$ has the same value, the retardation is the same; thus on examining a model in monochromatic light we would find that the loci of points where the retardation is equal to an integral number of wavelengths of the light used, would be defined by black lines (remembering that the light transmitted through the model is extinguished when the retardation is a multiple of one wavelength). The dark line corresponding to a retardation of one wavelength is termed the *first order fringe*; the line corresponding to two wavelengths' retardation is the *second order fringe*, and so on.

A simple example is shown in fig. 25 which shows the fringe photograph for a beam under pure bending. In this case the principal stress at right angles to the axis of the beam is zero and the other principal stress, parallel to the axis, is given by

$$P = \frac{My}{I},$$

where M is the bending moment, y the distance of the point from the neutral axis, and I is the moment of inertia of the section. At any point, $(P - Q)$ and thus the relative retardation is proportional to the distance of the point from the neutral axis. The fringes are thus parallel lines to the neutral axis, which also appears as a black line, since here the retardation is zero.

A more complicated fringe pattern is shown in fig. 26, which shows the appearance of an L-shaped model subjected to a tensile load through pin connexions at the ends of the legs of the L.

The fringe orders may be identified by observing the model as the load is applied or by counting from some point where the fringe order is known to be zero. For example, in the model of fig. 26 it is known that the sharp corner on the outer edge of the model is stress free, and therefore the retardation there is zero; such a point is known as an *isotropic point* (see under). Nearest to this point is the first order fringe, next the second order, and so on, until all the fringe orders have been determined. Fringe orders may also be conveniently counted from isotropic points in the interior of the model.

The Growth of the Fringe Pattern

Figures 27 (*a*), (*b*), (*c*) and (*d*) show the changing appearance of the fringe pattern in a beam specimen carrying a single load spread over a short length of its upper edge. The fringes naturally appear first at the points of maximum $(P - Q)$ and gradually spread to the lower stressed regions as the load is increased. Thus in fig. 27 (*a*), a 1st order fringe appears as a curved line intersecting the lower edge of the beam at two points; the maximum fringe order on the lower edge is about 1·7. In the second photograph the 3rd order fringe has just appeared at the lower edge while the 1st and 2nd order fringes have moved in towards the centre; the zero order fringe appears as a point. Figs. (*c*) and (*d*) show still later stages in the loading; the maximum fringe orders on the lower edges are respectively 4·8 and 7·3 in these photographs.

From the foregoing, it will be clear how the fringe orders may be found by observing the model as it is loaded.

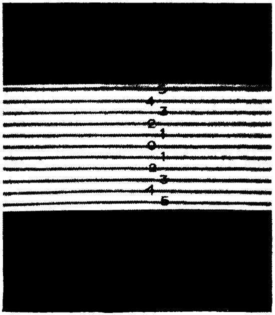

Fig. 25.—Fringe pattern for beam under pure bending.

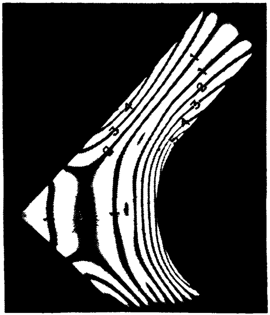

Fig. 26.—Fringe pattern for L model.

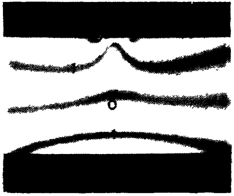

Fig. 27*a*

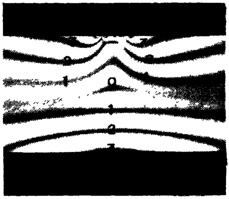

Fig. 27*b*

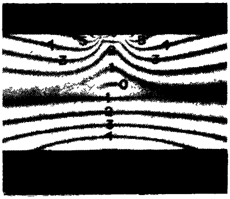

Fig. 27*c*

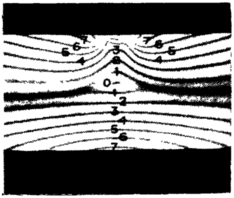

Fig. 27*d*

Fig. 27.—Development of fringe pattern in a beam specimen. Loads: (*a*) 17 lb., (*b*) 30 lb., (*c*) 47 lb., (*d*) 72 lb.

Isotropic Points

At any point in a model where $(P - Q)$ is zero the retardation is zero, and that point appears in the fringe pattern as a black dot; such a point is known as an *isotropic point.* In the special case where $P = Q = 0$, it is called a *singular point.* In some models, a point at which $(P - Q)$ reaches a maximum value may also appear as a black dot for certain values of the applied load, but in practice these are not likely to be confused with isotropic points which remain unaltered irrespective of the value of the applied loads.

The model of fig. 26 shows three black points near the curved edge; the central point is an isotropic point, where $P = Q \neq 0$ and the other points are singular points at which $P = Q = 0$. The black point in the fringe pattern of fig. 27 is also a singular point.

The Information given by the Fringe Pattern

Every fringe is a line along which $(P - Q)$ has a constant value, that is, the fringes are contours of $(P - Q)$. Since the maximum shearing stress at any point is equal to $\frac{1}{2}(P - Q)$, the fringe pattern gives the maximum shearing stress at every point in the model, provided that the stress equivalent of the fringes is known. Also, at a free boundary the principal stresses are respectively parallel and normal to the boundary, and the latter is equal to zero. Therefore, the boundary stress at any point on a free edge is equal to $(P - Q)$, and can be determined directly from the fringe photograph.

It will be seen from the foregoing that the fringe pattern gives an immediate view of the magnitude of the stresses at every point in the model and shows up critical points and sections. In many practical cases either the maximum shearing stresses or the edge stresses are critical, and the fringe photograph effectively solves the problem.

The directions of the principal stresses can be determined by photo-elastic observations and, as we shall see in a later chapter, there are several methods of obtaining the separate principal stresses at any point from the photo-elastic data (i.e. the fringe pattern and isoclinic lines).

Calibration of the Fringe Pattern

In carrying out a photo-elastic analysis it is evidently necessary to establish the link between the relative retardation, or fringe order, and the principal stress difference in appropriate units. In some cases it is possible to do this simply by calculating the stress at some point in the model where the fringe order is known; for example, in the model of fig. 26 it is possible to calculate the edge stress at a point where one of the fringes intersects the boundary of the parallel part of the model. Thus, we may find that the stress at the point on the outer edge where the third order fringe intersects it is 468 lb/in^2. The principal stress difference corresponding to the first order fringe is therefore $\frac{468}{3} = 156$ lb/in^2; this is the *model fringe value.*

It may not, however, be convenient to calculate the stress at any point in the model, and it will then be necessary to determine the stress equivalent of the retardation by a subsidiary test on a simple specimen cut from the same sheet of material as the model and loaded for the same length of time (in order to avoid errors due to creep in the material). The calibration specimen may be subjected to tension, compression or pure bending.

If a test piece of rectangular cross-section, width b and thickness t, is subjected to an axial tensile or compressive load, W, which produces a retardation of $n\lambda$, where λ is the wavelength of the light, then the stress in the specimen is

W/bt, and the stress equivalent of the first order fringe is W/nbt.

In comparing different materials it is often convenient to state this value for a plate of standard thickness, usually one inch, so that this *unit fringe value*, F, is equal to $W/nbt \times t/1$, i.e. $F = W/nb$. The material unit fringe value can therefore be determined without actually measuring the thickness of the test specimen. The wavelength of the light used in the calibration experiment must of course always be stated.

The stress-optical sensitivity may also be defined by the *stress-optical coefficient* (see p. 41); this constant is independent of the wavelength of the light used, and can be determined in a similar manner. Thus

$$n\lambda = 1{\cdot}752C \times \frac{W}{bt} \times t,$$

and

$$C = \frac{bn\lambda}{1{\cdot}752W}.$$

It is obviously a simple matter to change from unit fringe value to stress-optical coefficient as

$$C = \frac{\lambda}{1{\cdot}752F}.$$

As an alternative to a tensile or compressive test, the fringe value or stress-optical coefficient may be determined by subjecting a beam specimen to pure bending and calculating the stress at the distance from the neutral axis corresponding to any convenient fringe (see fig. 25). The well-known "four point" loading arrangement shown in fig. 28 provides a suitable means of applying pure bending to a specimen, but care must be taken to avoid axial forces on the beam. For this reason, the loads should be applied through pins passing through the centre line of the specimen and the links of the loading gear should be made fairly long. This method is rather less accurate than the tensile test, but quite satisfactory for most purposes provided that the precautions mentioned are observed.

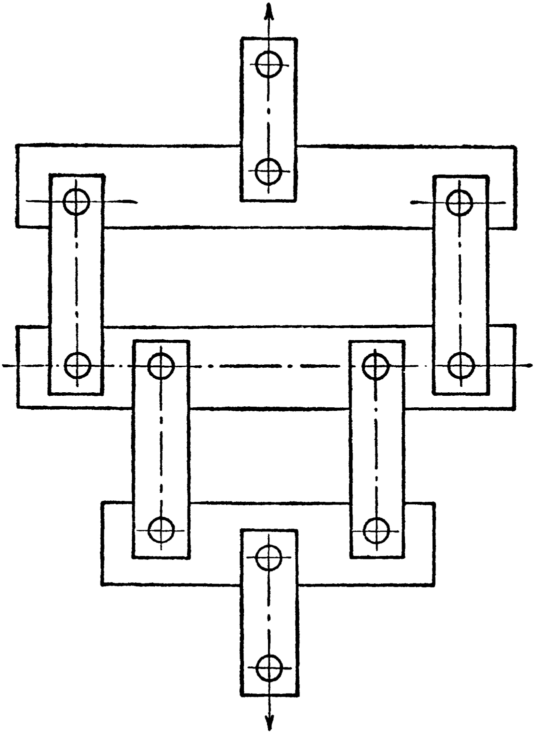

Fig. 28.—" Four point " loading gear for subjecting a specimen to pure bending

Stress Patterns in White Light

As we have already seen, a tensile specimen subjected to an increasing load will, when examined in white light, exhibit a series of colours; for each value of $(P - Q)$

there is a corresponding colour, and in a field of non-uniform stress the same colour will appear wherever $(P - Q)$ is the same. Contours of $(P - Q)$ will therefore appear as colour bands and for this reason they are called *isochromatic lines*.

There is a fairly sharp change in colour from a red to a blue tint when the relative retardation is about 5890 A.U. or an integral multiple of that value. The *tint of passage* associated with this change becomes, in a field of non-uniform stress, a mere line between contrasting colours, and is thus accurately located. For quantitative purposes the tint of passage isochromatics serve the same purpose as the monochromatic fringes. However, as it is much more difficult to produce a photograph of a coloured pattern, and as the isochromatics become faint and indistinct above the fifth order, the use of white light is mainly restricted to demonstration work where the brilliant colours are of great psychological value. For accurate quantitative work the monochromatic fringe pattern is now always used.

As regards calibration of a white-light colour pattern, the principal stress difference corresponding to the tint-of-passage isochromatic can be determined in exactly the same way as the fringe value for monochromatic light. For very approximate work, the $(P - Q)$ values may be inferred from the colours; for this purpose, a tensile specimen may be subjected to a gradually increasing load and a table of stresses and corresponding colours drawn up. For example, for a particular specimen, a first order green may be found to correspond to a stress of 200 lb./sq. in.; thus in the actual model the value of $(P - Q)$ will be 200 lb./sq. in. wherever this colour is identified. This is known as *colour matching*, and is obviously a very rough method of stress measurement.

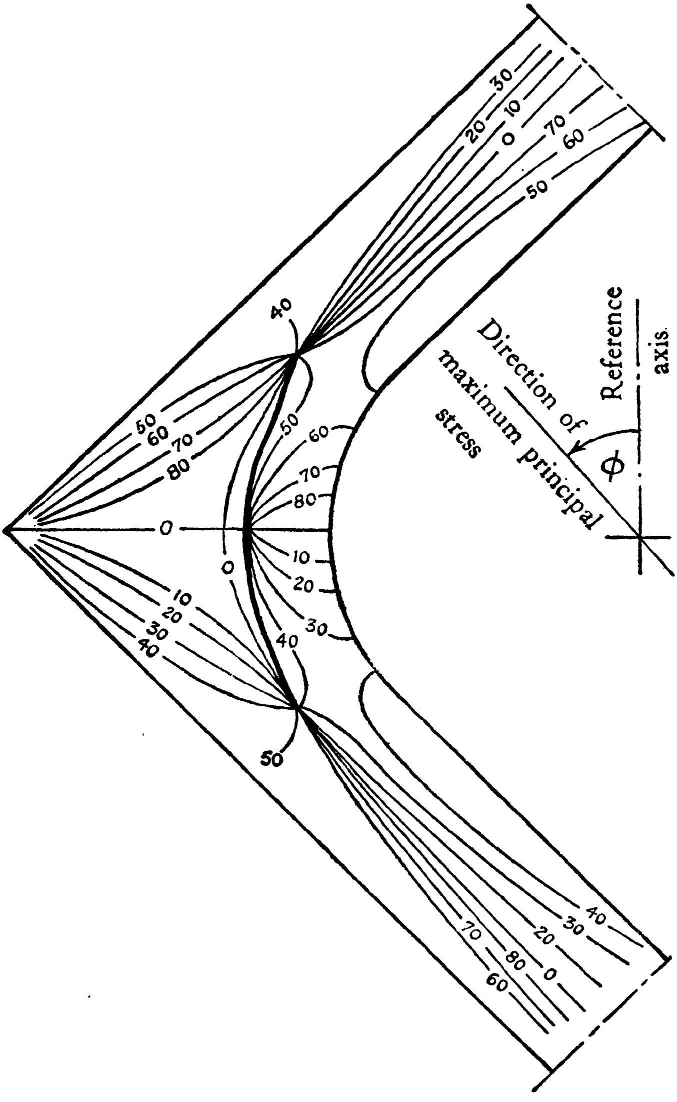

Fig. 29.—Isoclinic lines in model of fig. 26

The Isoclinic Lines

We have so far assumed in our discussion of stress patterns that the models are examined in circularly polarized light. If the models are examined in plane-polarized light, and if at any point the direction of one of the principal stresses coincides with the direction of polarization of the incident light, that point will appear dark when viewed through the analyser. The locus of points at which the principal stress direction coincides with the direction of polarization appears as a dark line across the model. Such lines are known as *isoclinic lines.*

In general, the isoclinic lines move across the model as the polarizer and analyser are rotated together. Fig. 29 shows, for the L model of fig. 26, the isoclinic lines obtained for different settings of polarizer and analyser. These curves, which give the directions of the principal stresses at every point in the model, are plotted by varying the setting of the polarizer in steps of, say, 10°, and plotting the isoclinics for each setting.

The isoclinic lines are not so sharply defined as the monochromatic fringes, and at best it is possible to determine the direction of the principal stresses only to about ±1°. However, for most practical purposes this is quite adequate.

CHAPTER IV

The Reduction of Data from Photo-elastic Tests

From the foregoing chapter it will be remembered that a photo-elastic test on a model gives the difference of the principal stresses and their direction at every point. For a complete analysis, we require to know the separate principal stresses and the main problem is to determine these from the experimental data. When this is done it is a simple matter to determine the stress distribution across critical sections by well-known methods.

However, it is important that the analysis should be presented in a systematic manner, so that a clear picture of the stress distribution is immediately obtained. Thus, diagrams showing the lines of principal stress, edge stresses and stresses across critical sections will generally be required, and may sometimes be supplemented by further diagrams showing principal stress contours and lines of maximum shearing stress. A series of photo-elastic tests is very often carried out to investigate the effect of varying the radius of a fillet at a discontinuity in the section of a member, or some similar problem, and it is then necessary to plot graphs showing, for example, the variation of the maximum stress with the size of the radius.

When a detailed analysis of the stresses in a model is required, the necessary work in reducing the experimental data may be summarized as follows:

(*a*) The lines of principal stress and lines of maximum shearing stress are plotted from the isoclinic lines.
(*b*) The fringe pattern is calibrated in terms of stress units.
(*c*) The edge stresses are plotted from the fringe photograph.
(*d*) The separate principal stresses are determined by calculation or by a subsidiary experiment.
(*e*) The magnitudes of the separate principal stresses at every point in the model are indicated by principal stress contours.
(*f*) The stress distribution across critical sections is investigated; the magnitudes and directions of the principal stresses being known, the normal, tangential and shearing stresses are readily found.

It will not usually be necessary to carry out all these operations on any one model; in many cases, the edge stresses are critical and (*a*), (*b*) and (*c*) together with the fringe photograph give an adequate picture of the stress distribution.

We may now consider each of the above procedures in detail.

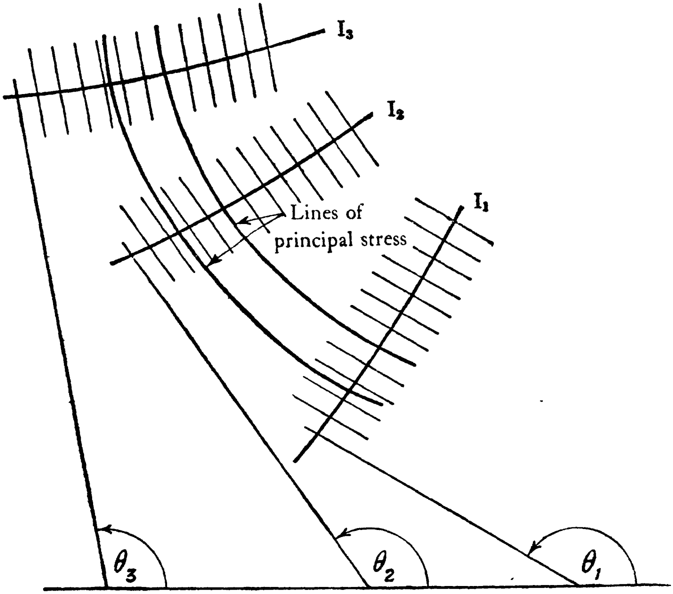

Fig. 30.—Construction of the lines of principal stress from the isoclinic lines

Construction of the Lines of Principal Stress

The lines of principal stress are drawn directly from the isoclinic lines. Several methods of carrying out the construction are available, the most rapid one being illustrated in fig. 30. I_1, I_2, I_3, &c., are the isoclinics of parameters θ_1, θ_2, θ_3, &c. Short lines, inclined at the appropriate angles to the reference axis, are drawn at closely spaced intervals along the isoclinics and the lines of principal stress are sketched in so as to be tangential to these short lines. The orthogonal system of principal stress lines can be sketched in by eye.

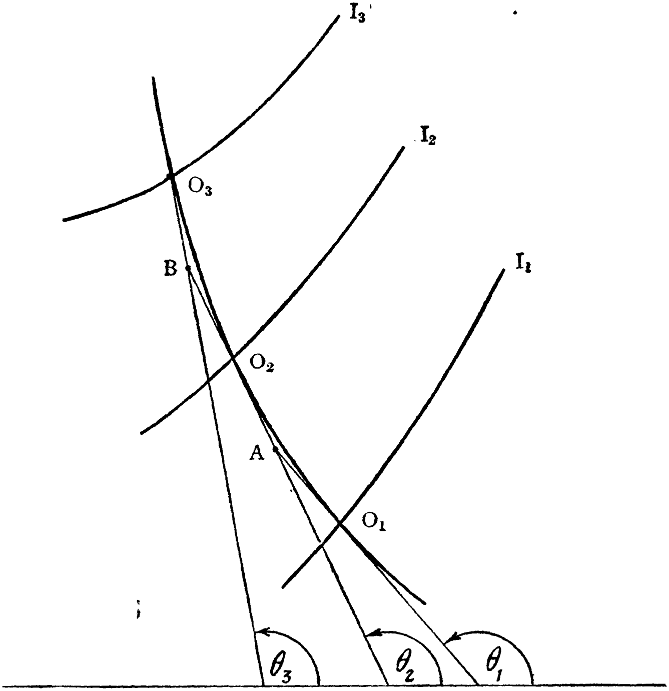

Fig. 31.—A more accurate construction for the lines of principal stress

The above method is sufficiently accurate if the principal stress lines are required only for qualitative examination, but if measurements are to be made from them the following construction should be used for greater accuracy.

Through an arbitrary point O_1 (fig. 31) on isoclinic I_1 draw a line O_1A inclined at angle θ_1 to the axis, so that

A is midway between I_1 and I_2; through A draw AO_2 at angle θ_2 to cut isoclinic I_2 at O_2, and produce AO_2 to B midway between I_2 and I_3. Through B draw BO_3 at angle θ_3 to cut I_3 at O_3. Then the required line of principal stress is the curve tangent to O_1A, O_2B, &c., at points O_1, O_2, &c.

Both these constructions are most conveniently carried out by laying a sheet of tracing paper over a diagram of the isoclinics and using an adjustable set square to draw the necessary construction lines.

The direction of the maximum shearing stress at any point is at 45° to the principal stresses, and the lines of maximum shearing stress can be constructed directly from the isoclinics by one of the above methods by altering the parameters by 45°.

Calibration of the Fringe Pattern and Plotting the Edge Stresses

The fringe pattern may be calibrated in terms of stress by one of the methods discussed in Chapter III, i.e. by testing a simple tensile or bending specimen cut from the same sheet of material as the model, or by calculating the stress at some point in the model where the fringe order is known.

The principal stresses at a free boundary are normal and parallel to the boundary, and as the latter stress is zero, the edge stresses are given directly by the fringes, which are lines of equal $(P - Q)$.

Knowing the model fringe value, the edge stresses are easily plotted by laying a sheet of tracing paper over the fringe photograph and tracing the outline of the model together with the points at which the various fringes intersect the boundary. Then at each of these points a normal to the boundary is erected, the length of which represents the edge stress to any convenient scale.

It sometimes happens that the fringes are running more or less parallel to the edge of the model and points at which they intersect the boundary are rather far apart. In such a case it may be necessary to determine the edge stress at intermediate points by plotting $(P - Q)$ across sections, and extrapolating the curve to meet the edge. This procedure is illustrated in fig. 32.

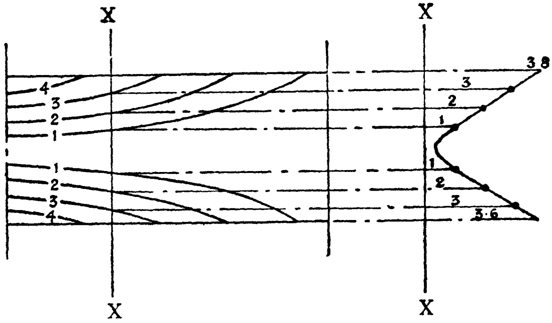

Fig. 32.—Determination of edge stress at points between fringes by plotting $(P-Q)$ across a section

Determination of the Separate Principal Stresses

There are several methods of calculating the stresses within the boundary of a model directly from the fringe pattern and isoclinic lines. Two of these methods will be described, but both are apt to be rather unsatisfactory due to the practical difficulty of locating the isoclinic lines with sufficient accuracy. If, however, the *sum of the principal stresses* can be determined at every point, by calculation or experiment, the separate principal stresses can be obtained immediately, since their difference is known from the fringe pattern. Three methods for the determination of $(P + Q)$, one arithmetical and two experimental, will be discussed, none of which involve the isoclinics with their attendant uncertainties.

Filon's Method.—In this method use is made of an expression giving the variation of a principal stress along its own line. Thus, by a step-by-step process, it is possible to determine the principal stresses at any point in the model, starting from a point at which they are known —for example, a point on a free boundary.

Referring to fig. 33 it can be shown that

$$P_N - P_A = \int_{\phi_A}^{\phi_N} (P - Q) \cot \beta \, d\phi,$$

where P_A is the known value of the major principal stress at point A, P_N the value of this stress at some other point N on the same line of principal stress, $(P - Q)$ the principal stress difference at any point on the line, β the angle at which the isoclinic of parameter ϕ cuts the line, and $d\phi$ the difference in parameter between successive isoclinics cutting the line under consideration (in fig. 33 $d\phi = \phi_1 - \phi_2$, $\phi_2 - \phi_3$, &c.). A, B, C, &c., are the points at which the line of principal stress cuts the isoclinic of parameter ϕ_1, ϕ_2, ϕ_3, &c.

The method of calculating the principal stress P along the line A, B, C, . . . N, will now be clear: starting at A, where $P = P_A$, $(P - Q)\cot\beta$ is calculated at each of the points A, B, C . . . N, and the mean of these quantities at A and B, B and C, &c., is multiplied by $d\phi$ (in radians). Denoting the resulting average quantities by δP_{A-B}, δP_{B-C}, &c., we have

$$P_B = P_A + \delta P_{A-B}$$

$$P_C = P_A + \delta P_{A-B} + \delta P_{B-C} = P_A + \sum_A^C \delta P$$

. . . .

$$P_N = P_A + \sum_A^N \delta P.$$

In this way the integration is carried out numerically and the value of P is obtained at points along the line of principal stress. It is convenient to take A on the boundary of the model, and to follow the line of principal stress normal to the edge. If it is necessary to follow along a line of Q-stress, the variation of this principal stress along its own line is given by

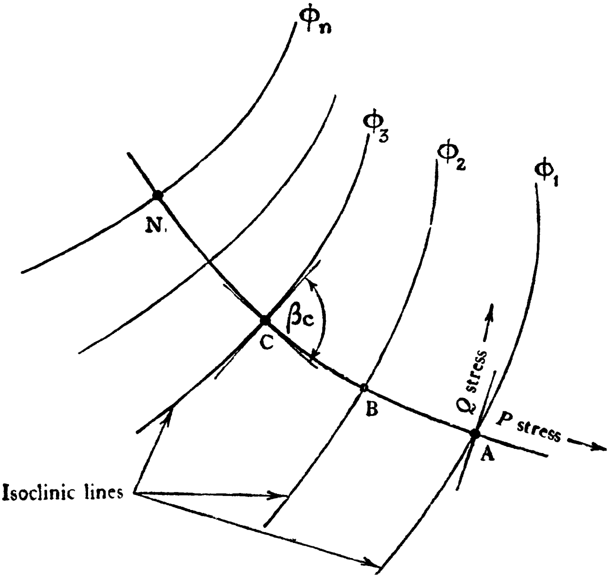

Fig. 33.—Filon's method for calculating the separate principal stresses

$$Q_N - Q_A = \int_{\phi_A}^{\phi_N} (Q - P) \cot(\beta - \pi/2) \, . \, d\phi,$$

where $(\beta - \pi/2)$ is the angle at which the isoclinic cuts the line of Q-stress.

If the isoclinic lines are almost parallel to the line of principal stress along which the separate principal stresses are required, the angles β are very small and difficult to measure accurately. It is then better to use the equation

$$P_N - P_A = d\phi \int_A^N \frac{Q - P}{ds_2} ds_1,$$

where the line of principal stress is divided off in small lengths ds_1; ds_2 is the distance between two neighbouring isoclinics measured transverse to the path of integration, and $d\phi$ is the difference between the parameters of these isoclinics (see fig. 34 (*a*)).

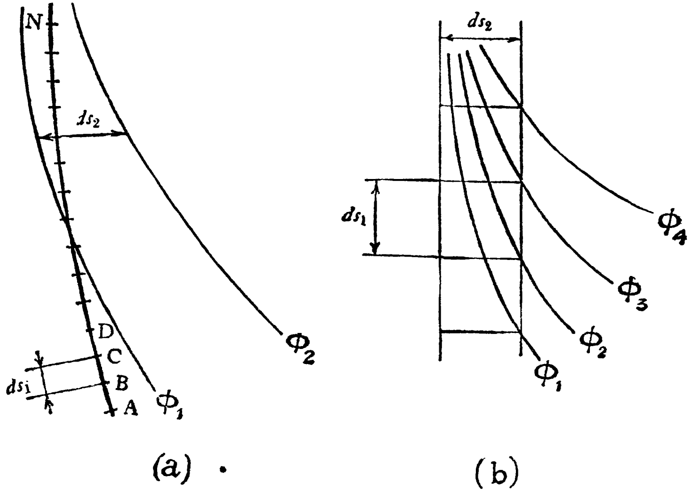

Fig. 34.—Filon's method where the path of integration is almost parallel to the isoclinics

The integration is carried out in the same manner as in the previous case, $(Q - P)/ds_2$ being calculated at each of the points A, B, C, &c., the mean values multiplied by ds_1, and the results summed up to give P at successive points.

In certain cases, the isoclinics tend to become asymptotic to a line of principal stress, which is also an axis of symmetry in the model, and in calculating the stresses along this line it becomes increasingly difficult to measure ds_2 accurately. In such a case, as has been suggested by Frocht, it is convenient to keep ds_2 constant and make ds_1 variable, as indicated in fig. 34 (*b*). A line is drawn parallel to the line of principal stress at distance ds_2 from it, and the intersections of this line with successive isoclinics are projected across to give ds_1. The integration from this stage is carried out as before.

The great difficulty which besets the use of Filon's method is that of accurately locating the isoclinic lines and of measuring the angles β or intercepts ds_2. Nevertheless, it gives reasonably good results in favourable cases, and is useful when the stresses are required only at a few interior points or across a section.

Frocht's Shear-difference Method.—This is a method for calculating the normal and tangential stresses along an arbitrary line, from the fringe pattern and isoclinics.

Suppose that in fig. 35 OX is a line in a model along which it is desired to calculate the normal and tangential stresses; OY is the axis at right angles to OX. Then it can be shown that

$$f_{xn} = f_{xo} - \int_0^{\mathrm{N}} \frac{\partial s_{xy}}{\partial y} \, . \, dx,$$

where f_{xo} and f_{xn} are the stresses at O and N respectively, parallel to the X-axis and s_{xy} is the shearing stress parallel to this axis at any point.

It is clear that this equation can be dealt with by the same sort of step-by-step integration process as was used for Filon's method, provided that $\partial s_{xy}/\partial y$, i.e. the rate of change of s_{xy} in the Y-direction, can be calculated from the photo-elastic data. This can be done approximately by calculating s_{xy} at points along the auxiliary lines AE and BF, which are parallel to OX and distant $dy/2$ on either side of it, from the expression

$$s_{xy} = \tfrac{1}{2}(P - Q)\sin 2\theta,$$

where θ is the angle measured clockwise between the normal to OX, and the maximum principal stress P. Then at a typical point on ON

$$\frac{\partial s_{xy}}{\partial y} = \frac{(s_{xy})_C - (s_{xy})_D}{dy} \text{ approximately,}$$

where C and D are the corresponding points on AE and BF.

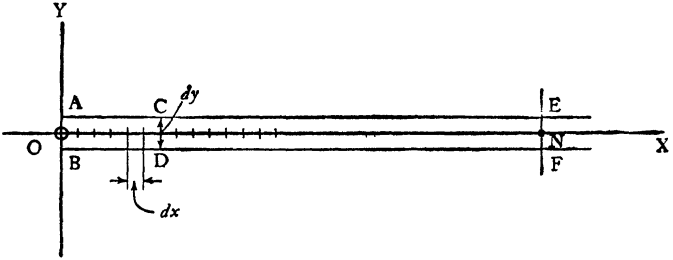

Fig. 35.—Frocht's shear-difference method

In carrying out the calculations it is convenient to plot curves of $(P - Q)$ and θ across the auxiliary lines from the fringe pattern and isoclinics; from these, s_{xy} across the lines may be calculated and subtracted graphically to give ∂s_{xy}. If dx and dy are made equal, $dx/dy = 1$ in the equation with consequent saving in arithmetic. Starting from point O, where f_x is known, this stress is calculated by summing ∂s_{xy} from point to point.

The normal stress across the section is obtained now from the relation

$$f_y = f_x \pm \sqrt{(P - Q)^2 - 4s_{xy}^2}.$$

The plus before the quantity under the square root sign is used if f_y is algebraically greater than f_x, and vice versa.

The normal stress, f_y, is greater than f_x at any point if the direction of the major principal stress, P, makes an angle of less than 45° with f_y.

This method is rather more laborious than Filon's, but somewhat greater accuracy may be expected. The signs of θ, dx, dy and ∂s_{xy} must conform to the convention of fig. 36, and considerable care is necessary to avoid errors due to wrong signs.

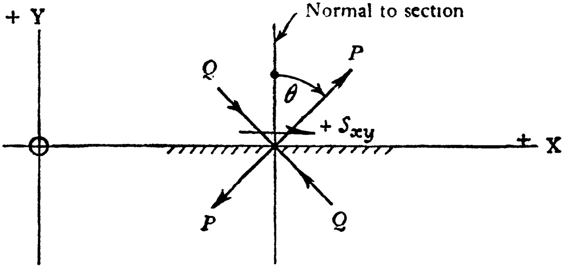

Fig. 36.—Sign convention for Frocht's shear-difference method

$(P + Q)$ by the Numerical Solution of Laplace's Equation

The following method for the calculation of $(P + Q)$ was first published by Shortley and Weller, and further developed by Frocht. It provides the most satisfactory method of determining the separate principal stresses from the photo-elastic results alone without recourse to an auxiliary experiment, since the only data required are the edge stresses from the fringe photograph. It is beyond the scope of this book to deal with the various refinements which have been suggested for shortening the arithmetical work involved, but a solution can be obtained for most problems without undue labour using only the simple procedures to be described.

It has been found by the theory of elasticity that the sum of the principal stresses at points in an elastic plate under two-dimensional stress obeys the Laplace differential equation

$$\frac{\partial^2(P+Q)}{\partial x^2}+\frac{\partial^2(P+Q)}{\partial y^2}=0.$$

To obtain an approximate numerical solution of this equation, it is necessary to know the value of $(P+Q)$ along the edges of the model and to take into account the requirement that, at any point, the value of $(P+Q)$ must be the mean of that quantity at four equidistant nearby points. The solution is obtained by an iterative process of improvement of an arbitrary set of values; although the arithmetical work may be considerable, it is simple and by no means prohibitive.

The procedure is best illustrated by an example, and fig. 37 shows part of a symmetrical L model which was subjected to tensile loads at the ends of its legs. The model is first covered by a coarse square net and the intersections of the network lines suitably boxed off to separate figures pertaining to the different points. The edge stresses in fringe units are now written down at the points where the sides of the net intersect the boundaries. It will be remembered that at a free boundary one of the principal stresses is zero, so that the edge stresses are equal to the boundary values of $(P+Q)$. In the present case a section across which the distribution of $(P+Q)$ is known to be linear is taken as one of the boundaries and, since the model is symmetrical, only half of it need be considered.

We must now put an initial value for $(P+Q)$ in each of the squares and proceed to improve it by a systematic application of an improvement formula until it approaches the correct value to within the limits of accuracy required. The nearer the initial values are to the correct ones, the more rapidly will the desired result be obtained, but any arbitrary set of initial values could eventually be corrected to give the solution. Usually the investigator will be able to choose approximate values at a few special points in the model or values for these *key points* may be calculated by Frocht and Leven's " four-point influence method ". Another alternative would be to find $(P+Q)$ at these points experimentally. The question of obtaining initial values will be referred to later when both of these methods for obtaining rational starting values for the iterative process will be discussed.

Suppose that in the present example arbitrary values of $-1 \cdot 0$ and $-4 \cdot 5$ are placed in squares E4 and E8 respectively. The points E4 and E8 are at the corners of blocks of four

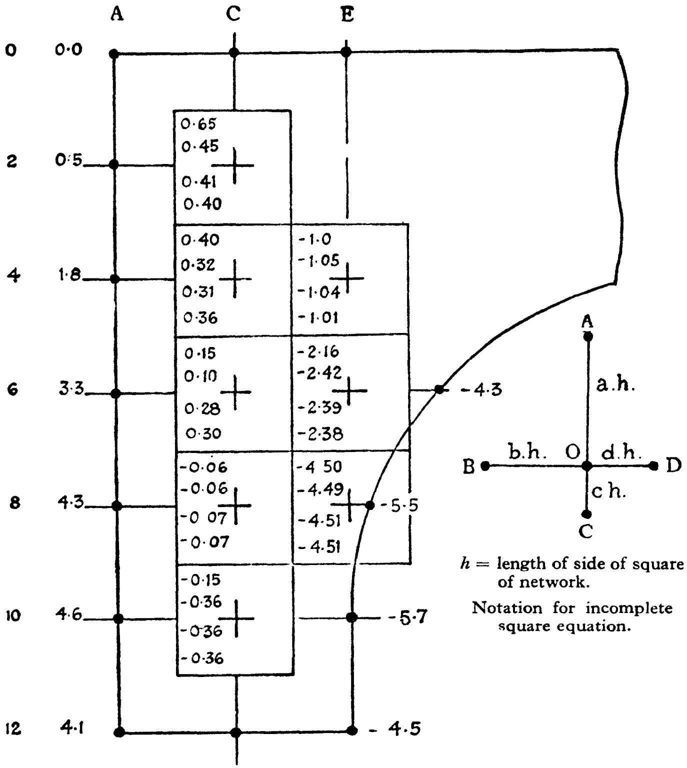

Fig. 37.—Determination of $(P + Q)$ at points within the boundary of a model by the numerical solution of Laplace's equation: preliminary network

squares and are key points in this network; the reason for calling them key points will be self-evident as the work proceeds. A first value for $(P + Q)$ at C2 is obtained next by taking the mean of the values at the four equidistant points A0, E0, E4 and A4, i.e.

$$(P + Q)_{C2} = \tfrac{1}{4}(0 + 1 \cdot 8 - 1 \cdot 0 + 1 \cdot 8) = 0 \cdot 65.$$

Similarly

$$(P+Q)_{C6} = \tfrac{1}{4}(1\cdot8 - 1\cdot0 - 4\cdot5 + 4\cdot3) = 0\cdot15,$$

$$(P+Q)_{C10} = \tfrac{1}{4}(4\cdot3 - 4\cdot5 - 4\cdot5 + 4\cdot1) = -0\cdot15,$$

and

$$(P+Q)_{C4} = \tfrac{1}{4}(0\cdot65 - 1\cdot0 + 0\cdot15 + 1\cdot8) = 0\cdot40.$$

This procedure is continued until a first value is calculated for each point in the network from the fixed boundary values and trial key-point values. The equation used is known as the *Liebman equation.*

Returning now to point C2, an improved value is obtained by taking the mean of the values at equidistant points normally disposed about it, i.e.

$$(P+Q)_{C2} = \tfrac{1}{4}(0\cdot5 + 0\cdot4 + 0\cdot4 + 0\cdot5) = 0\cdot45,$$

and

$$(P+Q)_{C4} = \tfrac{1}{4}(0\cdot45 - 1\cdot0 + 0\cdot15 + 1\cdot8) = 0\cdot35.$$

This is done to each of the squares in sequence and the cycle repeated until the alterations in the values become very small. It will be observed that the value in square E8 cannot be improved by the simple Liebman procedure and the expression

$$s_O = \frac{1}{1/ac + 1/bd}\left\{\frac{s_A}{a(a+c)} + \frac{s_B}{b(b+d)} + \frac{s_C}{c(c+a)} + \frac{s_D}{d(d+b)}\right\}$$

must be employed where a, b, c and d have the meaning indicated in fig. 37. In square E8, $a = c = d = 1$ and $b = 0\cdot4$, so that, where s_B is the boundary value where line 8 cuts the edge,

$$s_{E8} = (0\cdot143 s_{E6} + 0\cdot510 s_B + 0\cdot143 s_{E10} + 0\cdot204 s_{C8}).$$

It should be noted that the coefficients in the above always add up to unity.

The values obtained after completing the " harmonization " procedure give a first approximation to $(P+Q)$ at a relatively small number of points in the model, so that it is necessary to repeat the calculations for a network in which the sides of the squares are half that of the original net in order to get a more accurate analysis. The final values from the preliminary coarse network form the initial values for the second network and are accordingly transferred to the corresponding squares in the latter. These values are now broken down to give initial values in the remaining squares of the new network and the same process of harmonization is applied and continued until the values become stationary, or the changes negligible. The final result is shown in fig. 38.

The calculations are conveniently carried out in fringe units; conversion to stress units can be left to a later stage in the work. It is usually sufficient to calculate $(P + Q)$ to the second

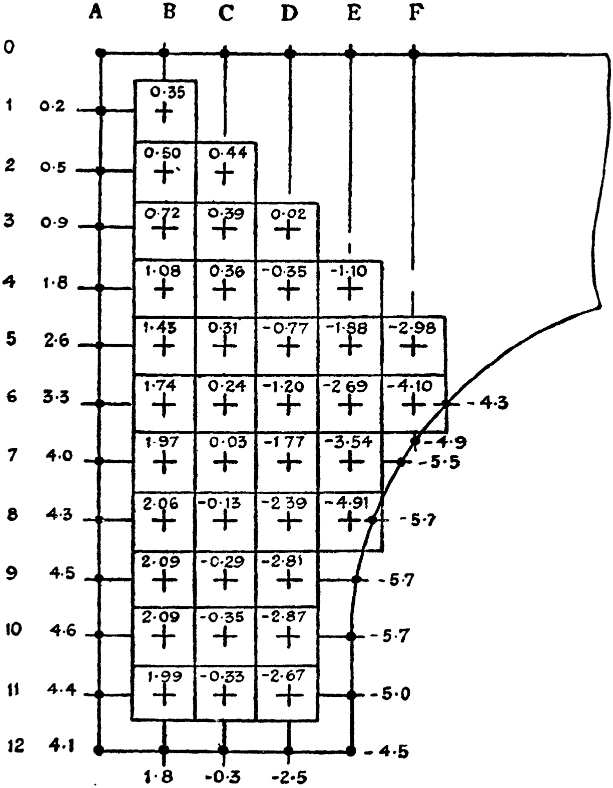

Fig. 38.—Determination of $(P + Q)$: final network

decimal place—this will be well within the limits of accuracy to which $(P - Q)$ can be estimated from the fringe photograph.

If a still more detailed analysis of certain areas of the model is required, for example in the region of a stress concentration, the size of the net can be still further reduced. It is not necessary to reduce the size of the net over the entire model, as this would involve an immense amount of needless work; it is sufficient to reduce it locally where required. The procedure in reducing the net size locally will be seen from fig. 39. The large black points form the coarser net; the intermediate points D2, F2, H2 are now introduced and $(P + Q)$ at these points calculated by taking diagonal Liebmans to equidistant points on the coarse net, e.g.

$$s_{D2} = \tfrac{1}{4}(s_{C1} + s_{E1} + s_{C2} + s_{C3}).$$

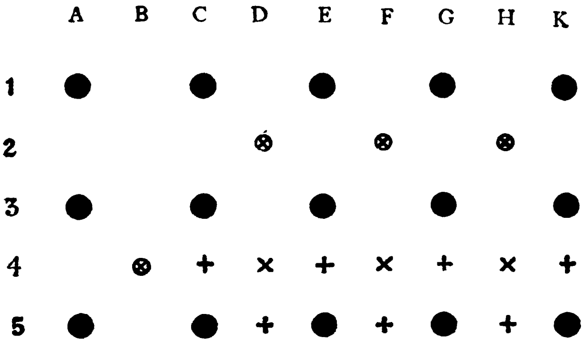

● – Points in coarse network

⊗ – Intermediate points from diagonal Liebmans

+ – Points in fine network from normal Liebmans

× – Points in fine network from diagonal Liebmans

Fig. 39.—Reduction of net size locally

Similarly the values at D4, F4, H4, &c., are calculated. The remaining points in the fine net are now filled in by taking normal Liebmans and, finally, the fine network values are improved by harmonization.

Initial Values by Frocht's Four-point Influence Method.—The procedure outlined above is quite satisfactory and rapid convergence is obtained by taking the initial values for the final net from a preliminary coarse network. It is possible to dispense with the preliminary network by calculating key-point values for the final net by the "four-point influence equation". As already stated, $(P + Q)$ at a point O is given by

$$s_O = \frac{1}{1/ac + 1/bd}\left\{\frac{s_A}{a(a+c)} + \frac{s_B}{b(b+d)} + \frac{s_C}{c(c+d)} + \frac{s_D}{d(d+b)}\right\},$$

where A, B, C, D are four nearby points, as in fig. 37. If A, B, C and D are not close to O the result will not be accurate, but if several sets of points such as A, B, C, D are taken and s_O calculated for each case, then the average value obtained is found to give a good first approximation to the correct value of s_O. This leads to a method of calculating $(P + Q)$ at key-points within a model from the known boundary values. Thus in fig. 40 the key points for a network in an L model are O_1, O_2 and O_3. s_O is calculated in each case for several inclinations, θ_1, θ_2, &c., of the axes, s_A, s_B, s_C and s_D being taken equal to the edge stresses at the points where the axes intersect the boundary. The average value of s_O is obtained by plotting it against θ and finding the mean ordinate of the resulting curve. The calculations are set down in Table II.

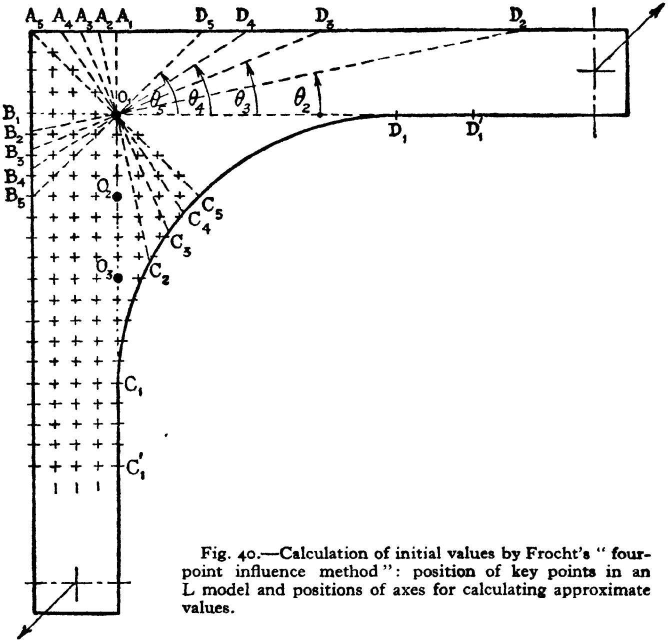

Fig. 40.—Calculation of initial values by Frocht's "four-point influence method": position of key points in an L model and positions of axes for calculating approximate values.

TABLE II

Four-point Influence Method

Point	Angular Posn. (θ)	$\frac{1}{ac}$	$\frac{1}{bd}$	$\frac{1}{1/ac+1/bd}$	(1) $\frac{\Psi_a}{a(a+c)}$		(2) $\frac{\Psi_b}{b(b+d)}$		(3) $\frac{\Psi_c}{c(c+a)}$		(4) $\frac{\Psi_d}{d(d+b)}$		$\sum_{(1)}^{(4)}$	Ψ_o	$P+Q$
o_1	0−	0·087	0·087	5·75	·016 × 2·9	−0·896	·072 × 5·9	−·159	·072 × 1·2	·086	·072 × 1·15	·083	−·089	−·512	+0·38
	0+	0·12	0·12	4·16	·027 × 5·9	−·159	·016 × 2·9	−·046	·09 × 1·2	·108	·09 × 1·15	·104	0·003	0·012	
	11¼	0·20	0·085	4·64	·025 × 2·9	−·368	·016 × 1·8	+·288	·13 × ·85	·110	·07 × 1·6	·112	0·142	0·659	
	22½	0·24	0·150	2·56	·098 × 4·1	−·402	·041 × 5·25	+·216	·14 × ·60	·084	·10 × 2·0	·20	0·098	0·251	
	33¾	0·235	0·18	2·41	·11 × 3·5	−·385	·071 × 4·2	·298	·125 × ·30	·038	·12 × 2·4	·248	0·201	0·485	
	45	0·20	0·19	2·56	·10 × 3·4	−·340	·095 × 3·3	·314	·10 × 0	0	·10 × 3·1	·31	0·284	0·727	
o_2	0−	·41	·084	2·02	·21 × 3·4	−·714	·038 × 5·9	−·224	·2 × 3·3	·66	·045 × 1·15	·052	−·226	−·456	−0·75
	0+	·41	·057	2·24	·21 × 3·4	−·714	·02 × 2·9	−·058	·20 × 3·3	·66	·035 × 1·15	·052	−0·160	−0·356	
	15	·48	·052	1·88	·27 × 3·5	−·945	·019 × 2·0	+·038	·20 × 2·7	·55	·034 × 2·2	·075	−0·282	−0·530	
	30	·47	·085	1·80	·26 × 3·95	−1·03	·045 × 5·35	·24	·18 × 2·0	·36	·038 × 3·5	·133	−0·296	−0·533	
	45	·36	·098	2·18	·24 × 4·3	−1·03	·065 × 4·9	·318	·125 × 1·2	·15	·033 × 4·9	·162	−0·400	−0·87	
	60	·23	·082	3·20	·17 × 4·7	−0·8	·065 × 4·2	·272	·066 × 0·2	·132	·018 × 4·5	·081	−0·315	−1·01	
	69½−	·19	·077	3·75	·13 × 5·0	−0·65	·063 × 3·9	·246	·06 × 0·2	·12	·014 × 0·4	·006	−0·280	−1·05	
	69½+	·19	·16	2·86	·13 × 5·0	−0·65	·11 × 3·9	·429	·06 × 0·2	·12	·05 × 5·4	−·27	−0·371	−1·03	
	80	·16	·32	2·08	·10 × 5·4	−0·54	·17 × 3·55	·604	·06 × 0·6	·036	·14 × 3·5	−·49	−0·390	−0·81	
o_3	0−	1·40	0·10	·67	1·0 × 5·15	−5·15	·069 × 5·9	−0·40	·31 × 4·8	1·49	·03 × 1·15	·044	−4·016	−2·69	−2·99
	0+	1·40	0·052	·69	1·0 × 5·15	−5·15	·028 × 2·9	−0·081	·31 × 4·8	1·49	0·24 × 1·15	·029	−3·712	−2·56	
	15	1·40	·049	·69	1·25 × 5·25	−6·55	·26 × 0·6	+0·016	·30 × 4·2	1·26	·023 × 2·7	·062	−5·212	−3.60	
	30	1·35	·057	·71	1·05 × 5·35	−5·62	·036 × 4·05	+0·14	·24 × 3·9	·935	·021 × 4·5	·095	−3·544	−2·52	
	44−	0·85	·067	1·09	0·81 × 5·4	−4·37	·05 × 5·2	0·26	·17 × 3·3	·561	·017 × 5·15	·088	−3·461	−3·76	
	44+	0·85	·210	0·94	0·81 × 5·4	−4·37	·10 × 5·2	0·52	·17 × 3·3	·561	·06 × 3·45	−·207	−3·496	−3·29	
	60	0·56	·80	·74	0·53 × 5·5	−2·92	·22 × 5·3	1·17	·084 × 1·7	·143	·57 × 4·9	−2·79	−3·397	−2·52	
	75	0·27	1·30	·64	·25 × 5·1	−1·43	·28 × 5·1	1·43	·036 × ·15	·005	·94 × 5·0	−4·70	−4·695	−3·0	

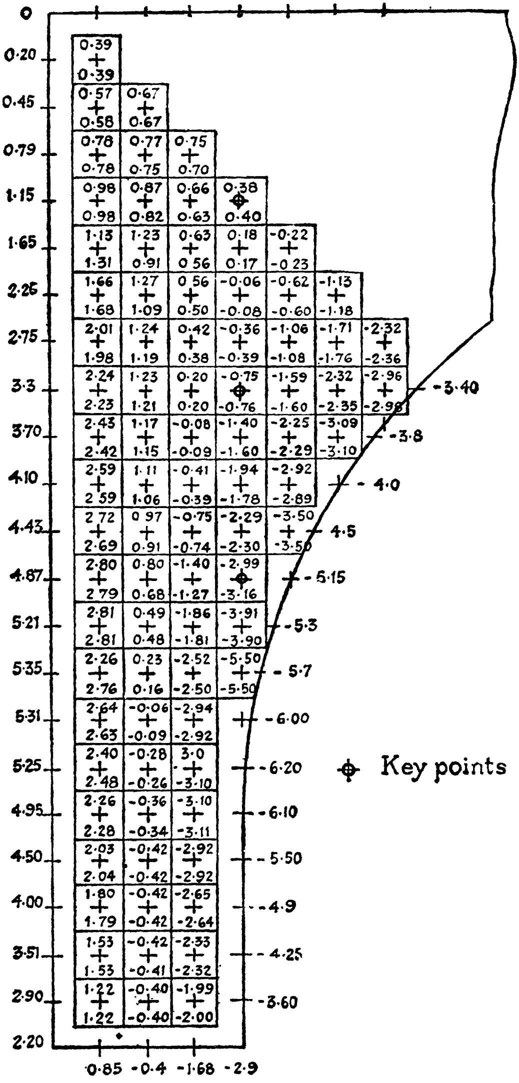

Fig. 41.—(*P* + *Q*) network in the model of fig. 40

The work then proceeds as in the previous example and is shown in fig. 41. A close approximation to the correct values of $(P + Q)$ is obtained simply by breaking down the key-point values of $(P + Q)$ calculated by the four-point influence method. This will be seen by comparing the two figures in each square of the network in fig. 41, the first figure being the value obtained by breaking down the key points, and the second the value after two cycles of harmonization. In many cases it will be unnecessary to carry out this process at all, although it would be advisable to carry out one cycle as a check.

The Experimental Determination of $(P + Q)$

As the calculation of the separate principal stresses from the photo-elastic data tends to be rather laborious, several experimental methods have been developed, two of which will now be described.

Lateral Extensometer Method.—If P and Q are the principal stresses at a point in a model of thickness d, cut from material for which Young's modulus is E and Poisson's ratio $1/m$, then the change in thickness due to P and Q is

$$e = \frac{1/m(P + Q)d}{E}.$$

For a given model $1/m$, E and d are constants and thus the lateral strain is proportional to $(P + Q)$. It is not necessary that the model used for making these lateral strain readings should be of the same material as the photo-elastic model—a plastic with low creep will be most suitable, e.g. unplasticized Perspex.

The lateral strains are, of course, very small, and the lateral extensometer to be used must be able to read to a few millionths of an inch; two suitable instruments will be described in Chapter VI. The usual procedure is to set up the instrument with the model unloaded, then measure the change of thickness due to a convenient load; the instrument can be calibrated to read $(P + Q)$ in lb/in^2 directly by means of a simple tension specimen of the same thickness and material as the model. Readings are taken in this manner at as many points as necessary—usually they are taken across various sections in the model, and if a complete analysis is required, a considerable number of readings is necessary.

There is no reason, however, why the lateral extensometer should not be used in conjunction with the arithmetical method for the determination of $(P + Q)$; if the key-point values for the arithmetical method are measured by the lateral extensometer, then only a few readings will be necessary and the remaining values can be determined arithmetically by breaking down the key points by the Liebman equation. Values of $(P + Q)$ for incomplete squares should also be measured experimentally, so that only the Liebman equation is required in the arithmetical work. A very rapid solution is thus obtained with the minimum of arithmetical and experimental work.

$(P + Q)$ by the Membrane Analogy Method.—It has been established that the transverse deflection of a stretched elastic membrane obeys the same differential equation as $(P + Q)$ in a stressed plate. Thus, if the stretched membrane is made to the same outline as the plate and its deflection is proportional to $(P + Q)$ round the boundary, then its deflection will be proportional to $(P + Q)$ at internal points as well.

The method is, then, to lay the model on a horizontal plane and erect round the boundary a vertical template, the height of which is at every point proportional to $(P + Q)$. A uniformly stretched rubber sheet is now clamped over the template, and $(P + Q)$ is determined by measuring the height of the rubber sheet wherever required. A soap film may be used for the membrane instead of the rubber sheet, but in this case the measurements are rather more troublesome.

The mathematical analogy underlying the method requires that the deflections of the membrane should be small relative to its dimensions, thus at a point of stress concentration the readings may not be accurate; this is especially true if a rubber sheet is used as the sheet may be pinched in clamping it down and so result in inequalities in the tension. However, there are a large number of problems which do not involve very sudden changes in the edge stress, and in these cases the method could be applied with confidence.

CHAPTER V

Photo-elastic Apparatus

Complete photo-elastic analyses can be carried out using only the plane or circular polariscope, which is in fact the basic apparatus of photo-elasticity. It is proposed therefore to describe the various types of polariscope in this chapter, and to devote a further chapter to a description of instruments and apparatus which are auxiliary to the polariscope.

We may begin our discussion of photo-elastic apparatus by considering the various types of polarizing filters, light sources, and other components which go to make up the polariscope. Following that, the complete optical systems of several polariscopes will be described.

Polarizing Filters

(*a*) *Calcite prisms.*—It is possible to make use of the phenomenon of double refraction in natural crystals to produce a polarizing filter. This is done in the *Nicol prism* by cutting a block of calcite in such a way that an entering ray is split into two components, the ordinary and extraordinary rays, plane-polarized in directions at right angles to one another, as indicated in fig. 42, which is a section through the prism. The block is cut through a diagonal section and recemented with Canada balsam. The index of refraction of the balsam film and its position within the calcite block is such that the ordinary wave suffers total internal reflection at the surface of the balsam while the extraordinary wave passes through; light emerging from the " Nicol " is thus plane-polarized. The ordinary ray is reflected to the side of the prism and is there absorbed by a coating of black paint.

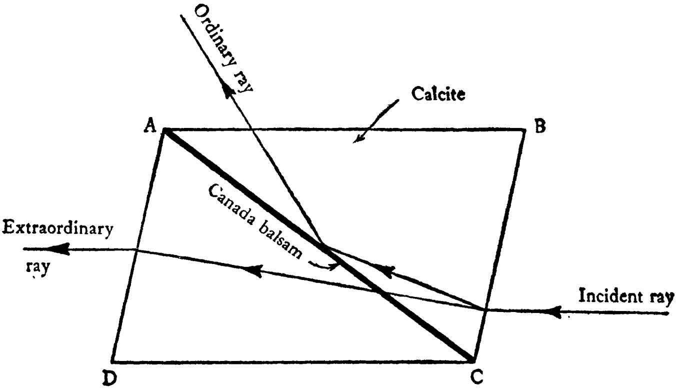

Fig. 42.—Principle of the Nicol prism

The Nicol prism is an extremely efficient polarizing filter but Nicols sufficiently large to be useful for photo-elastic polariscopes are expensive and difficult to obtain. In addition, the lateral displacement of the rays passing through the prism is a rather serious drawback. Small Nicols are, however, useful as analysing eyepieces.

To overcome the disadvantages of the usual prism several modified forms of the Nicol prism have been devised. These include the *Glan-Thomson* and *Ahrens* prisms, which are sketched in fig. 43. The faces of the Glan-Thomson prism are perpendicular to the direction of the transmitted rays, so that lateral displacement is avoided. The Ahrens prism is, in effect, a double Glan-Thomson prism, but the ordinary rays emerge obliquely from the prism instead of being reflected to one side. Another modified prism is the *glass spar prism*, which is rather like an inverted Nicol, consisting of a layer of Iceland spar cemented between flint glass blocks.

(*b*) "*Polaroid*" *filters*.—In certain natural crystals light which is transmitted through them is broken up into two plane-polarized components in the usual way, but one of the components is reduced in intensity to the point of extinction, while the other is transmitted with only slight loss; the emergent light is thus plane-polarized. Such a crystal is said to be *dichroic* and its action is illustrated in fig. 44. The natural crystal *tourmaline* behaves in this way, as does the synthetic substance *herapathite*, which is a complex salt containing quinine, hydriodic acid, and sulphuric acid.

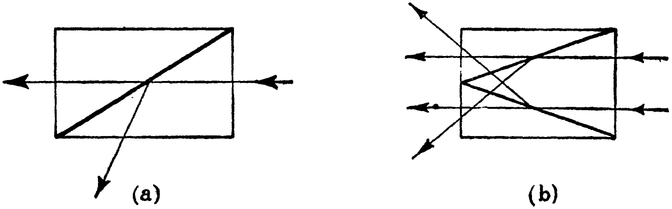

Fig. 43.—(*a*) The Glan-Thomson prism. (*b*) The Ahrens prism

In the manufacture of "Polaroid", ultramicroscopic, dichroic crystals of herapathite are embedded in a sheet of cellulose nitrate or acetate, and so oriented that the resulting sheet behaves exactly as shown in fig. 44. Exact details of the manufacturing process do not appear to have been revealed, but it would seem probable that the herapathite is held in colloidal solution in the cellulose and made to flow uniformly in one direction. This orients the crystals and on being forced through a narrow slot the solution sets to form a sheet.

Various grades of "Polaroid" are available in sheets up to 12 inches square. It is not quite as efficient a polarizer as a Nicol prism, but is entirely satisfactory for photo-elastic purposes.

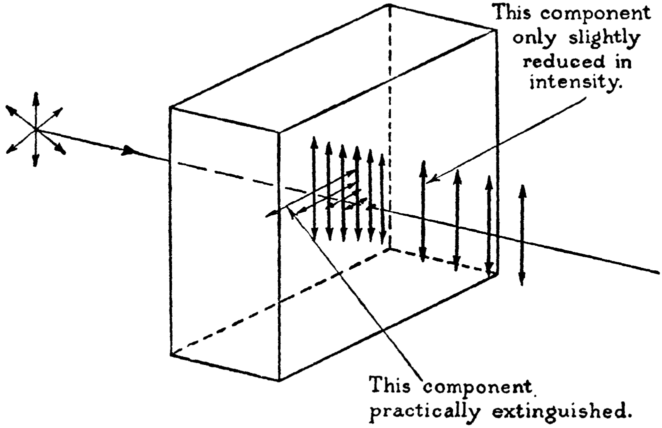
This component only slightly reduced in intensity.
This component practically extinguished.

Fig. 44.—Polarization by a dichroic crystal

(*c*) *Glass plate polarizers.*—It is found that light reflected from a glass plate is almost completely polarized when the angle of incidence is equal to a certain value termed the *polarizing angle*. This angle is the angle whose tangent is equal to the index of refraction of the glass, and is usually about 57°. The light reflected from the plate is polarized in the plane of incidence, i.e. the plane containing the incident ray and the normal to the plate.

The back of the plate is painted black to absorb the transmitted light, which is actually partially polarized in the plane at right angles to the plane of incidence. The transmitted component could be utilized, but a pile of say twelve plates would have to be used to obtain a sufficient degree of polarization. The two types of glass-plate polarizing filters are shown in fig. 45.

The reflection polarizer is the more effective of the two, and it provides a useful and cheap polarizer particularly where a large field is required. To overcome the disadvantage of the change in direction of the light beam the arrangement, originally suggested by Dr. F. C. Harris, shown in fig. 45 (*c*), may be adopted; there is no change in direction of the incoming beam so that this type of polarizer can be used in optical-bench type polariscopes (e.g. see fig. 51). The first glass plate may be replaced by a silvered mirror when the intensity of the transmitted light will be increased at the expense of polarizing efficiency; this, however, will still be satisfactory for most purposes.

Quarter-wave Plates

In order to study the fringe pattern in a model, it is preferable to examine it in circularly polarized light in order to eliminate the isoclinic lines, as they frequently obscure the fringes. To convert the plane polariscope to a circular polariscope two quarter-wave plates are put between the polarizer and analyser as described in Chapter II (see p. 38). These plates are usually of mica, which is easily split to the thickness required to give quarter of a wavelength retardation between the transmitted components.

The technique of cutting quarter-wave plates is fairly easily acquired with a little practice. From amongst the various methods which have been suggested, the following procedure has been found satisfactory. A sheet of mica is cut to a size slightly larger than the required quarter-wave plate. A corner of this sheet is now "burred"

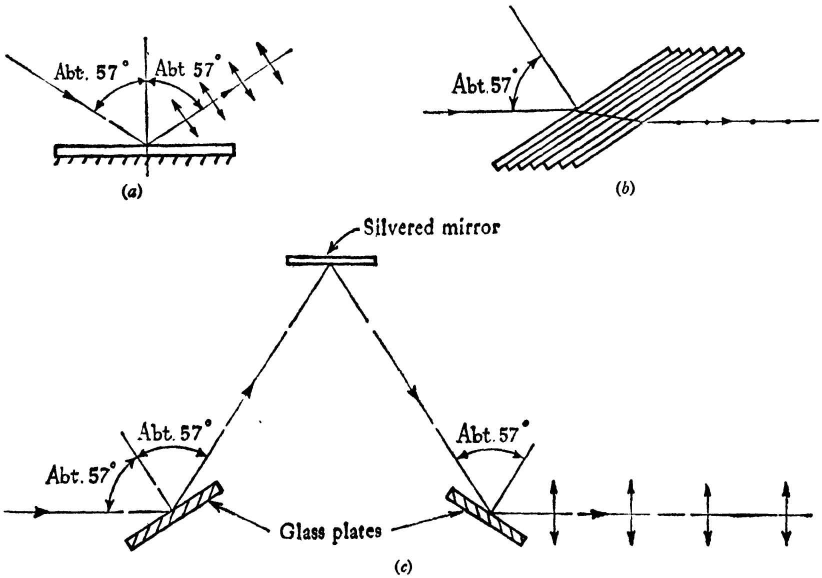

Fig. 45.—Glass-plate polarizing filters
(*a*) Reflection polarizer, (*b*) Transmission polarizer, (*c*) Triple reflection polarizer

and a needle point is inserted so as to split the sheet into two sheets of roughly equal thickness. Holding the corner open with the needle a drop of water is introduced, and the needle point worked *gently* round the boundary of the plate, propagating the cleavage round the sheet and toward the centre. This is repeated several times, always working gradually towards the centre. In this way the sheet will be split into two sheets of roughly equal thickness. One of the resulting sheets is next split in the same way, and so on until a quarter-wave plate is obtained. After a little experience it will be possible to judge when the correct thickness has been obtained, and the retardation can then be verified by superimposing four strips cut from the edge of the plate and examining them in the polariscope to see whether the combined retardation is one wavelength of the light used; eight thicknesses should, of course, give two wavelengths' retardation.

It is obvious that quarter-wave plates are accurate for only one particular wavelength, but it has been found that fairly large inaccuracies in the quarter-wave plates do not cause distortion of the fringe pattern provided that both the plates are of nearly equal thickness. That is, the plates will be quite satisfactory even if the retardation is as much as one-tenth of a wavelength greater or less then quarter of a wavelength, provided that the error is about the same for both plates.

Mica retardation plates are easily prepared for comparatively small sizes, say up to 3 inches diameter, but larger sheets are difficult to cleave uniformly and, if purchased, their cost is excessive. In view of this, various alternatives to mica for quarter-wave plates have been suggested. The well-known material "Cellophane" behaves as a uniaxial crystal, and large quarter-wave plates can be cut from it at negligible cost, provided that a sheet of the correct thickness can be obtained. The thickness necessary is rather less than that of the sheets usually employed for packing purposes.

The difficulty of obtaining Cellophane of the required thickness can be overcome by superimposing two sheets of equal thickness. If their principal axes coincide, the retardation will be twice that of a single sheet or zero, depending upon whether the "fast" axis in the first sheet coincides with the " fast " or " slow " axis in the second. Generally, the maximum retardation due to the two sheets will considerably exceed quarter of a wavelength. It is obvious therefore that there is some relative inclination of the axes of the two plates between these two positions which will give the required retardation of quarter of a wavelength.

Another method of obtaining a large quarter-wave plate has been suggested by Z. Tuzi; this type of plate consists of a sheet of glass subjected to a uniform compressive stress on two opposite edges. The value of this compressive stress is adjusted so that the retardation due to the plate is quarter of a wavelength.

Light Sources

As it is usually desired to project a magnified image of the model under examination on a screen for demonstration purposes, a concentrated white light source and condenser lens must be provided to give an intense parallel beam. A 500-watt " Point-o-lite " or a bunched-filament projector lamp is therefore suitable for this purpose.

In certain special types of polariscopes for examining very large models, it is impracticable to employ a collimated light beam, and the white light source may then be a bank of ordinary filament lamps behind a frosted-glass diffusing screen.

For monochromatic light various electric gas discharge lamps are available. As monochromatic light is mainly necessary for photography and not for large-scale projection a much less powerful source is sufficient, and for most purposes a 125-watt "Osira" high-pressure mercury-vapour lamp, with the outer envelope removed, is satisfactory. In order to isolate monochromatic light from the spectrum of this lamp, colour filters are necessary; Wratten gelatine filter No. 22 will give yellow light of wavelength 5780 A.U., while No. 77 will isolate the green of wavelength 5461 A.U. Alternatively, the following double-cell liquid colour filters may be used:

For yellow light—

Cell A (30 mm thick): Saturated aqueous solution sodium dichromate.
Cell B (10 mm thick): Aqueous solution copper sulphate 11·1 g/100 c.c.

For Green Light—

Cell A (26 mm thick): Sol. cupric chloride in ethyl alcohol 4·75 g/100 c.c.
Cell B (10 mm thick): Sol. cobalt chloride in acetone 1·4 g/100 c.c.

These cells are very effective, and although they transmit rather less light than the corresponding Wratten filters, they are cheaper and not liable to damage by heat from the lamp.

Sodium-vapour discharge lamps, which give practically monochromatic light without filters, are also available. Although they are more expensive than mercury-vapour lamps the saving in cost, and the greater convenience, due to the absence of colour filters should be borne in mind when deciding between the two.

Cameras

Photo-elastic polariscopes are usually built up by individual investigators rather than purchased complete, so that it is usual to adapt a standard type of camera to suit particular requirements and preferences. Thus, if a large number of photographs are to be taken, and if suitable enlarging facilities are available, it is convenient and economical to use a 35 mm. miniature camera. If large-size glass negatives are preferred a half-plate camera of orthodox design is very suitable. The essential requirements are a good quality anastigmat lens, and ample extension of the bellows. (Miniature cameras will require extension collars.)

A plate camera possesses the great advantage that the model can be focused and examined on the ground glass screen at a reasonable magnification before taking a photograph. Special focusing arrangements are necessary in the case of miniature cameras.

Optical Systems of Typical Polariscopes

The optical system of a polariscope using "Polaroids" for polarizer and analyser is shown in fig. 46. The light from the source L is brought to a parallel beam by the small lens B and condenser lens C_1 and polarized by the "Polaroid" P. If a suitable type of lamp is used, lens B may be omitted. The analyser may be placed before or after the second lens C_2, which together with the camera or projection lens D throws an image of the model on the photographic plate or screen, S. Particular attention should be paid to the selection of the lenses C_2 and D; the former should be of good quality, free from internal strains, and may conveniently have a focal length of from 12 to 15 inches. A bi-convex lens in this position appears to be preferable to a plano-convex from the point of view

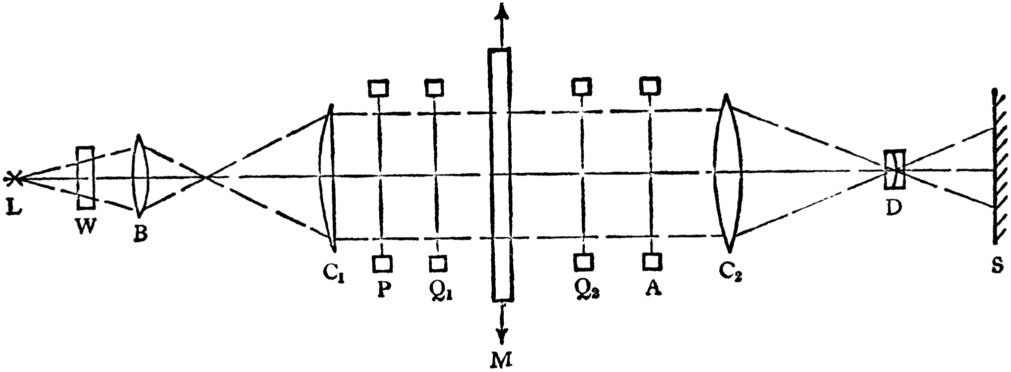

Fig. 46.—Optical system of a polariscope using " Polaroid " filters

L—Light source; W—Water cell and/or colour filter; B—Focusing lens; C_1C_2—Condenser lenses; P—Polarizer; A—Analyser; Q_1Q_2—Quarter-wave plates; M—Model; D—Projection or camera lens; S—Screen or photographic plate

of avoiding distortion. When it is required to project a large image on a screen for demonstration purposes, lens D should be an achromatic doublet of about 17 inches focal length; with a 15-inch biconvex lens at C_2 this will give an image of the model magnified about twelve times at a distance of ten feet.

If circularly polarized light is required the quarter-wave plates Q_1 and Q_2 are placed before and after the model. When colour filters are required for isolating monochromatic light from a mercury-vapour lamp, these are placed at W. If liquid colour filters are used they also serve as a water cell protecting the apparatus from the heat of the lamp; if white light is being used it is advisable to include a clear water cell for this purpose.

If economy has to be studied, the size of the second quarter-wave plate and the analyser may be reduced by placing them at the focus of C_2, or the optical system of fig. 46 may be modified in such a way as to use only one large diameter lens, Polaroid, and quarter-wave plate. The arrangement in this case is indicated in fig. 47.

The system of fig. 48 using Ahrens or Glan-Thomson prisms for the polarizing filters gives the highest possible degree of polarization and greatest intensity of transmitted light. The concave lenses bringing the beam parallel to pass through the prisms may be omitted, with some sacrifice in performance. A polariscope of this type would be very expensive, and is employed only where the greatest accuracy is required.

For certain special experiments in which the models show only a few fringes, reflecting polariscopes are employed. The optical system of such a polariscope is shown in fig. 49. From this it will be seen that the light beam passes twice through the model, so that the retardation is doubled. The surfaces of the model must be flat and parallel to each other and to the reflector, otherwise the

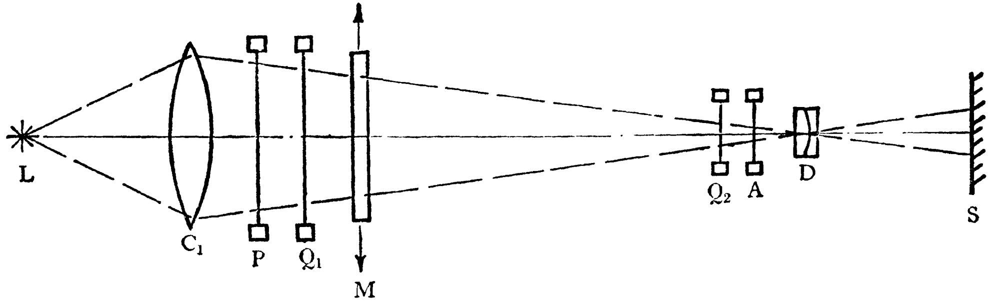

Fig. 47.—Modified optical system using only one large-diameter lens, " Polaroid " and quarter-wave plate

Fig. 48.—Optical system of a polariscope using Glan-Thomson or Ahrens prisms for polarizer and analyser

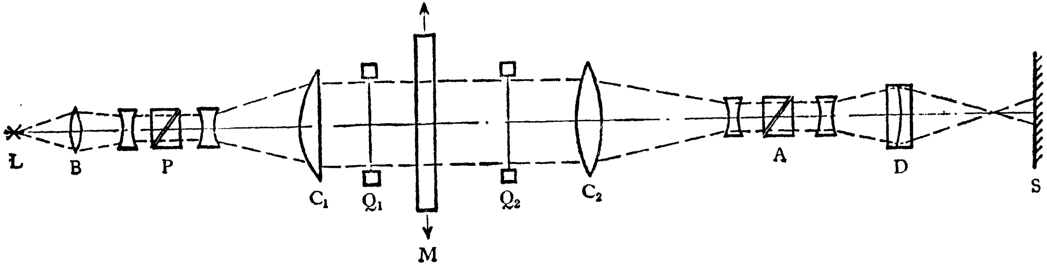

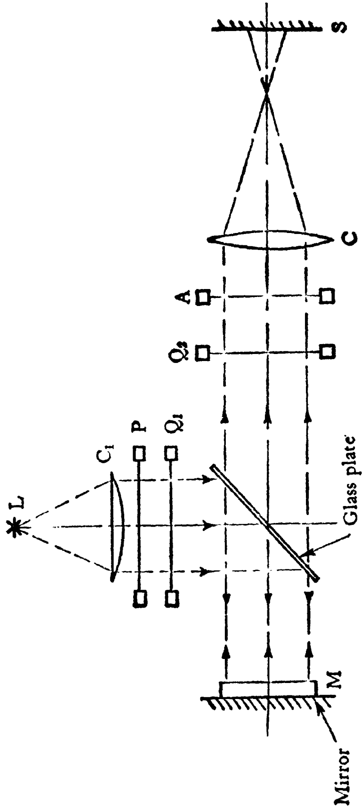

Fig. 49.—Optical system of a reflection polariscope

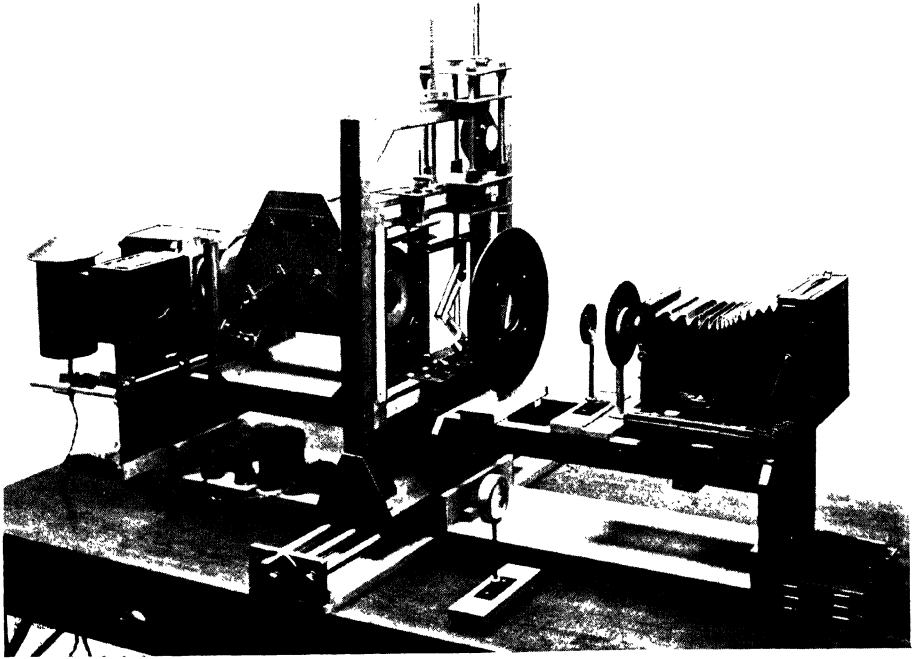

G 314

Fig. 51.—General view of polariscope with glass-plate reflection polarizer

fringe pattern will be blurred. Reflection polariscopes are not recommended for general use.

Polariscopes using lenses and Polaroids are very expensive if the diameter of the field is greater than about six inches; it has been suggested in this connexion that large concave mirrors might be used in such a case instead of lenses, with some saving in cost. However, a very satisfactory large-field polariscope can be constructed using a sheet of plate glass for the polarizer and a Polaroid disc for the analyser. In this case the light source consists of a bank of lamps behind a diffusing screen, and the first quarter-wave plate is a sheet of Cellophane. The apparatus is shown in outline in fig. 50. A polariscope of somewhat similar type was used by the late Prof. E. G. Coker for several of his investigations.

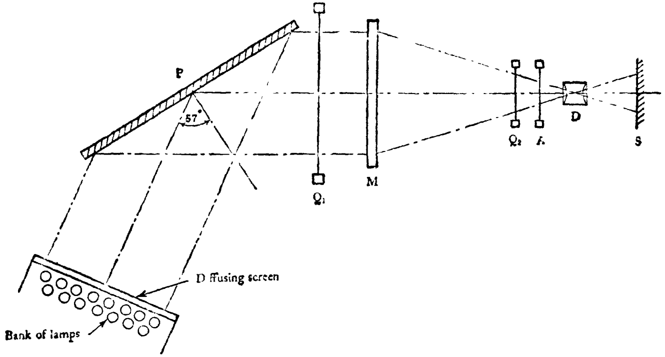

Fig. 50.—A large-field polariscope with glass plate polarizer and "Polaroid" analyser

The Design of Polariscopes

As examples of the actual design of polariscopes, figs. 51 and 52 show the general arrangement of the two polariscopes in use in the Engineering Department of Aberdeen University.

The apparatus of fig. 51 has a three-inch diameter field and can be used either for projection or for photographic work. Alternative light sources fitted at the end of the optical bench give either white or monochromatic light; the latter may be either the green or yellow from the mercury spectrum according to the liquid colour filter employed. Both lamp-houses are fitted with collimating lenses, and in both provision is made for centring and focusing the lamp. The polarizer is of the triple-reflection glass-plate type, and the analyser is a small Polaroid disc placed near the focus of the second condenser lens.

The camera is a standard half-plate one with a 7½-inch, *f*/8 Ross anastigmat lens. For projection, the camera is replaced by a 17-inch achromatic doublet.

The model under test is carried in the straining frame shown in fig. 53 (facing p. 92). As will be seen from this, the straining frame is constructed in such a way as to enable any part of the model to be brought into the light beam from the polarizer. The model and loading gear are carried by an inner frame, which can be moved vertically within the outer frame by a screw gear. The whole frame is mounted on rails and can be moved transversely to the axis of the polariscope by a lead screw and hand wheel. The frame is so designed that many different types of models and loading arrangements can be set up within it. Three methods of loading a specimen in tension are shown in fig. 53. Girder models can be accommodated by fixing two steel flats horizontally across the inner frame; these flats are shown in front of the straining frame in fig. 53 with a Vierendeel girder model resting on adjustable roller supports

The second polariscope shown has a 6-inch diameter field and uses Polaroids for the polarizer and analyser. Only one lamp-house is used in this case; the projector and mercury-vapour lamps are carried on adjustable

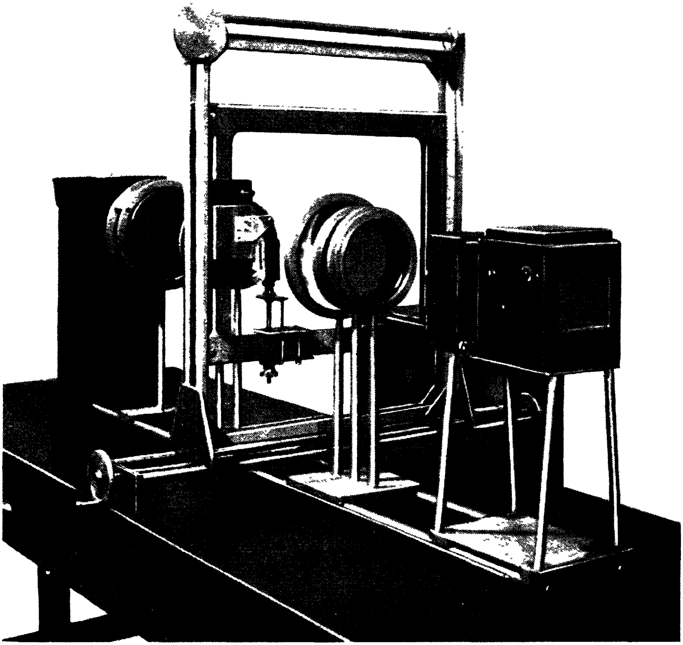

G 314

Fig. 52.—General view of a large polariscope with " Polaroid " filters

stands, which rest on the rails of the optical bench and are thus very easily interchanged. The straining frame is built up from Duralumin plate and angle; the inner frame is suspended by steel wires instead of a central screw, thus leaving the top bar entirely unobstructed for the attachment of loading gear.

The polariscopes shown here are typical designs for general photo-elastic testing. Many variations are, of course, possible, and may be necessary to suit the requirements of a particular investigation.

CHAPTER VI

Compensators and other Instruments

While the polariscope forms the essential apparatus for photo-elasticity, there are a number of other instruments which may have to be employed in the course of photo-elastic investigations. These include various types of compensators for measuring relative retardations in models and crystal plates, an interferometer specially adapted for the measurement of absolute retardations due to strain, and apparatus for the measurement of the sum of the principal stresses.

Compensators

A compensator is an instrument consisting essentially of a crystal plate, the effective thickness of which can be varied at will, so that the relative retardation between the emergent plane-polarized components is variable between certain limits. The variation in the effective thickness is controlled by a micrometer screw, or other device, calibrated to read the corresponding retardation. The purpose of the instrument is to measure the relative retardation at any point in a crystal plate or photo-elastic model. This is done by setting the compensator so that the retardation imposed by the instrument is exactly equal and opposite to the retardation being measured.

Compensators are employed in photo-elastic work in cases where the stresses being measured are too small to produce a satisfactory fringe pattern in the model. They may also be employed for carrying out quantitative analyses with white light; this method was used frequently by Coker and Filon, but is rarely necessary with the sensitive materials now available for models.

It should be mentioned that the manipulation of compensators requires considerable care, and the position of compensation is not always easy to determine with accuracy. This is especially true if the observations are made with white light, as the retardation produced by a crystal plate varies according to the wavelength of the light transmitted; unless this *dispersion* effect is the same in the test-piece and compensator, exact compensation cannot be obtained. As a rule, better results are obtained using monochromatic light.

The Babinet Compensator

The Babinet compensator consists of two superimposed wedges of quartz, which is a uniaxial crystal. As shown in fig. 54*a*, the first wedge is cut so that the optic axis of the crystal is parallel to the line of intersection of the wedge faces, while the optic axis of the second wedge is at right angles to this. The effective thickness of the combination is at every section equal to the difference in thickness of the two wedges; thus at point O in fig. 54*b* the wedges are of equal thickness and the effective optical thickness is zero for the combination.

If the wedges are examined in the polariscope in mono-

G 314

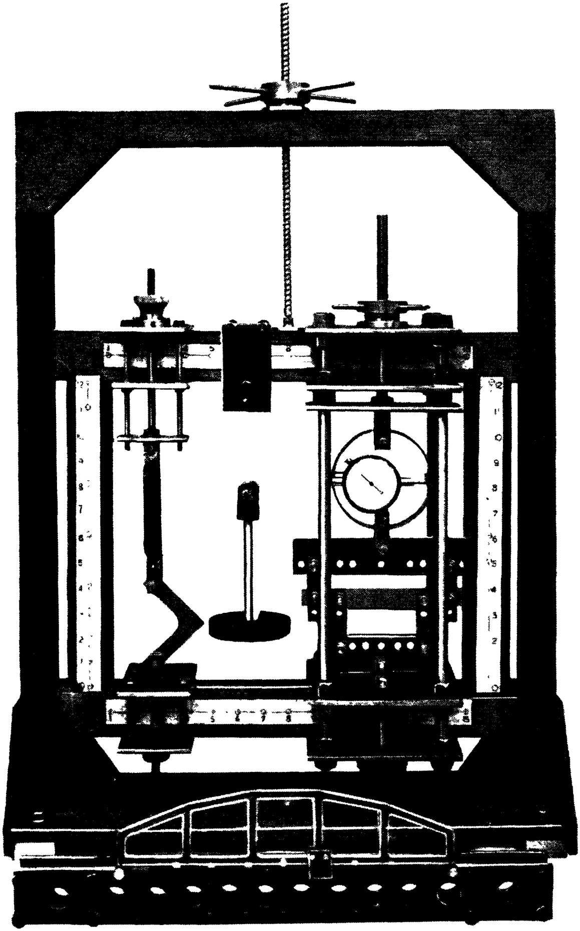

Fig. 53.—Straining frame for polariscope of fig. 51

chromatic light, their appearance will be as in fig. 54*c*, that is, there will be a central band, along which the retardation will be zero, flanked on each side by a series of dark bands corresponding to sections where the combined thickness produces a retardation of an integral number of wavelengths of the light used.

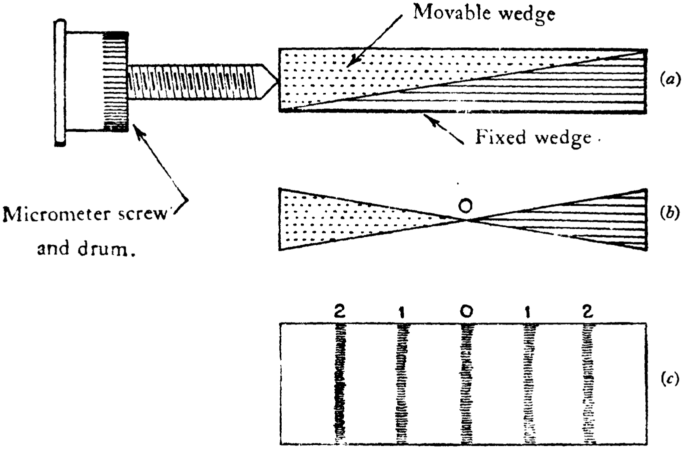

Fig. 54.—The Babinet compensator
(*a*) Construction of the compensator. (*b*) Effective thickness of the combination
(*c*) Appearance in the polariscope in monochromatic light.

In the actual instrument, one of the wedges is fixed and the other can be displaced laterally by means of a micrometer screw. When the movable wedge is centrally placed with respect to the fixed wedge, the micrometer reads zero and the position of the zero-order fringe is marked by a line engraved on the fixed wedge.

Suppose now that it is desired to measure the retardation produced by a uniform crystal plate. The compensator and specimen are set in the field of the polariscope so that their polarizing axes coincide and are at 45° to the azimuth of polarization of the light from the polarizer.

The set of parallel fringes crossing the compensator will be displaced and the zero-order fringe will now appear at one side or the other of the fixed reference line. The micrometer screw is then rotated until the zero-order fringe once more coincides with this line; when this is done, the change in effective thickness of the plates produces a relative retardation exactly equal to that produced by the specimen. The " fast " axis in the compensator, however, coincides with the " slow " axis in the specimen, and so this change in the effective thickness of the plates exactly cancels out the retardation due to the specimen and restores the initial conditions. The micrometer screw carries a graduated drum, calibrated to read relative retardations in appropriate units.

The retardation at any point in a photo-elastic model can be measured in exactly the same way, the directions of polarization being determined from the isoclinic lines.

Retardations as small as one-hundredth of a wavelength can be measured with considerable accuracy with this instrument.

The Soleil-Babinet Compensator

This instrument is a modified form of the Babinet compensator consisting of two similar quartz wedges and a quartz plate of uniform thickness arranged as shown in fig. 55. In this case the optic axes of the wedges are parallel, so that the two wedges combine to form a plate of uniform effective thickness. The optic axis in the plate is at right angles to the optic axes in the wedges so that if the wedges are adjusted to form a plate of the same thickness as the parallel plate, the overall retardation will be zero.

If the movable wedge is displaced by the micrometer screw, the composite plate will be thicker or thinner than the uniform plate, depending on the direction of the displacement, and the overall effect will be to introduce a relative retardation between the two plane-polarized components emerging from the compensator. The Soleil-Babinet compensator thus amounts to a uniform crystal plate whose effective thickness can be varied at will, within certain limits; its appearance in the polariscope in monochromatic light will thus be uniformly light or dark, as compared with the banded appearance of the Babinet.

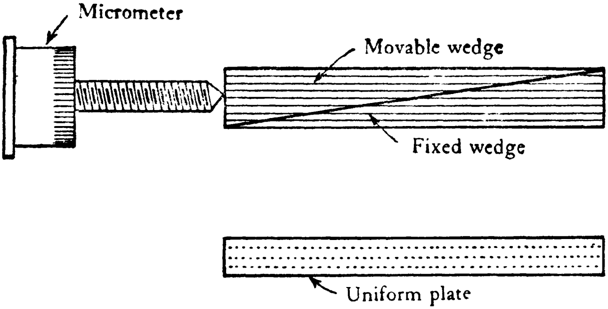

Fig. 55.—The Soleil-Babinet compensator

In use, the instrument is set with its polarizing axes parallel to the polarizing axes in the specimen and the micrometer drum is adjusted until extinction is obtained.

A Mica-plate Compensator

The quartz wedges required for the Babinet and Soleil-Babinet compensators require very careful preparation, and the instruments are consequently rather expensive. For photo-elastic work, an inexpensive but effective compensator has been devised using a single mica plate. The principle of the instrument was suggested by Prof. T. C. Phemister of Aberdeen University.

As is well known, muscovite mica can be easily cleft into thin plates; if such a plate is examined in the plane polariscope, being held so that the light beam is incident normally on the plate, two orientations will be found for which no light will be transmitted through the analyser. These correspond to two of the *principal axes* of the mica plate, the third principal axis being at right angles to these. The indices of refraction for light travelling in the directions of the principal axes are known as the *principal indices of refraction* for the crystal and their values are found to be about 1·57, 1·588 and 1·60 respectively. If a plate (fig. 56) lies with its face in the XY-plane and oriented with the principal axes along XX and YY, the axis associated with the intermediate index of refraction of the plate lying along XX, then a light disturbance originating at a point O will be transmitted through the plate as a two-sheeted wave. The trace of the wave surface on the YZ-plane is shown in the diagram by a circle (C) and an ellipse (E). Consider now a wave whose normal N_i lies in the YZ-plane, to enter the plate at an angle of incidence i. Corresponding to the refracted wave normal N_r are two wavefronts whose traces on the YZ-plane are F_1 and F_2. Thus on leaving the mica plate, the incident light will have been broken up into two components having a certain relative path retardation; in addition, these two components are plane-polarized in directions at right angles to one another.

If the angle of incidence is such that the refracted wave normal lies along OP or OP′, there is only one wavefront, the line at right angles to OP being a common tangent to C and E. OP and OP′ are the *optic axes* of the crystal. In this case there is obviously no relative retardation, and if the plate is examined in the polariscope at this inclination, the field will remain dark. The value of i corresponding to this condition is about 34·5°. If the incident beam enters along the Z-axis, i.e. normal to the face of the plate, the retardation is at its maximum, the value depending on the thickness of the plate.

The construction of a compensator of this type is illustrated in fig. 57 (facing p. 102); the mica plate is set as described above and so arranged that it can be rotated

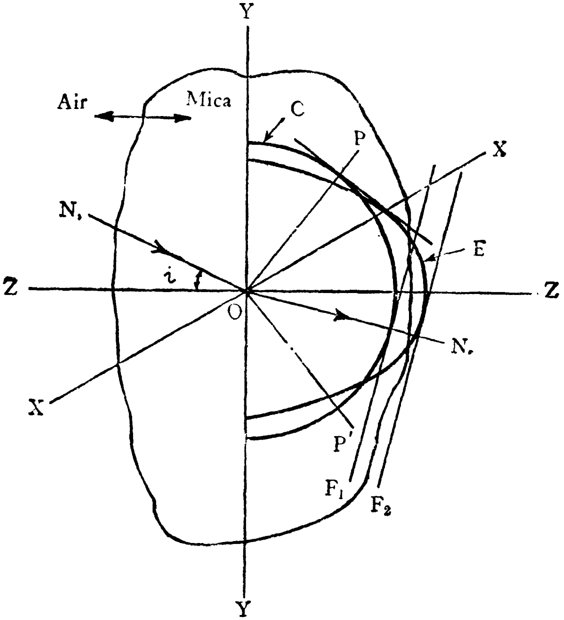

Fig. 56.—The mica-plate compensator

about the X-axis, so that any retardation from zero to a certain maximum can be obtained by varying the inclination of the mica plate relative to the incident light beam. The angle of rotation is measured to half a degree by a suitable scale, and the corresponding retardation is obtained from a calibration graph which may be constructed by means of plates of known retardation.

The calibration can also be effected by calculation and in a typical mica plate, for which the intermediate index of refraction was 1·588 and the apparent angle between the optic axis and the normal to the surface of the plate 34° 36′, it was found that the relation between the angle of incidence, i, and the retardation was given by

$$R = n\lambda \, . \, k,$$

where k is a function of i.

i	0°	5°	10°	15°	20°	25°	30°	34·5°
k	1·00	0·98	0·92	0·82	0·69	0·52	0·31	0

As will be observed, $n\lambda$ is the retardation produced by the plate when its surface is normal to the light beam. In the absence of an instrument for measuring this, the mica plate can be cleft so that it gives a retardation of $\frac{1}{4}$, $\frac{1}{2}$ or 1 wavelength of the light being used—this can be verified in the manner described on p. 81. The values quoted for k will be sufficiently accurate for most purposes, and, when $n\lambda$ is known, a calibration curve can be drawn of retardation in Ångström units against angle of rotation.

The mica-plate compensator is used to measure retardations in the same way as the Soleil-Babinet compensator.

The Coker Tensile Strip Compensator

A useful compensator for photo-elastic purposes consists simply of a strip specimen cut from the same sheet of material as the model under test, arranged so that it can be subjected to tensile stress and oriented in any desired direction in a plane parallel to the plane of the model.

To use the instrument, it is set in the polariscope (using white light), and its inclination adjusted so that the axis of the compensator lines up with the direction of the minor principal stress in the model at the point under consideration. The stress on the compensator specimen is then gradually increased until compensation is obtained. The stress in the compensator specimen gives the principal stress difference in the model directly.

This type of compensator was developed by Coker and employed extensively in his investigations, in which he used celluloid models and white light.

The Photo-elastic Interferometer

As we have seen in the foregoing chapters, the relative path retardation between the two plane-polarized components transmitted through a photo-elastic model is proportional to the difference between the principal stresses, and it is this quantity which we obtain from the monochromatic fringe pattern. If, instead of the *relative* retardation between the two components, the *absolute* retardation of *each* component is measured, then the separate principal stresses will be obtained directly.

This can be done by means of an *interferometer*, the most suitable type being the modified form of the Jamin interferometer used by Favre and others for this purpose. The optical system of the instrument is shown in fig. 58. Monochromatic light from the source L is brought to a parallel beam and polarized by the filter P. The beam is then divided by the half-silvered mirror M_1, being partly reflected and partly transmitted. The latter component passes through a glass block C_1, and is reflected by the silvered mirror M_2 through two lenses arranged to narrow the light beam to a point as it passes through the model M. Half-wave retardation plates are placed on each side of the model at H_1 and H_2; the purpose of these plates is to enable the plane of polarization of light entering the model to be set at any desired azimuth, the effect of a half-wave plate being merely to alter the direction of polarization. This component of the light beam

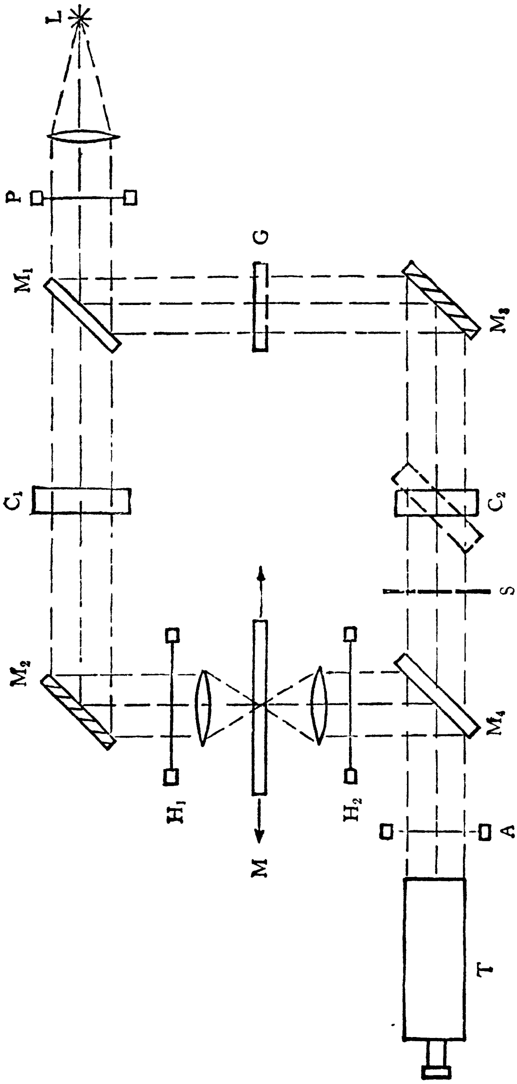

Fig. 58.—The photo-elastic interferometer

is now reunited with the component reflected by M_1 and M_3, at the half-silvered mirror M_4, and after passing through the analyser A enters the viewing telescope T. Glass plates C_1, C_2 and G are also introduced in the positions shown; C_1 and C_2 are of the same thickness, and G introduces a retardation roughly equal to that due to the lenses and the model.

In using the instrument, the model is loaded and the direction of polarization of the light passing through the model is measured by rotating the half-wave plates together, until the field of the telescope is dark. The azimuth of polarization of the light passing through the model now coincides with the direction of one of the principal stresses, so that the light wave comes through the model without being split into two components, and the retardation suffered by its passage is due only to this principal stress.

The analyser is now removed, the component of the light beam from M_3, which has meantime been cut out by a stop S, is allowed to enter the telescope and the model is unloaded. The total effective path lengths of the components coming round the two sides of the interferometer will be slightly unequal, so that an interference fringe pattern will be observed in the field of the telescope. If the model is now reloaded, the interference fringes seen in the telescope will be displaced laterally due to the additional retardation introduced by strain; this retardation is proportional to the magnitude of the principal stress corresponding to the direction of polarization of the light wave passing through the model. The fringes are next restored to their original position in the telescope field by increasing the effective path length of the component which does not pass through the model; this is done by rotating the glass plate C_2 so that the light has to travel through a slightly greater thickness of glass. The rotation of this compensator plate can be calibrated to read retardation, or stress direct.

The other principal stress at the same point is measured in the same way by rotating the direction of polarization of the light entering the model by 90°.

A complete stress analysis is obtained by carrying out these measurements at closely spaced points over the model. The procedure is therefore rather laborious and the apparatus is much more delicate than the ordinary polariscope—for example, it must not be subject to any vibration and considerable care is necessary in setting it up. Further, it is necessary that the models should be optically flat, otherwise the interference fringes will be blurred.

In spite of these disadvantages, the fact that a complete solution is obtained without further experiment or calculation makes the interferometer method attractive and worthy of further development.

Lateral Extensometers

As we have seen in Chapter IV, it is possible to determine the sum of the principal stresses at any point in an elastic plate by measuring the change in thickness of the plate due to the stresses; to do this, a very sensitive lateral extensometer is necessary. Although mechanical and optical instruments have been devised, the most convenient lateral extensometers convert the small mechanical deformation into a change of electrical resistance, inductance or other quantity which can be conveniently measured. Two typical electrical instruments for the measurement of small changes of thickness will therefore be described.

The first makes use of the well-known electrical resistance strain gauge and is shown diagrammatically in fig. 59. As will be observed, the gauge consists simply of a U-shaped brass frame with resistance elements placed in

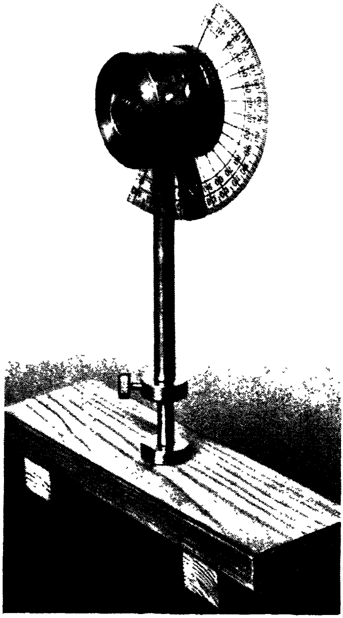

Fig. 57.—Mica-plate compensator

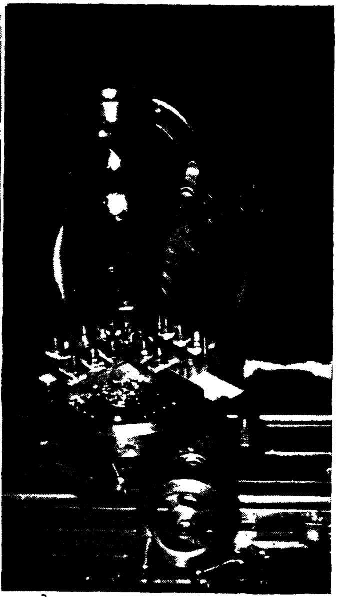

Fig. 66.—Model being cut in a vertical milling machine

the positions shown. The instrument is clamped lightly over the specimen by means of the adjusting screws, so that subsequent alterations in its thickness produce corresponding alterations in the strains in the limbs to which the gauges are cemented.

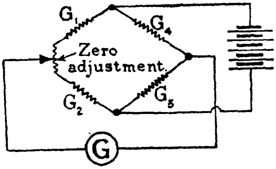

Circuit diagram

The gauges are arranged to form a bridge circuit, and the out-of-balance potential across the bridge is indicated by a suitable galvanometer calibrated to read the lateral strain of the test piece by means of a simple tension specimen. By making the calibration specimen of the same material and thickness as the model on which the actual readings are to be taken, the galvanometer can be calibrated to read $(P + Q)$ directly, which is of great convenience in photo-elastic work.

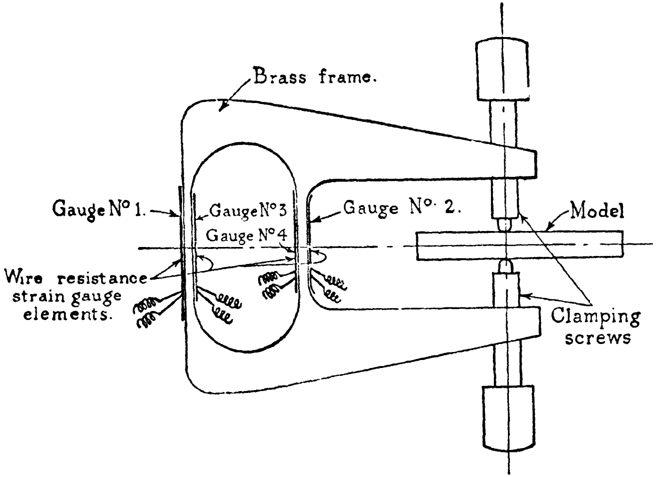

Fig. 59.—Electrical lateral extensometer

Fig. 60 shows a Taylor and Hobson " Talymit " comparator adapted for use as a lateral extensometer. In this instrument, change of thickness of the specimen causes an alteration in the inductance of an electrical circuit, and the change of thickness is indicated directly on a suitably calibrated microammeter.

The gauging head is carried in a stand, which allows readings to be taken at every point in the model under test.

Membrane Analogy Apparatus

In this method of measuring $(P + Q)$ in a stressed elastic plate, a template is erected round the boundary of the plate, the height of which is at every point proportional to the edge stress (see fig. 61). A uniformly stretched rubber sheet is now clamped over the template, and the height of the surface which the rubber takes up is measured with a depth gauge to give the value of $(P + Q)$ at any required point. Alternatively, the model and edge-stress template can be made to a smaller scale, and a soap film stretched over it to serve as the membrane.

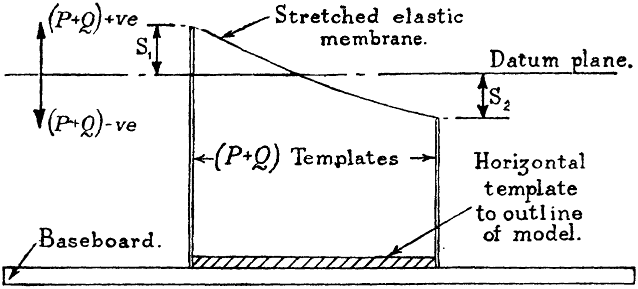
(P+Q)+ve
S₁
Stretched elastic membrane.
Datum plane.
S₂
(P+Q)-ve
(P+Q) Templates
Horizontal template to outline of model.
Baseboard.

Fig. 61.—Sectional diagram illustrating the construction of templates for the membrane analogy method. Dimensions s_1, s_2 &c., are made proportional to the edge stresses at the corresponding points in the model.

In both cases the apparatus is relatively simple and, using a rubber sheet, the set-up is as indicated in fig. 62.

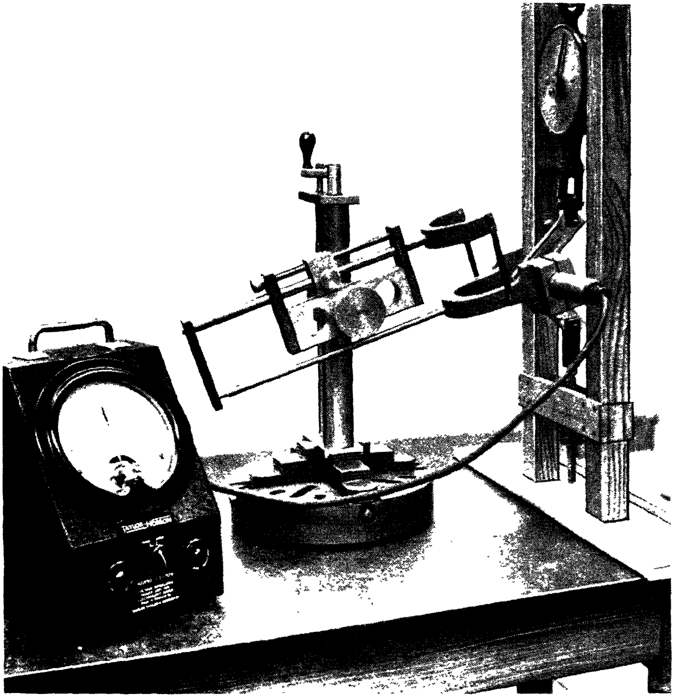

G 314

Fig. 60.—Taylor and Hobson " Talymit " gauge

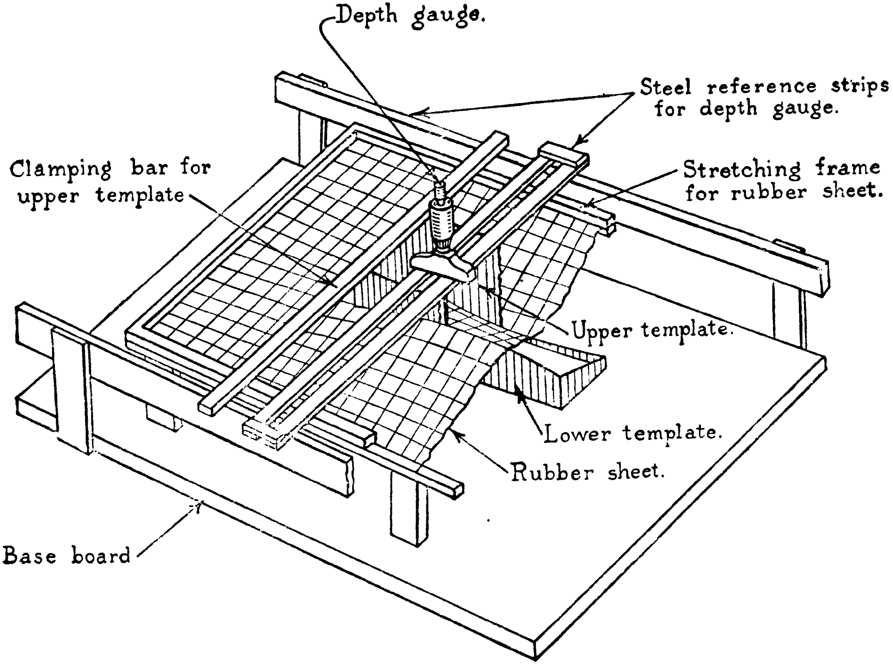
Depth gauge.
Steel reference strips for depth gauge.
Clamping bar for upper template
Stretching frame for rubber sheet.
Upper template.
Lower template.
Rubber sheet.
Base board

Fig. 62.—General view of apparatus for the membrane analogy method using a stretched rubber sheet

In carrying out an experiment using the rubber sheet apparatus, the sheet must be uniformly stretched before it is clamped over the template; this is achieved by ruling it off in, say, one inch squares, and stretching it in a suitable frame until the squares are one and a half times their original size. The template is made in two mating sections and the rubber sheet is clamped between them, great care being taken to avoid pinching it at any point and thus preventing it from taking up its correct surface.

Using a soap film, the apparatus is rather easier to set up, the main precaution being to keep the under-side of the template open—if this is not done the air trapped under the soap film may cause it to bulge upwards, and thus lead to false readings. The film has to be renewed frequently during an experiment as it is easily punctured by the point of the depth gauge.

In both cases the depth gauge is carried by a carefully levelled system of steel strips.

The membrane analogy method has a good deal to commend it in that the apparatus is inexpensive and the experimental technique fairly simple. A considerable amount of work, however, is involved in making the necessary templates and in setting up the apparatus, but once this is done results are rapidly obtained and gross errors are unlikely.

CHAPTER VII

Photo-elastic Materials

The essential properties of a transparent material for photo-elastic models may be summarized briefly under the following headings:

(1) The material must be isotropic, i.e. must show no double refraction before the application of external loads.

(2) The material must be easily machined without chipping or showing appreciable machining stresses. It must also be hard enough to withstand without injury any moderate pressures due to jig clamps and fixtures used in the machining operations.

(3) The material should be transparent, as nearly colourless as possible and easily polished.

(4) The material should possess reasonably high elastic moduli, so that the deflections of the model are not excessive. Moderate tensile strength and freedom from strain creep are also desirable. (If a material is subjected to stress, there is an immediate corresponding strain; if, now, the material continues to elongate or contract under constant stress, this additional strain is known as *creep*.)

(5) The stress-optical sensitivity should be high and the optical creep effect small. (The latter manifests itself as a continuous decrease in the model fringe value with time.)

(6) The stress-strain and stress-retardation relations should be linear.

(7) The optical and mechanical properties of the material should remain constant at room temperatures.

(8) The cost of the material should be moderate and supplies readily available.

No known material satisfies all these requirements, and the material selected will depend on the type of model being investigated and the information required. For example, high sensitivity is usually an advantage, but if only the isoclinic lines are being studied, an insensitive material is desirable as the isoclinics can then be observed without a fringe pattern.

The properties of a number of suitable materials are tabulated on p. 109. This list includes the materials most commonly used in this country, but as the number of transparent plastics available is large and steadily increasing, it is not necessarily complete. The phthallic anhydride (glyptal), polyvinyl, and polystyrene groups, for example, may contain plastics suitable for photo-elasticity. Again, the figures quoted above are only intended to be typical values; the physical properties in many cases vary considerably with time, and from one sample to another. The properties must therefore be determined when required for the material actually being used.

Bakelite BT-61-893

This colourless, transparent Bakelite, which is perhaps the best material so far available, is manufactured specially for photo-elastic purposes by the Bakelite Corporation of America, and supplied in Great Britain through Bakelite, Ltd., London.

The properties of the material have been fully investigated in America by Frocht, Hetényi and others. It is obtainable in sheets about 12″ × 6″ and in various thicknesses.

Usually, initial double refraction is small, but if not, annealing is possible by heating the sheet in a suitable oven to about 120° C. and allowing it to cool down very slowly over a period of 24 hours. The sheet being annealed should be laid flat on a glass plate; no weights of any sort should be placed on top of it. The Bakelite frequently warps when it is annealed, so that the plate must be machined flat before cutting a model from it.

The machineability is good and models can be cut by turning, milling, sawing, &c., with ordinary tools.

TABLE III

Properties of Materials for Photo-elastic Models

Material	Composition	Tensile Strength (lb/in²)	Young's Modulus (lb/in²)	Poisson's Ratio	Unit Fringe Value* (lb/in²)	Stress-Optical Coefficient (Brewsters)
Bakelite: BT-61-893 †	Cast phenol-formaldehyde	17,000	615,000	0·365	91·0	36·3
Catalin 800 (uncured)	Cast phenol-formaldehyde	2,000	200,000	—	20·2–31·2	164–106
Catalin 800 (fully cured)	Do.	7,000	300,000	0·42	39·5	83·5
Perspex (unplasticized)	Methyl-methacrylate	7,000	500,000	0·38	856	3·9
Transpex II	Do.	7,000	500,000	0·38	338	13·7
Celluloid	Camphorated nitrocellulose	7,000	300,000.	0·4	225	14·7
Plate glass †	—	—	9,000,000	0·25	1040 3180	3·2–1·0
Gelatine †	13% aqueous solution	—	6	—	0·15	20,000

*Value of $(P-Q)$ for 1st order fringe in plate 1" thick, for light of wavelength 5780 A.U.

† Value from Frocht.

The stress-optical sensitivity is satisfactory, and both stress-strain and stress-fringe order relations remain linear up to about 6000 lb/in^2. Optical and mechanical creep are present, but are usually inappreciable.

The properties of Bakelite are sensibly constant at room temperatures, so that no errors due to alterations in room temperature during a photo-elastic test need be expected.

Bakelite is strongly recommended for work where a high degree of accuracy is required. Its cost, however, is extremely high, and for ordinary work a material such as Catalin, available at a fraction of the cost, is entirely satisfactory. There are also a number of less expensive grades of Bakelite, made in America, with properties intermediate between those of BT-61-893 and Catalin.

Catalin-800

Catalin is made in Great Britain by Messrs. Catalin, Ltd., Waltham Abbey. Like Bakelite, it is a phenol-formaldehyde condensate, but its properties differ considerably from the BT-61-893 material just described.

Catalin is readily available in sheets of any desired thickness; it is very sensitive to the photo-elastic effect, is colourless and usually practically free from initial double refraction. Its main disadvantages are low elastic modulus and high creep rate. Fortunately, the nature of the creep in such that it does not cause distortion of the fringe pattern.

Recently manufactured Catalin has a low elastic modulus and its creep rate is excessive; this is illustrated in fig. 63, which shows the variation of the unit fringe value in a specimen four months old up to one hour after loading. Mechanical or strain creep is correspondingly large, and Young's modulus varies continuously; thus, in carrying out a tensile test to obtain the stress-strain relation, it is necessary to measure the total strain at some

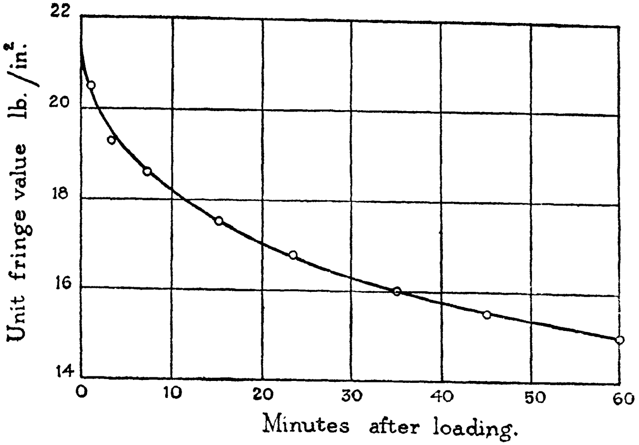

Fig. 63.—Variation of unit fringe value with time in uncured " Catalin "

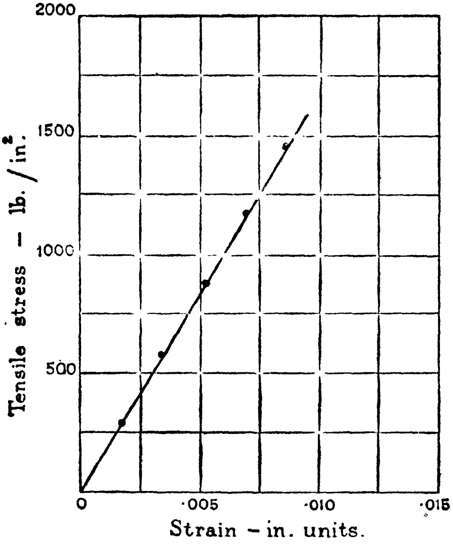

Fig. 64.—Stress-strain relation for " Catalin " specimens four months old, uncured, 10 minutes loading (E = 167,000 lb/in^2)

definite time after loading for several values of the applied load. Fig. 64 shows the result of such a series of tests. E for the material of this specimen was 167,000 lb/in^2, based on a ten-minute loading period. The stress-strain relation is practically linear up to about 1500 lb/in^2. It has been found that analyses can be carried out even with the material in this state, provided that the model fringe value is determined from a specimen loaded for the same length of time as the model itself.

The mechanical properties are considerably improved simply by storing the material at room temperature. The effect of ageing is shown in the following table:

Specimen No.	Age (Months)	Minutes after Loading	Unit Fringe Value (lb/in^2)	Remarks
1	17	10	31·2	Material stored at room temperature.
2	10	10	29·5	
3	6	10	20·1	
3	6	30	15·7	
4	6	10	39·5	Cured at 80° C. for 20 hours.
4	6	30	37·6	

From this table it will be observed that the stress-optical sensitivity diminishes very considerably as the material ages; the strength and elastic moduli, however, increase. A comparison of the unit fringe values for Specimen No. 3, 10 minutes and 30 minutes after loading, shows that considerable optical creep which has taken place.

By baking the material at a suitable temperature its properties can be considerably improved. A satisfactory procedure is to place the Catalin on a glass plate inside a steel container and keep it at a constant temperature of 80° C. for 20 hours or more, according to the age of the material. The container is placed in an oil bath, the temperature of which is raised from room temperature to 80° C. in about one hour and, after the required length of time at the latter temperature, is cooled down over a period of about eight hours. This slow cooling rate is to ensure that the material cools uniformly, thus avoiding the possibility of uneven contraction and consequent internal strain. The action of this heat treatment, known to chemists as " curing ", is believed to be the expulsion of small particles of water formed as a by-product of the chemical combination of phenol and formaldehyde, and also a continuation of the cross-linking of the molecules in the material. Curing at 80° C. does not appear to remove large initial double refraction if this is present, but the material might be annealed by heating to a rather higher temperature (100–120° C.). This should only be done after prolonged baking at 80° C., and then with the greatest caution to avoid damage to the plate. It is inadvisable to heat Catalin in direct contact with oil as it tends to absorb the liquid, and thus some arrangement such as that suggested above should be employed.

The effect of curing on the photo-elastic properties is shown by comparing the tests on specimens Nos. 3 and 4 above; the stress-optical sensitivity has been almost halved, but the creep effect has been quartered—the unit fringe value has altered 5·4% between 10 and 30 minutes after loading as compared with a 21·7% decrease in the uncured material.

Catalin which has been aged or cured is quite satisfactory for general use, but in view of its rather low elastic modulus models should preferably be not less than $\frac{1}{4}$ inch thick to avoid unduly large deflections. Small models as thin as $\frac{1}{8}$ inch can, however, be used on occasion as the sensitivity is very high and enables a satisfactory fringe pattern to be developed without over-stressing the material.

Catalin is easily machined and polished, and with ordinary precautions large machining stresses are rarely observed.

The author has found that Catalin is suitable for the construction of flanged models which can be milled out of, say, half-inch thick plate. The sensitivity of the material is high enough to allow the web stresses to be studied from the fringe pattern, and its favorable machining characteristics allow the large amount of machining necessary to be carried out without appreciable stresses being developed.

Xylonite Celluloid

Celluloid was the first plastic to be used for photo-elastic models and the wide application of the method to engineering problems was made possible by its introduction, in the early years of the present century, by the late Prof. Coker.

Chemically, celluloid is entirely different from Bakelite and Catalin, being made from nitrocellulose and camphor. Compared with the phenolic resins it is comparatively insensitive to the photo-elastic effect, and its use is now more or less confined to the construction of built-up models, where the fact that it can be very easily cemented to itself is an advantage.

The grade of celluloid known as Xylonite is suitable for photo-elastic models. Its properties are rather variable and are found to improve with ageing. Creep is observed in the material and is found to be rather more complicated than in Catalin, so that it cannot be overcome by the expedient of calibrating the fringe pattern from a tensile specimen loaded for the same length of time as the model. However, the creep in celluloid several years old is quite small.

Large sheets of Xylonite in various thicknesses are obtainable from the British Xylonite Co., Ltd. The sheets are polished by the makers and the material is very easily machined; it is not so brittle as Bakelite and thus not so liable to chip during machining.

Glass

Although a glass model has been used for the solution of a practical engineering problem by photo-elasticity, it is rarely employed owing to its low stress-optical sensitivity and the great difficulty of cutting models from it. As already mentioned, however, an insensitive material is sometimes required, and in a limited number of cases where the model is of a very simple shape, glass might be used.

Unplasticized Perspex

Perspex, made by Imperial Chemical Industries, Ltd., is a methyl methacrylate plastic. The unplasticized material possesses a number of useful properties for photo-elastic purposes. It has a reasonably high elastic modulus, its transparency is excellent and it can be easily machined. The stress-optical sensitivity is low, approaching that of glass, so that when such a material is required, unplasticized Perspex is invaluable.

Its applications include the construction of models for the study of isoclinic lines and models of riveted and other connexions involving overlapping plates. For the latter purpose one of the plates would be of a sensitive material and the others of Perspex, so that the stress distribution in the sensitive plate could be studied without the fringes in it being confused by the passage of the light through the other plates in the connexion. An example of this type of model is shown in Chapter IX.

Samples of ordinary Perspex to which the plasticizer has been added have been examined, but do not appear to be suitable for photo-elastic models due to large initial

Catalin is easily machined and polished, and with ordinary precautions large machining stresses are rarely observed.

The author has found that Catalin is suitable for the construction of flanged models which can be milled out of, say, half-inch thick plate. The sensitivity of the material is high enough to allow the web stresses to be studied from the fringe pattern, and its favorable machining characteristics allow the large amount of machining necessary to be carried out without appreciable stresses being developed.

Xylonite Celluloid

Celluloid was the first plastic to be used for photo-elastic models and the wide application of the method to engineering problems was made possible by its introduction, in the early years of the present century, by the late Prof. Coker.

Chemically, celluloid is entirely different from Bakelite and Catalin, being made from nitrocellulose and camphor. Compared with the phenolic resins it is comparatively insensitive to the photo-elastic effect, and its use is now more or less confined to the construction of built-up models, where the fact that it can be very easily cemented to itself is an advantage.

The grade of celluloid known as Xylonite is suitable for photo-elastic models. Its properties are rather variable and are found to improve with ageing. Creep is observed in the material and is found to be rather more complicated than in Catalin, so that it cannot be overcome by the expedient of calibrating the fringe pattern from a tensile specimen loaded for the same length of time as the model. However, the creep in celluloid several years old is quite small.

Large sheets of Xylonite in various thicknesses are obtainable from the British Xylonite Co., Ltd. The sheets are polished by the makers and the material is very easily machined; it is not so brittle as Bakelite and thus not so liable to chip during machining.

Glass

Although a glass model has been used for the solution of a practical engineering problem by photo-elasticity, it is rarely employed owing to its low stress-optical sensitivity and the great difficulty of cutting models from it. As already mentioned, however, an insensitive material is sometimes required, and in a limited number of cases where the model is of a very simple shape, glass might be used.

Unplasticized Perspex

Perspex, made by Imperial Chemical Industries, Ltd., is a methyl methacrylate plastic. The unplasticized material possesses a number of useful properties for photo-elastic purposes. It has a reasonably high elastic modulus, its transparency is excellent and it can be easily machined. The stress-optical sensitivity is low, approaching that of glass, so that when such a material is required, unplasticized Perspex is invaluable.

Its applications include the construction of models for the study of isoclinic lines and models of riveted and other connexions involving overlapping plates. For the latter purpose one of the plates would be of a sensitive material and the others of Perspex, so that the stress distribution in the sensitive plate could be studied without the fringes in it being confused by the passage of the light through the other plates in the connexion. An example of this type of model is shown in Chapter IX.

Samples of ordinary Perspex to which the plasticizer has been added have been examined, but do not appear to be suitable for photo-elastic models due to large initial double refraction; however, it is possible that strain-free samples might be selected.

Gelatine

Gelatine has entirely different properties from the materials already described, and is used only for special investigations, particularly in cases where the stresses in the model due to its own weight are comparable with those due to the external loads. Thus, gelatine models have been used for the photo-elastic study of stress-distribution problems in soil mechanics. For example, the stress distribution in embankments and in the foundations of a gravity dam have been investigated and, although there are obvious differences between soils and gelatine, the information obtained from these tests has been most instructive and, in some cases, has been corroborated by the known behaviour of earth masses.

Gelatine is extremely sensitive to the photo-elastic effect, which of course leads to its use for models of the type mentioned above. The exact value of the stress-optical coefficient is very variable, depending on the concentration used and on the presence or absence of glycerine. The models are made by casting the gelatine in suitable moulds and the fringe pattern may be calibrated by making a rectangular slab and setting it up vertically; examined in the polariscope, this shows a series of equally spaced horizontal bands due to the weight of the block itself. The pressure on any horizontal section is vertical and is determined by calculating the weight of gelatine per unit area above the section. Thus the stress corresponding to any of the horizontal fringes in the calibration model can be found.

The technique used in making and testing gelatine models is, however, rather specialized, and it is not proposed to discuss these matters in detail.

CHAPTER VIII

The Preparation of Models and Test Procedure

Although it is one of the advantages of the photo-elastic method that gross errors in the test results are improbable, the accuracy of the analysis is very largely dependent on the careful preparation of the model and attention to detail in the actual test procedure. The technique of the method, however, is not unduly difficult and is soon acquired.

As the models for most photo-elastic tests are cut from plates of cast phenolic resin, such as Bakelite or Catalin, the procedures to be described refer mainly to these materials. Celluloid, Perspex, and other plastics can be machined in the same way, but some are, for example, difficult to cut by sawing and the polishing technique may be different.

Selection of Material

The sheet of material from which a model is to be cut should preferably not be of very recent manufacture, as many plastics appear to improve with ageing. The sheet is first examined in the polariscope to make sure that it is free from initial double refraction. In general, the edges of the plate will show pronounced double refraction and will have to be discarded along with any other unsatisfactory areas; these areas are conveniently marked with a wax pencil. A simple, large-field, glass-plate polariscope may be fitted up for carrying out this inspection as it is usually inconvenient to examine large plates in the optical bench type of polariscope used for the analysis of relatively small models.

If the plate has been annealed or cured, it may be warped, and it will then be necessary to machine it flat at this stage; this is best done by surfacing it in a lathe.

Polishing

Before polishing, the plate should be cut roughly to the shape of the finished model, leaving a margin of about $\frac{1}{16}$ inch round the boundaries; there is no point in polishing areas which are later to be cut away and scrapped.

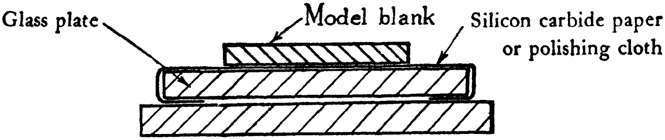

Fig. 65.—Grinding and polishing model blanks

The plate is now ground flat by hand. This is best done by laying a sheet of silicon carbide paper on a glass plate in the manner indicated in fig. 65. The type of papers used by coachbuilders for cellulose finishing, e.g. " Hydro-durex-sil " made by the Durex Abrasive Co., is very suitable and can be obtained in a number of different grades. The grinding should be carried out first with a coarse paper, using plenty of water, to remove deep scratches and machining marks. The model is now ground on a fine paper until the scratches due to the first paper disappear. Having repeated this with a third, finer, paper, the blank will be ready for polishing. Throughout the grinding process, the thickness of the plate should be checked with a micrometer at numerous points to ensure uniformity.

Polishing is done in the same way, using a " Selvyt " cloth and alumina instead of the silicon carbide paper.

Dry polishing is not recommended, but any fine liquid metal polish will give satisfactory results.

It is essential that all the polishing operations should be completed before machining the model to its final dimensions, as polishing unavoidably rounds off the edges of the plate.

Machining

The polished blank is now cut to its final dimensions by sawing and filing, turning or milling according to the outline of the model and the degree of accuracy required.

Where the analysis is of a qualitative nature, the outline may be scribed on the plate, the model trimmed to within $\frac{1}{16}$ inch of its final dimensions by fret-saw, and completed by careful filing to the scribed lines. It is rather difficult to see fine scribed lines on the transparent material, so that a coat of marking-off paint may be applied and carefully removed when the model is completed. Alternatively, the photo-transfer method of marking off could be employed.

If strict dimensional control is required, and particularly if a series of models is being examined differing only, say, in the size of a fillet, it is convenient to use steel templates. The blank is clamped between a pair of accurately made templates, and the excess material removed by filing. This method ensures that the edges of the model are accurately square, which would not necessarily be the case if only a single template was used.

A rotary filing machine may be used, but it is advisable to complete the filing by hand in order to avoid machining stresses.

Discs, rings and similar shapes are most conveniently made by turning in a lathe, which should also be employed for boring large-diameter holes. Low speeds and feeds and light cuts are necessary to avoid chipping, and the cutting tool should be frequently honed. No coolant is necessary.

Vertical milling is an extremely useful and accurate method of cutting models, although it is rather slow. A pantagraph engraving machine can be employed to cut elaborately shaped models from templates, but a wide variety of models involving straight and circular profiles can be cut in an ordinary vertical milling machine fitted with a rotary table.

Fig. 66 (facing p. 102) shows a model being cut in a milling machine; a circular stud plate is fitted to the rotary table and the model is fixed down on it by small wooden clamps. Two steel reference bars, fixed at right angles to one another near the edge of the stud plate, and a countersunk centre point facilitate the setting-up operations. A piece of thick cardboard should be placed under the model, and when machining an edge, the final cut should be taken well into the cardboard as this ensures that the lower corner will not be chipped. As in turning, low speeds and feeds and light cuts are essential to avoid chipping and setting up machining stresses. Also, a sharp cutter is of paramount importance in avoiding these defects in the finished model—this point can hardly be over-emphasized. The use of a coolant makes little difference to the machining stresses and is not really necessary if the above precautions are observed.

The edges of the model may be machined by a combination of side and end milling, using a cutter of not less than ½-inch diameter. The use of smaller cutters should normally be restricted to end milling as their rigidity is deficient and they tend to chip the material if used for side milling.

The materials can be drilled with twist drills, but care must be taken to avoid chipping when the drill breaks through—it is advisable to drill through into another

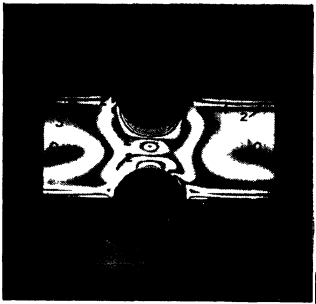

Fig. 68.—Time-edge effects in a notched beam subjected to pure bending, showing complete distortion of the fringe pattern.

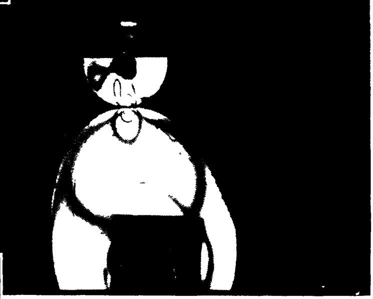

Fig. 70.—Fringe pattern in cam and roller in plane polarized light.

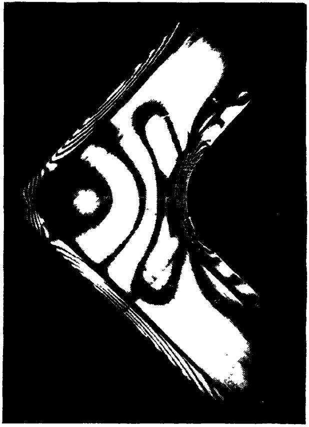

Fig. 71.—Fringe photograph for flanged L frame

plate of the same material to avoid this. Twist drills leave quite large machining stresses, so that holes around which the stresses are to be examined should be bored in the lathe or milling machine.

Preparation of Flanged Models

Flanged models, for example of I section, can be satisfactorily milled from thick plates of Catalin in the following manner. The model blank is cut and polished as already described; polishing the blank ensures that the edges of the flanges in the finished model are transparent. The blank is now fixed down on the milling-machine table, and the outer boundaries of the model machined; the clamps holding down the model must, of course, be shifted from time to time as each edge is cut.

The flanges and web are next formed by a combination of end and side milling, the depth of cut being measured as the work proceeds so as to get the correct web thickness. When one side is completed and the model turned over, the first side is carefully packed to prevent any distortion of the web when the second side is being cut. To avoid leaving deep circular marks on the web at the end of a finishing cut, the end play on the milling machine spindle must be kept down to a minimum. When the machining is finished, the web is ground and polished, using strips of silicon carbide paper and small wooden blocks. It is difficult to polish the web of a flanged model to the same finish as can be obtained on a flat plate, particularly at re-entrant corners in the flange, but satisfactory results can usually be obtained.

Test Procedure

When the preparation of a model is completed, it must be tested immediately; if left for even a few hours, edge effects may appear and cause distortion of the fringes near the edges.

The model is placed in the straining frame of the polariscope, and adjusted so that it is accurately at right angles to the light beam. This can be checked by examining the appearance of the edges on the screen; if they appear as broad black lines, the edges are not parallel to the light beam (see fig. 67*a*). In some cases this " space effect " may be due to the edges of the model not being square to the surface, as indicated in fig. 67*b*. In the latter case, it will not be possible to get rid of the effect on all the boundaries at the same time, and it will then be necessary to adjust the inclination of the model so as to get a well-defined boundary at important points. If the model has been machined carefully, the edges should be accurately square, but if the space effect is excessive it may be necessary to make another model.

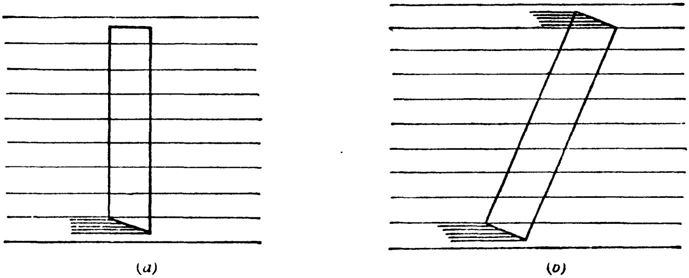
(*a*) (*b*)

Fig. 67.—Space effects (*a*) owing to inclination of model to light beam, (*b*) owing to edge of model not being square to its surface

The model is next examined for machining stresses or other defects and, if found satisfactory in this respect, the load is applied. The development of the fringe pattern as the load is applied should be observed on the camera screen, so that the fringe orders can later be identified from the photograph. If the fringe pattern is to be calibrated by a separate test, the model should be photographed at a definite time after loading, to allow for optical creep. The fringe photograph is taken in circularly polarized monochromatic light.

If the isoclinics are required, the white light source is next set in position, the quarter-wave plates removed, and an image of the model projected to a convenient scale on a glass screen from which the isoclinics are traced on to a sheet of paper. Using a mirror, it is a simple matter to arrange the glass screen so that it is horizontal, with the paper on top of it; the isoclinics can then be plotted with greater facility than if a vertical screen is used.

It may sometimes be desired to photograph the isoclinics and, in this case, it is better to make a separate Perspex model which will show these lines clearly without a fringe pattern. An alternative procedure is to photograph the model used for obtaining the fringe pattern in white light on a panchromatic plate. The panchromatic plate will give an approximately equal rendering of all the colours, so that, with a fairly long exposure, the stress pattern will appear simply as a white blur on the print, against which the black isoclinics will stand out distinctly.

Photography

It is obviously impossible to quote exposure times for photographing the fringe pattern, as these will vary from one apparatus to another, depending on intensity of the light source, type of polarizer and analyser, and on many other factors. The exposure time for any particular polariscope must therefore be determined initially by exposing a few test plates; once this has been done, the investigator will be able to judge the exposure for any subsequent test with reasonable accuracy.

The plates used should have a fine-grained, contrasty emulsion, and if the monochromatic light used is yellow, a panchromatic plate is necessary. Kodak P.150, rapid process panchromatic plates are thus satisfactory for general purposes.

The plates may with advantage be *slightly* over-exposed and fully developed; subsequent reduction in ferricyanide-hypo solution will then bring about maximum possible contrast between the black and white areas on the print. If there is a stress concentration in the model, however, considerable care is necessary to get the exposure exactly correct in order that the very fine lines in the vicinity of the stress concentration should show up clearly.

Prints off the negatives may either be contact or enlargements; generally, it will be necessary to use enlarged prints for making measurements on the fringe pattern. A contrasty bromide paper, such as Kodak B.G.4, is suitable.

Colour photographs are not required for quantitative work, although it may be desired on occasion to make such photographs for demonstration purposes. In this case, " Kodachrome " cut film may be employed with satisfactory results.

For full details of plates, formulæ for developers, and similar information, reference should be made to a standard manual of photography.

Sources of Error in Photo-elastic Tests

As in all experimental work, there are in photo-elasticity various sources of error which must be guarded against. Errors may arise due to defects in the optical apparatus and due to the imperfect elastic behaviour of the model material, but these are likely to be small in comparison with errors arising from the following causes, which should be carefully noted.

(*a*) *Initial Anisotropy in the Model.*—This may be due to a variety of causes. If the model appears uniformly light, or approximately so when examined in the polariscope before being loaded, this would indicate that the plate from which it was cut was not isotropic. This is, of course, avoided by inspection and selection of the material before cutting the model; it is advisable to inspect the material before and after polishing as rough handling during the grinding and polishing operations may quite easily introduce internal strains.

Machining stresses are always recognized by the bright appearance of the edges of the model; they are rarely appreciable in the interior. Machining stresses are always compressive at the edge and may lead to slight distortion of the fringes where they intersect a boundary.

If the model is not tested immediately after machining, a " time-edge " effect may appear, due, apparently, to the release of some volatile constituent and to rounding off on the edges due to spontaneous cold flow in the material. After a time, quite high order fringes appear near the edges, and in this condition the model is quite useless as the fringe pattern is entirely distorted; this is illustrated in fig. 68 (facing p. 121). The effect is much less marked in phenolic resins which have been aged or cured for a considerable time.

If initial double refraction is at all appreciable, say of the order of a tenth of a fringe, there is no remedy but to prepare a new model; the amount of initial double refraction which can be tolerated, however, will vary according to circumstances.

(*b*) *Accuracy of Model.*—It is hardly necessary to point out that the accuracy of a test is entirely dependent on the dimensional accuracy of the model. The tolerances which can be allowed in machining will depend to some extent on the size of the model. For example, if we consider a beam specimen 0·750 inch deep, the variation in depth must be restricted to about ±0·002 inch to ensure that the stresses in it, when it is subjected to pure bending, will not vary by more than 2% along its length. This degree of accuracy is not difficult to achieve, but to attain the same degree of accuracy in a beam 0·500 inch deep, a variation of only ±0·001 inch would be permissible.

Small variations in thickness are not so serious, as retardation is proportional to stress and to thickness; thus, reducing the thickness may be expected to increase the stress proportionately and the retardation would remain constant. The variation in the thickness of a plate, however, need not exceed about 0·002 inch if ordinary precautions are taken in grinding and polishing.

Space effects, as we have already seen, may be due to careless machining. Where they are noticeable in the fringe photograph they cause inaccuracy in the determination of the edge stresses. The image of the model on the camera screen should be very carefully examined for this effect before photographing, and if it cannot be eliminated by adjustments in the polariscope, it is almost certainly due to the edges of the model not being square to the surface. This can arise in hand-filing operations, and even in milling and turning if the model is not clamped flat on the working table or face plate.

(*c*) *Faulty Loading Conditions.*—Loads, where possible, should be applied by hanging weights, with or without a lever arrangement. Where spring balances are used they must be adjusted frequently to maintain a constant load, as the load will tend to fall off due to strain creep.

Frictional effects giving rise to indeterminate reactions must be guarded against. For example, the end reactions for a simply supported beam on knife edges would not be vertical, as assumed in elementary mechanics—an unknown horizontal thrust would be developed due to frictional resistance to the stretching of the fibres in its lower edge. This would certainly affect the fringe pattern in a photo-elastic test but could, of course, be overcome by placing a roller support at one end.

Care must also be taken to avoid the introduction of irrelevant stress systems due to buckling or eccentric loading. Unintentional stresses of this sort may sometimes be detected by inspection, but this may not always be the case. The loads should therefore be applied through carefully designed fixtures, carefully adjusted and not large enough to cause excessive stresses in the model.

(*d*) *Creep.*—If photo-elastic grade Bakelite is used for the model, creep may be neglected, but if Catalin is used it is essential to calibrate the fringe pattern from a specimen loaded for the same length of time as the model or by calculating the stress at some point in the model where the fringe value is known; the latter is the more accurate procedure but cannot always be applied.

According to Filon, the creep in celluloid cannot be allowed for in the above manner and the results inevitably contain an error due to this cause. Fortunately, the creep in celluloid which has been aged for a number of years is very small and the error inappreciable.

(*e*) *Temperature Effects.*—As has been mentioned, the properties of Bakelite BT-61-893 are sensibly constant at room temperatures, but this is by no means true in the case of most other phenolic resins, which show marked changes in stress-optical coefficient and other properties with a change in temperature of even a few degrees. It is therefore important to observe that the model and calibration specimen are tested at the same temperature; if this precaution is observed there will be no error due to this cause.

CHAPTER IX

Practical Applications of Photo-elasticity

During the past thirty years, the photo-elastic method has been applied to a large number of engineering problems, particularly to the investigation of stress concentrations due to holes, notches and discontinuities in structural and machine elements, and to the stress analysis of rings, chain links, hooks, and other parts of complicated shape not readily dealt with by mathematical methods. Other problems investigated by photo-elasticity range from the analysis of highly redundant bridge girders to the study of cutting stresses in machining operations.

To illustrate in greater detail the type of problem in which the photo-elastic method is likely to be of value, a few applications will be described in this chapter. It is not intended to deal with each example exhaustively, the aim being merely to bring out the possibilities and limitations of the method.

Stress Concentration Problems

If a straight, parallel tie-bar has a notch or a hole cut in it, the maximum stress set up in the bar when subjected to load would, in general, be considerably greater than the average stress obtained by dividing the load by the reduced cross-sectional area. The ratio of the actual maximum to the average stress is termed the *stress concentration factor.* It is quite difficult to determine the stresses in such a member by mathematical analysis, but the solution by photo-elastic methods presents no difficulty whatever. Graphs of the stress concentration factors for different sizes of holes or notches can be drawn for design purposes and, of course, more complicated examples can be dealt with in a similar manner.

In machine design, it is frequently necessary to reduce the section of a shaft, for example at its end where it enters a journal bearing. The section at which the diameter decreases is thus subject to bending and shear, and has long been known as a section of weakness in the shaft out of proportion to the reduction of the diameter. This problem has been investigated by flat photo-elastic models, representing a longitudinal section or slice out from the shaft, and it has been found that a stress concentration exists at the section of the discontinuity; this stress concentration can be greatly reduced by a fillet, and numerous experiments have been carried out to determine the variation of the stresses with the size of the fillet under various loading conditions, with a view to establishing just how large the fillet should be.

The results of such a set of tests are summed up in a graph showing stress concentration factor plotted against the ratio of the size of radius to the depth of the smaller section. A typical graph of this type is shown in fig. 69.

Stress concentrations reduce the fatigue strength of a shaft and the photo-elastic tests give a valuable indication of the existence of dangerously high stresses. At this point, however, it is necessary to remark that the fatigue strength of different materials is affected in varying degrees by stress concentrations, and in the case of a low-carbon steel shaft, the fatigue strength is not reduced as much as would be expected from consideration of the stress concentration factor alone.

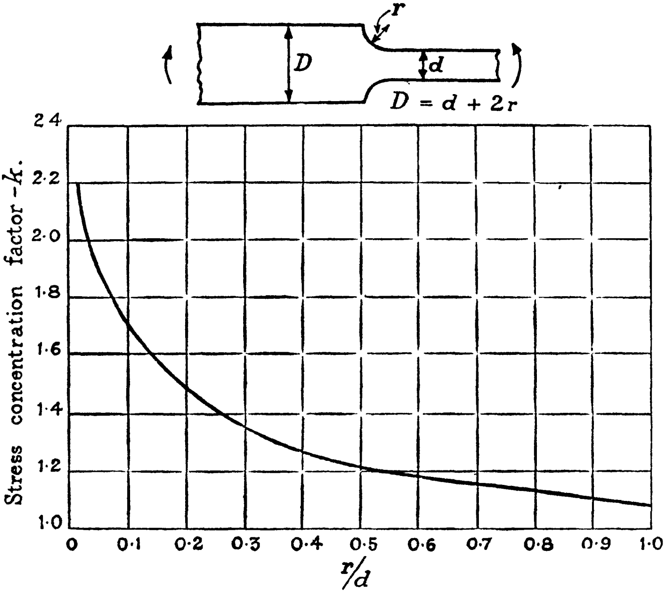

Fig. 69.—Stress concentration factors for shaft of varying diameter (Frocht, *Journal of Applied Mechanics*, 1935)

Contact Stress Problems

Another type of problem investigated by the photo-elastic method is the analysis of stresses in rollers, cams, gear teeth, and the like. Again mathematical solutions are possible in a number of simple cases, but are usually rather complex, and problems involving irregular boundaries or complicated load systems cannot be dealt with by the theory of elasticity.

As an example of a contact stress problem fig. 70 (facing p. 121) shows the fringe patterns in a cam and its roller follower at one particular position; the stresses in both parts can be followed as the camshaft is rotated through a full revolution.

Other problems in this category which either have been or might be investigated include the stress distribution in foundation blocks, the stresses in beams resting on an elastic continuum, and the local stresses in crane gantry girders due to wheel loads.

The Stress Distribution in Structural Members and Details

The stress distribution in various kinds of beams has been investigated by photo-elasticity. For example, Coker and Filon have shown that the ordinary bending theory is inaccurate for short, deep beams, and more recently Frocht's investigation of the shear-stress distribution in rectangular beams has shown this to be very much more complicated than is usually assumed.

The author has recently used the photo-elastic method to study the stress distribution in a particular type of structural connexion met with in rigid frame bridges and building frames. The members in these structures carry bending and direct loads, and the connexions between them must be able to transmit bending moments from one member to another. In this way they differ from the so-called " pin-jointed " structures in which the member loads are assumed to be axial and the connexions incapable of transmitting bending moments. The stress distribution in rigid frame connexions is difficult to analyse mathematically, and a series of experiments using flanged photo-elastic models was carried out to study the stress distribution in one particular type.

The joints examined connected two parallel flanged beams the axes of which intersected at right angles. The fringe photograph of fig. 71 (facing p. 121) shows the appearance of a typical model in the polariscope, and from it the shear-stress distribution in the web is obtained.

Tests were carried out on a number of other frames, varying the radius on the inner flange and the length of the legs of the L. Fig. 72 shows the variation of the maximum shearing stress in the connexion for different radii and leg lengths.

In order to check the photo-elastic results, three steel frames, dimensionally similar to the small-scale models, were tested using an electrical resistance strain gauge to measure the strains. Comparisons between the results were fairly good as can be judged from the points in fig. 70 showing corresponding values for the steel frames and photo-elastic models plotted on the same diagram.

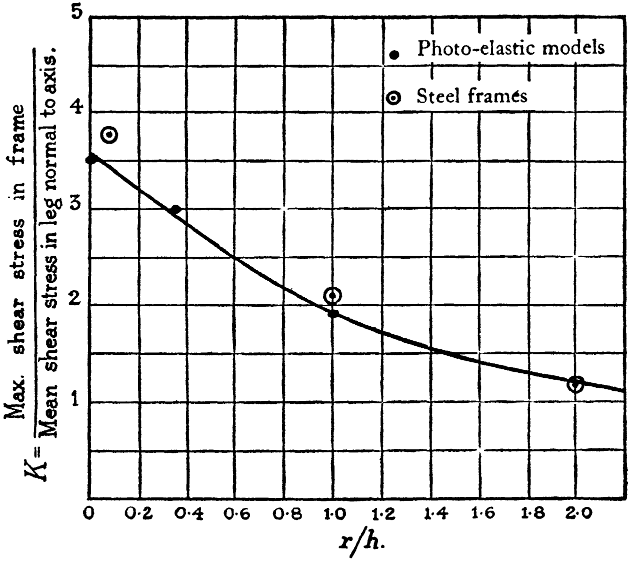

Fig. 72.—Variation of coefficient *K* in steel frames and photo-elastic models with size of radius

It was also found possible to determine the actual stresses in the steel frames from the photo-elastic model by applying dimensional similarity principles; the web of the model was made geometrically similar in outline to that of the steel frame, and it was assumed that the loads applied to the webs of the model and steel frame by the flanges were proportional, the areas and inertias having been made proportional in the following manner. The cross-section of the leg of the model was such that the ratios of the moment of inertia of one flange to the moment of inertia of the whole section, and the area of the web to the area of the whole section, were the same in the model as in the steel frames. The formula

$$f = f_m \cdot \frac{d_m}{d} \cdot \frac{t_m}{t} \cdot \frac{P}{P_m}$$

was then applied (see Chapter I, p. 18) to find the ratio between the stresses in the steel frame (f) and the stresses in the model (f_m). On this basis, the maximum shearing stress in the steel frame corresponding to the model shown in fig. 71 was estimated at 1·35 tons/in^2 as compared with the measured value of 1·4 tons/in^2.

It may be concluded from this and from a number of other comparisons, that photo-elastic tests of this sort give a reliable representation of the stresses in flanged steel constructions.

The Analysis of Highly Redundant Structures

Photo-elasticity can be profitably employed for the analysis of certain types of highly redundant structures where the calculations for a mathematical solution, although perhaps not fundamentally difficult, tend to be rather tedious. This is especially true as the calculations have usually to be repeated two or three times due to modifications necessary in the sections of the members originally selected.

The Vierendeel girder, shown in fig. 73*a*, is a typical example of this type of structure. As will be observed

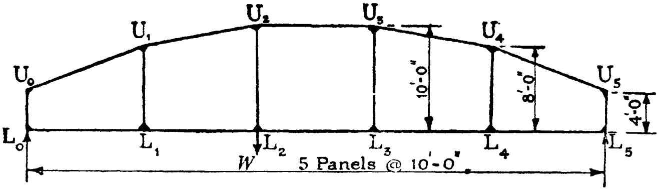

(*a*) Outline of Vierendeel girder

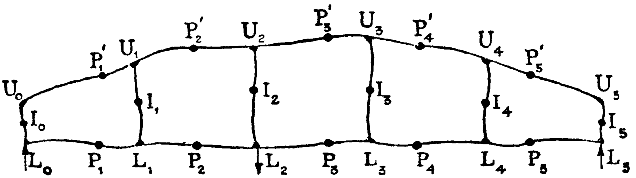

(*b*) Deflected form of girder

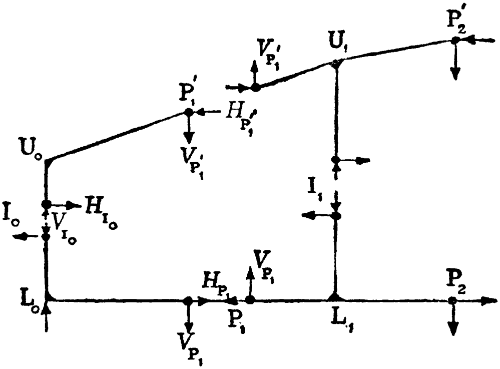

(*c*) " Free-body " diagram

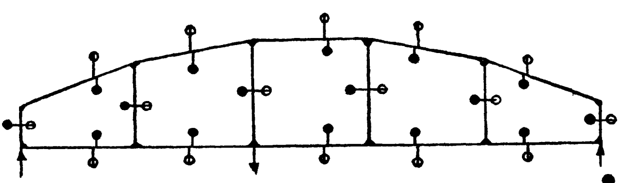

(*d*) Points of inflexion

Fig. 73.—Photo-elastic analysis of an inclined chord Vierendeel girder. For a full discussion of the analysis of this truss, see paper by D. Young, *Trans. A.S.C.E.*, 1937, Vol. 102.

from fig. 73*b*, which shows the deflected form of the girder under a single panel load, there is a point of inflection in each member where the bending moment changes sign, and if the positions of these points are known, it is possible to calculate the axial loads, moments and shears in every member by simple statics. At a point of inflection the bending moment is, of course, zero, and the forces in the members are found by breaking down the truss and applying the conditions of statical equilibrium. Thus, the section $P_1L_0U_0P_1'$ is first considered: taking moments about P_1' we obtain H_{P1}, which is equal to $H_{P'1}$. Then considering the part $P_1L_0I_0$, and taking moments about I_0, we obtain V_{P1}, and so on until all the forces at the points of inflection are known. It is then a simple matter to calculate the bending moments at the connexions. The arithmetical work is short and self-checking.

Now it is possible to locate a point of inflection in a member of a photo-elastic model with reasonable accuracy simply by inspection, due to the characteristic appearance of the fringes and isoclinic lines. The appearance in the polariscope of one panel of the girder which we are considering is shown in fig. 74 (p. 136). Fig. 73*d* shows a comparison between the positions of these points determined in this manner with the positions found mathematically.

The suggested procedure in designing a structure of this sort, using the photo-elastic method, would be, first, to analyse a girder taking all the members of uniform section; the sections of the members are next adjusted in the light of this analysis to give a more uniformly stressed structure. With a few trials, suitable areas and inertias for the full-sized structure can be found, and the work completed by a final mathematical analysis. This is much less laborious than having to repeat the mathematical work several times, and the experimental analysis gives a reliable check on the final calculations.

Many other highly redundant structures could be dealt with in a similar manner with considerable saving in time and labour.

The Stress Distribution in Riveted and other Connexions

The stresses in plates around bolt holes, at the heads of eye-bars and in welded joints have all formed the subject of photo-elastic research at one time or another. Strictly speaking, the results of tests in which forces are applied to the boundaries of holes are subject to small corrections, as described in Chapter I, p. 15, if Poisson's ratio is different for the materials of the model and prototype. Usually, however, the corrections are small and local, and may often be neglected.

The stress distribution in eccentrically loaded rivet groups would undoubtedly be an interesting subject for photo-elastic investigation. The simple theory used for the design of such connexions is by no means conclusive, and experiments which would confirm the validity of this theory or lead to improvements would be most useful. The models used would be of the composite type, using plates of sensitive and insensitive materials. As an example, the fringe photograph of fig. 76 (facing p. 136) shows the results of a test on the simple bracket of fig. 75. The bracket consists of two Perspex plates, and is connected to a Catalin plate by a group of six close-fitting $\frac{1}{4}$-inch diameter brass pins.

✓Conclusion

The examples quoted above by no means exhaust the list of applications of the photo-elastic method to engineering problems, but they make it clear that photo-elasticity is likely to be of value in cases where a mathematical solution is difficult or impossible, and as a sub-

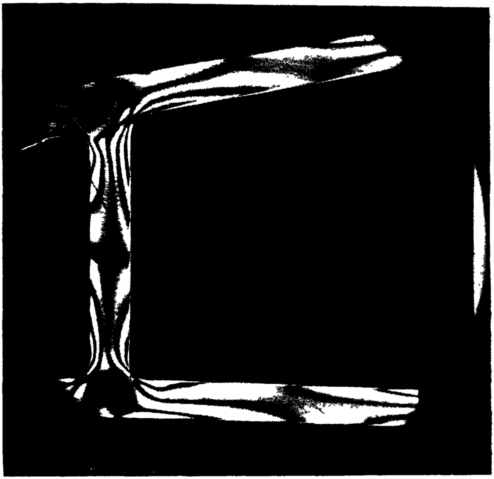

Fig. 74.—Vierendeel girder panel in polariscope.

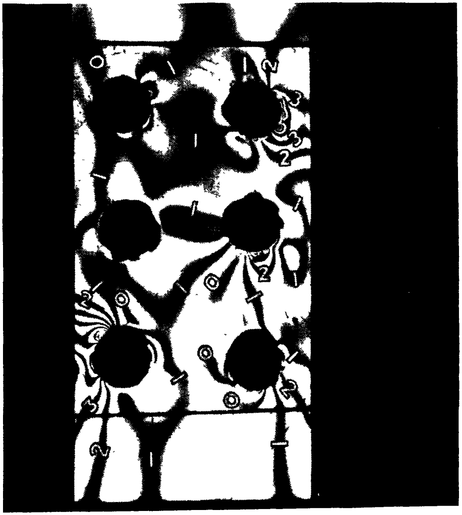

Fig. 76.—Fringe pattern for test on ecentrically loaded rivet group.

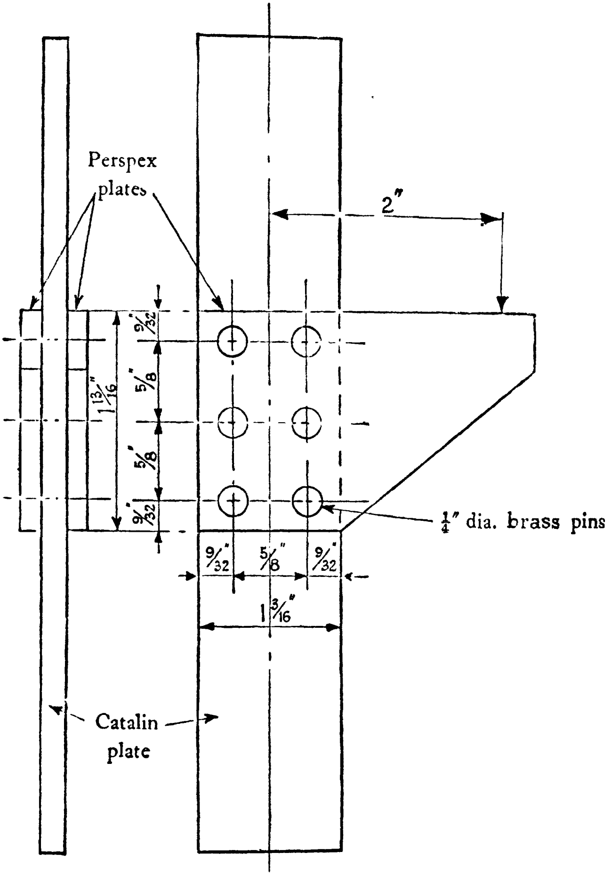

Fig. 75.—Model of bolted bracket connexion

stitute for or a check on long arithmetical solutions. One of the most valuable features of the method lies in the fact that the investigator obtains an immediate and striking picture of the stress conditions in the part under consideration.

Photo-elasticity is perhaps mainly an instrument of research, since, to make the fullest possible use of the method, considerable workshop and laboratory facilities are required. At the same time, however, it should be emphasized that valuable information can often be obtained using only comparatively simple and inexpensive equipment, and more use could be made of the method in design than is at present the case.

CHAPTER X

Frozen Stress Patterns and their Practical Applications

We may conclude this volume with a short description of " frozen " stress patterns and their application to the investigation of rotational stresses and the study of three-dimensional stress systems. The latter application is still in its early stages, and a good deal has yet to be done before the technique and methods of analysing results are fully developed. However, considerable advances in this direction have been made in recent years, and the potential value of the method is so great that it is felt that no modern book on photo-elasticity would be complete without some reference to these matters.

Frozen Stress Patterns

When the external loads are removed from a photo-elastic model, the fringe pattern produced by these loads disappears, either immediately or in a comparatively short time. Suppose, however, that a model is heated to a temperature of about 120° C, loaded, and cooled down very slowly to room temperature with the loads still acting. Then on removing the loads and examining the model in a polariscope it will be found that the fringe pattern due to the loads has not disappeared but has been " fixed " or " frozen " in the model. Careful tests have shown that this *frozen stress pattern*, as it is called, is identical with the pattern obtained at room temperatures under the same loading, although the magnitudes of the loads necessary to produce it are very much less.

Further, it is found that the frozen stress pattern is quite unaffected by cutting the model in pieces, the fringes in each piece remaining just as they were when the model was first examined.

This rather remarkable behaviour is due to the molecular nature of the material. The molecular structure of Bakelite is extremely complex, but for present purposes it is sufficiently accurate to assume that at room temperature there exists in the material a " skeleton ", or three-dimensional network, of strongly linked molecules surrounded by a mass in which the molecules are much less strongly bonded. Thus, when the Bakelite is heated to 120° C, the thermal energy imparted to it is sufficient to break down the bonds between the molecules of the latter constituent without appreciably affecting the strongly bonded molecular skeleton, which in fact remains stable to about 300° C. As a result of this breaking down of inter-molecular bonds, the interstitial material becomes effectively liquid, and any loads which are applied to the material in this state must be carried entirely by the infusible space network.

If now the material is slowly cooled down with the loads still acting, the molecular bonds within the fusible part are re-established, and this constituent returns to its original hard, resistant state. In doing so, however, it prevents the infusible network from returning to its undeformed shape when the loads are removed, and thus the high-temperature deformations of the network are preserved at room temperatures with the results already described.

Since the deformations are maintained purely by intermolecular forces, it is now apparent why the frozen stress pattern is not affected by cutting the model in pieces.

The Properties of Bakelite at High Temperature

It is obvious that, if frozen stress patterns are to be of practical value in photo-elasticity, the material from which the models are made must possess linear stress-strain and stress-retardation relations at the temperature to which the model must be heated in order to produce the frozen stress pattern. It has been established by Hetényi that Bakelite BT-61-893 satisfies these conditions; this is illustrated in fig. 77, showing the stress-strain and stress-retardation curves for this material at 115° C.

At this temperature, Young's modulus is about 1100 lb/in^2, and the unit fringe value 3·3 lb/in^2. Comparing these with the room temperature values, E is reduced in the ratio 1/640, while the stress-optical sensitivity is increased about 26 times.

Catalin also may be used for frozen stress models.

Practical Applications of the Frozen Stress Pattern

The frozen stress phenomena have been utilized in investigating the stress distribution in a rotating disc perforated at various points. To determine the centrifugal stresses in such a part is mathematically rather difficult, and to carry out a photo-elastic test using high-speed photography or stroboscopic technique is troublesome, although quite practicable. The problem has been solved by rotating the disc while immersed in a bath of paraffin

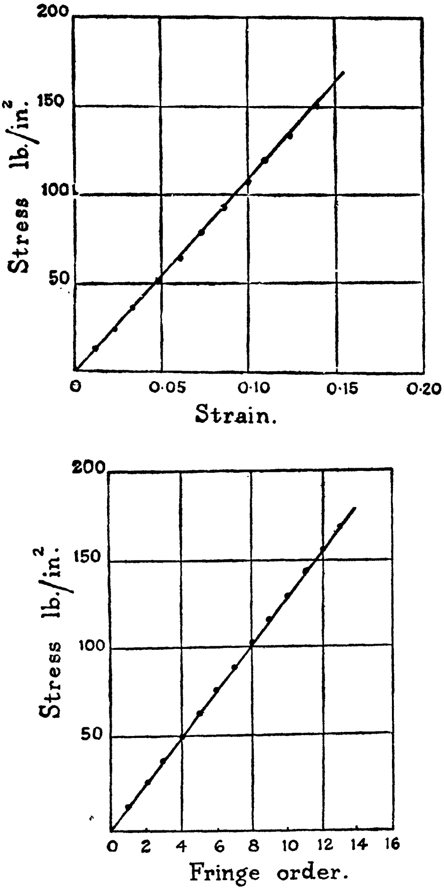

Fig. 77.—The properties of " Bakelite " BT-61-893 at 115° C. (From data published by M. Hetényi, *Trans. A.S.M.E.*, 1938, Vol. 60)

oil at 120° C, the rotation being continued while the bath was cooled slowly to room temperature. The resulting frozen stress pattern was subsequently analysed in the usual manner.

An even more important application of the frozen stress technique is to the study of three-dimensional stress systems. The method is again to load the model while immersed in an oil bath at 120° C, and to maintain the loads while the temperature is gradually lowered.

After removing the model from the loading apparatus, it is very carefully cut up into thin slices in a milling machine. After polishing, the slices are examined in the polariscope, and from observations on slices cut at several different inclinations, it is possible to calculate the state of stress at points in the model. It is, however, beyond the scope of this book to discuss the technique and the method of determining the three-dimensional stresses from the patterns exhibited by the slices.

The method has been used by Frocht in investigating the stresses in a shaft having a hole drilled through it at right angles to its longitudinal axis. Various other problems, including the stress analysis of thick rectangular slabs, have also been investigated by three-dimensional photo-elasticity.

It should be mentioned that the frozen stress method is not the only approach to the solution of the triaxial stress problem by photo-elasticity—there is in fact another method, known as the " scatter " method, in which a narrow beam of polarized light is directed into the stressed material; the beam is " scattered " and a fringe pattern is observed on looking through the model in a direction transverse to the direction of the beam, without the use of an analyser.

The extension of the photo-elastic method to the analysis of three-dimensional stress systems promises to be most valuable, as there is at present no other experimental method of determining the state of stress in the interior of a solid body.

BIBLIOGRAPHY

The following classified list of books and papers will be of value in further reading:

BOOKS ON PHOTO-ELASTICITY

E. G. Coker and L. N. G. Filon, *A Treatise on Photo-elasticity*, Cambridge University Press (1931).

L. N. G. Filon, *A Manual of Photo-elasticity for Engineers*, Cambridge University Press (1936).

M. M. Frocht and J. Wiley, *Photo-elasticity*, Vol. I (1941), Vol. II (In press, 1946).

BOOKS ON THEORY OF ELASTICITY, &C.

S. Timoshenko, *Strength of Materials*, MacMillan (1941), 2 Vols.

R. V. Southwell, *Theory of Elasticity*, Oxford University Press.

R. A. Houston, *A Treatise on Light*, Longmans.

PAPERS ON PHOTO-ELASTICITY

1. Optical Theory, etc.

J. Valsek, " Survey of Crystal Optics ", *J. App. Physics*, Vol. 10, 4, 1939.

R. D. Mindlin, " A Review of the Photo-elastic Method of Stress Analysis ", *J. App. Phys.*, Vol. 10, 1939.

" Photo-elasticity and Elasticity ", *Engineering*, Vol. 150, 1940.

R. E. Arthur, " Introduction to the Theory of Photo-elasticity ", *J. R. Aero. Soc.*, 1943.

2. Analysis of Results

G. H. Shortley and R. Weller, " Calculation of the Stresses within the Boundary of Photo-elastic Models ", *Trans. A.S.M.E.*, Vol. 61, 1939, and " The Numerical Solution of Laplace's Equation ", *J. App. Phys.*, Vol. 9, 1938.

M. M. Frocht and M. M. Leven, " A Rational Approach to the Numerical Solution of Laplace's Equation ", *Jour. App. Phys.*, Vol. 12, 1941.

L. N. G. Filon, " On the Graphical Determination of Stress from Photo-elastic Observations ", *Engineering*, October, 1923. See also " Report of the British Association ", 1923.

D. C. Drucker, " Photo-elastic Separation of the Principal Stresses by Oblique Incidence ", *Trans. A.S.M.E.*, Vol. 65, 1943.

G. H. Shortley, R. Weller and B. Fried, " The Numerical Solution of Laplace's and Poisson's Equations with Applications to Photo-elasticity and Torsion ", *Ohio State Univ. Engin. Exp. Sta.*, No. 107, 1940.

M. M. Frocht, " Isopachic Stress Patterns ", *J. App. Phys.*, Vol. 10, 4, 1939.

3. Photo-elastic Apparatus

A. V. De Forest and A. R. Anderson, " A New Lateral Extensometer ", *Trans. A.S.M.E.*, Vol. 63, 1941.

A. W. Hendry, " Photo-elastic Apparatus, Technique and Materials ", *J. Inst. C.E.*, 1946.

Z. Tuzi and H. Oosima, " On the Artificial Quarter-plate for Photo-elasticity Apparatus and its Theory ", *Sci. Papers. Inst. Phys. Chem. Research, Tokio*, 1939.

R. D. Mindlin, " Distortion of the Photo-elastic Fringe Pattern in an Optically Unbalanced Polariscope ", *Trans. A.S.M.E.*, Vol. 59, 1937.

J. H. A. Brahtz and J. F. Soehrens, " Direct Optical Measurement of the Individual Principal Stresses ", *J. App. Phys.*, Vol. 10, 4, 1939.

4. Photo-elastic Materials and Technique

A. W. Hendry, " Photo-elastic Apparatus, Technique and Materials ", *J. Inst. C.E.*, 1946.

G. H. Lee and M. Goldstein, " The Annealing of Photo-elastic Bakelite and the Resulting Effect on its Physical and Optical Properties ", *J. App. Phys.*, Vol. 12, 8, 1941.

J. Villey, " On the Selection of Transparent Materials for Photo-elastic Analysis ", *Pub. Scien. et Tech. de Sec. d'Etat à l'Aviation*, No. 96, 1941.

G. H. Lee and C. W. Armstrong, " The Effect of Temperature on Physical and Optical Properties of Photo-elastic Materials ", *Trans. A.S.M.E.*, Vol. 60, 1938.

W. Leaf, " Edge Effects in Photo-elastic Analysis ", *Plastics*, No. 7, 1943.

R. S. Monell (Ed.), *Synthetic Resins and Allied Plastics*, Oxford University Press (1943).

H. A. Robinson, R. Ruggy and E. Slantz, " Elasto-viscous and Stress-optical Properties of Commercial Polymerized Methyl Methacrylate as a Function of Temperature ", *J. App. Phys.*, Vol. 15, 1944.

M. L. Price, " Preparation of Photo-elastic Models ", *Proc. Eastern Photo-elasticity Conference*, 1946.

B. Dunn, " A Photographic Method of deriving Isoclinic Lines in Photo-elastic Methods of Stress Calculation ", *Nature*, 1945.

" Photographic and Cinematographic Records in Photo-elastic Analysis ", *Photographic J.*, 1941.

T. R. Cuykendall, " Gelatin Models ", *Proc. 9th Eastern Photo-elasticity Conference*, 1939.

5. Applications of Photo-elasticity to Engineering Problems

D. Sinclair and P. Bucky, " Photo-elasticity and its Application to Mine Pillar and Tunnel Problems ", *Mining Technology*, 1940.

Horger, " Photo-elastic Analysis Practically Applied to Design Problems ", *J. App. Phys.*, Vol. 9, No. 7, 1938.

R. E. Orton, " Photo-elasticity as a Designer's Tool ", *Experimental Stress Analysis*, Vol. 3, No. 1, 1945.

A. W. Hendry, " Photo-elasticity and its Application to Certain Problems in Structural Engineering ", *The Structural Engineer*, Vol. 22, 1944.

A. W. Hendry, " An Investigation of the Stress Distribution in Steel Portal Frame Knees ", *The Structural Engineer*, Vol. 25, 1947.

" Application of Photo-elasticity to Automobile Engineering ", *Proc. 13th Eastern Photo-elasticity Conference*, 1941.

A. G. Solakian, " Photo-elastic Analysis of Stress in the Lap Plates of Fillet-welded Joints ", *Amer. Weld. J. Suppt.*, Sept., 1939.

R. F. Tylecote, " A Photo-elastic Investigation of the Stress Distribution in Spot Welds ", *Weld. J. Suppt.*, Aug., 1941.

W. E. Cooper, " Photo-elastic Investigation of Stress in Spot Welds ", *Welding Res. Coun. Report*, No. R52/75, 1943.

M. Hetényi, " The Distribution of Stress in Threaded Connections ", *Experimental Stress Analysis*, Vol. I, 1943.

M. Hetényi, " A Photo-elastic Study of Bolt and Nut Fastenings ", *Trans. A.S.M.E.*, Vol. 65, 1943, also Vol. 66, 1944.

M. Hetényi, "Some Applications of Photo-elasticity in Turbine Generator Design", *Trans. A.S.M.E.*, Vol. 61, 1939, also Vol. 62, 1940.

J. J. Ryan and R. T. Rettaliata, "Photo-elastic Analysis of Stresses in a Steam Turbine Blade Root", *Trans. A.S.M.E.*, Vol. 62, 1940.

P. D. Edmondson, "Photo-elastic Investigation of W2/700 Blade Root", *Power Jets Memo.*, M. 1212, 1946.

R. V. Baud, "Photo-elasticity and Mechanical Model Experiments on the Stress in Commutator Sections", *Schweizer Archiv.*, 1941.

M. M. Frocht and H. N. Hill, "Stress Concentration Factors around Central Circular Hole in Plate loaded through Pin in Hole", *Trans. A.S.M.E.*, Vol. 62, 1940.

P. Grodzinski, "Investigations of Shaft Fillets", *Engineering*, 1941.

"Stresses in Axles, Photo-elastic Diagrams", *Engineering*, 1943.

F. O. Anderegg, B. Fried and R. Weller, "Photo-elastic Analysis of a Pre-stressed Beam", *Proc. A.S.T.M.*, Vol. 39.

M. M. Frocht and M. M. Leven, "On the State of Stress in Thick Bars", *J. App. Phys.*, Vol. 13, 5, 1942.

A. Robert, "An Experimental and Theoretical Study of the Stress Distribution in Built-in Beams", *Pub. of the Lab. for Photo-elasticity at the Fed. Inst. of Tech. (E.T.H.), Zurich*, No. 1, 1943.

A. H. Beyer and A. G. Solakian, "Photo-elastic Analysis of Stresses in Composite Materials", *Trans. Am. Soc. C.E.*, Vol. 99, 1934.

T. Dolan and D. Richards, "A Photo-elastic Study of the Stresses in Wing Ribs", *J. Aero. Sciences*, 1940.

T. J. Dolan, " Influence of Certain Variables on the Stresses in Gear Teeth ", *J. App. Phys.*, Vol. 12, 8, 1941.

T. J. Dolan and E. L. Broghamer, " A Photo-elastic Study of Stresses in Gear-tooth Profiles ", *Univ. Illinois Eng. Exp. Stn. Bull.*, 335.

W. N. Findley, " The Fundamentals of Photo-elastic Stress Analysis applied to Dynamic Stresses ", *Proc. 9th Eastern Photo-elasticity Conf.*, 1939.

R. E. Newton, " A photo-elastic Study of Stresses in Rotating Discs ", *Trans. A.S.M.E.*, Vol. 62, 1940.

I. G. Teverovski, " An Investigation of the Stresses in Rotating Discs with a Number of Apertures ", *M.A.P. Trans.*, No. 1493.

F. B. Farquarson and R. G. Hennes, " Gelatin Models for Photo-elastic Analysis of Stress in Earth Masses ", *Civil Engineering*, 1940.

6. Three Dimensional Photo-elasticity, etc.

M. Hetényi, " Photo-elastic Studies of Three-dimensional Stress Problems ", *Proc. 5th International Congress for Applied Mechanics.* See also *Trans. A.S.M.E.*, Vol. 60, 1938.

R. Weller, " A New Method for Photo-elasticity in Three Dimensions ", *J. App. Phys.*, Vol. 10, 4, 1939.

M. Hetényi, " The Application of the Hardening Resins in Three-dimensional Photo-elastic Studies ", *J. App. Phys.*, Vol. 10, 5, 1939.

D. C. Drucker and R. D. Mindlin, " Stress Analysis by Three-dimensional Photo-elastic Methods ", *J. App. Phys.*, Vol. 11, 1940.

R. Weller and J. K. Bussey, " Photo-elastic Analysis of Three-dimensional Stress Systems using Scattered Light ", *J. Roy. Aero. Soc.*, Vol. XLIV, 1940.

R. Weller, " Three-dimensional Photo-elasticity using Scattered Light ", *J. App. Phys.*, Vol. 12, 8, 1941.

R. D. Mindlin, " Optical Aspects of Three-dimensional Photo-elasticity ", *J. Franklin Inst.*, 1942.

R. D. Mindlin, " Present Status of Three-dimensional Photo-elasticity ", *Civil Engineering*, Vol. 12, 1942.

D. C. Drucker, " The Photo-elastic Analysis of Transverse Bending of Plates in the Standard Transmission Polariscope ", *Trans. A.S.M.E.*, Vol. 64, 1942.

J. Goodier and G. H. Lee, " An Extension of the Photo-elastic Method of Stress Measurement in Plates in Transverse Bending ", *Trans. A.S.M.E.*, Vol. 63, 1941.

J. L. Meriam, " Centrifugal Stresses in Impellers ", *Aircraft Eng.*, Sept., 1943.

M. M. Frocht, " Stress Concentrations in Shafts with Transverse Holes in Tension ", *J. App. Phys.*, Vol. 15, 1944.

M. M. Frocht, " Stress in Bent Circular Shafts with Transverse Holes ", *Trans. A.S.M.E.*, Vol. 66, 1944, also *Exp. Stress Analysis* Vol. 2, No. 1, 1944.

W. A. P. Fisher, " Photo-elastic Investigation of Three-dimensional Stress by the Freezing Method", *R.A.E. Report*, No. SME 3328, 1945.

W. A. P. Fisher, " An Investigation of the Suitability of Catalin 800 for the Frozen Stress Method of Photo-elastic Analysis ", *R.A.E. Report*, No. SME 3342, 1946.

W. A. P. Fisher, " Photo-elastic Determination of the Shear Load in Bolts by Means of the Freezing Method ", *R.A.E. Report*, No. SME 3365.

INDEX

Ahrens prism, 77.
Analyser, 32.
Angström unit, 21.
Anisotropic media, 25.
Anisotropy, initial, 124.

Babinet compensator, 92.
Bakelite, properties, 108.
— properties at high temperature, 140.
Beams, fringe pattern in, 45, 46.
Brewster (unit), 41.

Calcite, 28.
— polarizing filters, 75.
Calibration of fringe patterns, 49, 57.
Cameras, 84.
Catalin, 110.
— curing of, 112.
Cellophane, 81.
Celluloid, 114.
Circularly polarized light, 22.
Coker compensator, 98.
Colour filters, 83.
— matching, 49.
— patterns, white light, 49.
— sequence, 42.
Compensators, 91.
Contact stress problems, 130.
Creep, optical, 107, 127.
Crystal plate in polariscope, 33.
Crystals, biaxial, 28.
— dichroic, 77.
— propagation of light in, 26.
— uniaxial, 26.
Cupic points, 12.

Dichroism, 77.
Dislocations, 16.
Double refraction, 27.

Edge stresses, plotting the, 58.
Elliptically polarized light, 22.
Error, sources of, 124.
Extensometer, lateral, 73, 102.

Filon's method for calculation of principal stresses, 59.
Flanged models, preparation of, 121.
Four-point influence method, 69.
Framed structures, models of, 18.
Fringe order, 45.
— pattern, 45.
— — calibration of, 48.
— — growth of, 45.
— — use of, 47.
Frocht's shear-difference method, 61.
Frozen stress patterns, 138.

Gelatine, 116.
Geometrically similar plates, 15.
Glan-Thomson prism, 77.
Glass, 115.
— plate polarizers, 78.

Herapathite, 77.

Initial stresses, 124.
Interference, 29.
Interferometer, photo-elastic, 99.
Isochromatic lines, 51.
Isoclinic lines, 10, 55.
— — Mesnager's theorem of, 12.
Isotropic media, 24.
— points, 14, 47.

Laplace's equation, arithmetical solution of, 65.
— — experimental solution, 74, 104.

Lateral extensometer method, 73, 102.
Light, nature of, 20.
— sources, 82.
Lines of principal stress, 8.
— isochromatic, 51.
— isoclinic, 10, 55.

Machining of Catalin, 119.
Materials, photo-elastic, 106.
Maximum shearing stress, 8.
— — — lines of, 57.
Membrane analogy apparatus, 104.
— — method, 74.
Mercury-vapour lamps, 83.
— — filters, 83.
Mesnager's theorem, 12.
Mica retardation plates, 79.
Mica-plate compensator, 95.
Model, accuracy of, 125.
Models, preparation of, 117.
— scale requirements, 18.
Monochromatic light, 21, 83.
— fringe patterns, 45.

Nicol prism, 76.

Patterns, monochromatic fringe, 45.
— white light colour, 49.
Perspex, unplasticized, 115.
Photo-elastic effect, 40.
— interferometer, 99.
— materials, 106.
Photo-elasticity, practical applications, 128.
Photography, 123.
Plane polarized light, 22.
— strain, 3.
— stress, 3.
Points, cupic, 12.
— isotropic, 14, 47.
— singular, 14, 47.
Polariscope, circular, 38.
— crystal plate in, 33.
— design of, 89.
— optical systems of, 84.
— plane, 32.
— stresssed materials in, 40.
Polarization of light, 22.
Polarizer, 32.
Polarizing filters, 75.
Polaroid, 77.
Principal stress, 6.
— stresses, determination of sum of, 64.
— — lines of, 8.
— — — — construction of, 55.
— — separation of, 58.
Prism, Ahrens, 77.
— Glan-Thomson, 77.
— Nicol, 76.

Quarter-wave plates, 38.
— — preparation of, 79.

Redundant structures, 133.
Refraction, double, 27.
Refractive index, 25.
Retardation, relative path, 28.
Riveted connexions, 136.

Scale-model requirements, 18.
Sequence, colour, 43.
Shear diagonal, 4.
Shear-difference method, 61.
Shearing stresses, 8.
Similarity formulæ, 18.
Soleil-Babinet compensator, 94.
Sources, light, 82.
— of error, 124.
Space effect, 122, 126.
Strain, plane, 3.
Stress at a point, 3.
— concentration factor, 128.
— in similar plates, 15.
— plane, 3.
— trajectory, 8.
Stresses, principal, 6.
Structural members, stresses in, 131.
Structures, models of, 18, 133.

Test procedure, 121.
Three-dimensional analysis, 142.
Time-edge effect, 125.
Tint of passage, 42.
— — — isochromatic, 51.

Tourmaline, 77.
Triple-reflection polarizer, 79.

Uniaxial crystals, 26.

Vierendeel girder, 133.

Wavefront, 24.
Wave normal, 24.
— surface, 24.
— theory of light, 20.

Xylonite, 114.

CENTRAL LIBRARY
BIRLA INSTITUTE OF TECHNOLOGY & SCIENCE
Call No. PILANI (Rajasthan) Acc. No,
DATE OF RETURN 5 1167